Università degli Studi di Napoli “Federico II”

Facoltà di Ingegneria

Dottorato di Ricerca

Ingegneria Aerospaziale, Navale e della Qualità

XXVII Ciclo

Experimental Flight Test Management.

Optimization procedures and flight test techniques for test time efficiency and cost reduction

Relatori Ch.mi
Prof. Carlo de Nicola
Prof.ssa Lina Mallozzi

Candidato
Pierluigi De Paolis

Anno Accademico 2015-2016

CONTENTS

INTRODUCTION

Approaching to flight test is paramount to keep clear in mind that accurate test management is the cornerstone between failure and success. Flight testing remains an essential element of sound air vehicle development. The current emphasis on expanding the use of M&S has been promulgated with the intention that it can help to reduce flight test time and cost, enhance test safety, and increase testing efficiency.

The “predict-test-validate” (a.k.a. ”model-test-model”) paradigm is held forth as the most efficient combination of these development tools. In this paradigm the initial modelling and simulation guides the planning and conduct of flight testing, with incremental test results then used to enhance the accuracy and/or fidelity of the simulation before the process is repeated. The cycle would be repeated many times during the course of the test program, especially in an effort to avoid the "fly-fix-fly" paradigm that commonly proves inefficient and trying to avoid future operational shortfalls.

Although much of the technical leadership in the NATO aerospace industry and Italian Defence Department insist that M&S is not intended to replace flight testing, there remains concern among flight test practitioners that the result will be an overreliance on simulation. This has a potential for neglecting invaluable empirical test data verifying system performance. In addition, detrimental and potentially hazardous system characteristics may not be uncovered, and overall assessment of vehicle worthiness vis-a-vis its mission will suffer. Appreciation for a sound balancing of flight testing with simulation must be promulgated. In addition, a methodology appears to be needed to help insure this sound balance.

The term M&S is taken to include,[1]:

- Digital models and computer simulations using those models;
- Mathematical analytical tools such as Computational Fluid Dynamics;
- Simulated flight testing such as in wind tunnels and engine altitude test chambers;
- Hardware-in-the-loop simulations;
- Pilot-in-the-loop simulations, with and without hardware-in-the-loop;
- In-flight simulation;

−Other large-scale ground tests.

Each of these initially employ simplified system representations that become more complex as the systems engineering process defines the system during the course of development and as test data becomes available to improve model and simulation fidelity and accuracy. Present initiatives are expanding the application of verification and validation of M&S resources to ensure that they function as intended and suitably represent real-world behaviour. Flight testing itself can be considered a simulation if the test article is an experimental system or early prototype, if some internal or external system functions are contrived, and if test conditions do not truly match actual in-service scenarios (such as simulated combat). OT&E flight test relies heavily on constructive simulation and PITL tactical simulations. All this has become more popular as simulation capabilities have increased and flight test budgets and schedules have decreased.

However, the flight environment, with systems interacting and with a pilot (perhaps) in control, is not a simulation. Flight test remains the most dynamic and credible medium for collecting actual system performance data.

Test management holistic concept is much more, taking into account also the relevant phase of actual test preparation, test matrix identification (totality of test points to be performed), coordination, FTTs set-up, generation of new validation techniques and reporting, of course.

The purpose of this thesis work is to show how an accurate test management based on alternative geometry acquisition processes, test matrix generation algorithms, M&S, new FTTs and validation procedures can be used effectively and efficiently to support flight testing. In particular, in order to reduce the scope of the subject activity the focus is kept on a specific branch of the test field known as Store Integration and Safe Separation; the approach could be expanded to other branches of flight test, but customization would be required.

The question becomes how much flight testing can really be replaced by simulation before jeopardizing the safety of flight and increasing the cost of simulation prohibitively to make it worthwhile. Simulation is not a panacea for all test problems, but a valuable tool that must be used cautiously and wisely in the course of a test program, the key word is “balance” and its maidservants are “optimization, synchronization and coordination”.

CHAPTER 1

AIRCRAFT STORE INTEGRATION AND CERTIFICATION PROCESS

Approaching the optimization process for the whole flight test area of expertise could result pretty cumbersome and arduous, therefore a choice is necessary. This study is focused on the store integration, evaluating experimental relevant steps ride along the certification process starting from the task mandate up to the production of outcome necessary to the reporting phase, Figure 1.

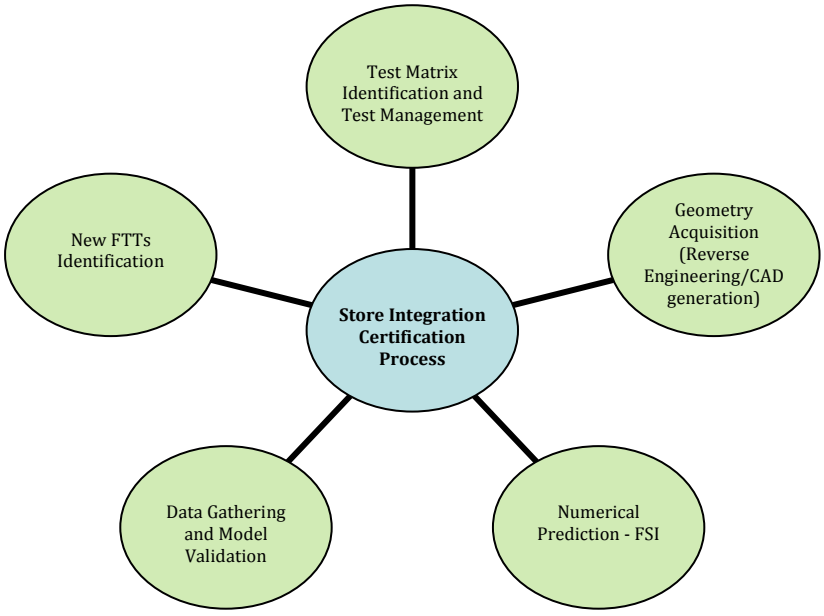

Figure 1: FT contribution to Store Integration Certification Process.

Historically, the management of the aforementioned process was based on the experience of few very skilful people, leading the activity, depriving the process itself from being standardized and depersonalized. Moreover, some steps of the process were not evaluated for many reasons: time deficiency, lack of necessary know-how, high costs, risk mitigation under-evaluation.

The purpose of the new "predict-test-evaluate" approach is to force the decision makers to take in due account all relevant steps concerning the experimental evaluation of the store integration certification process and to standardize, to the limit of depersonalization, the execution phase. The "predict-test-evaluate" represents a circular approach, Figure 2, producing the effect of a self-test process, leading the test team to the challenge-and-response test.

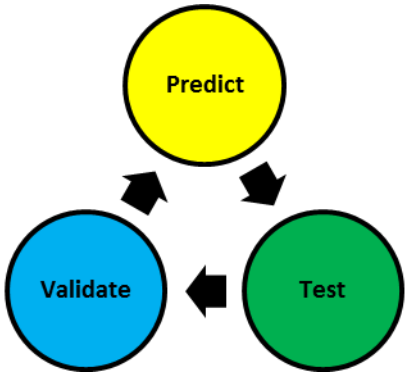

Figure 2: Predict-Test-Validate model.

Optimization of the entire process, cost reduction, time efficiency and risk mitigation effectiveness pass through the standardization and optimization of the single steps listed in Figure 1.

1.1 Test matrix identification and test management

Sizing and identifying the test matrix is the most time consuming and uncertain activity faced by every test team when approaching a new flight test task. The unkowns are countless and the proposed methods promising a solution in the academic world are much more. Different project managers in the same organization could decide to pursue different

solution tracks, all valid, but requiring different means, way and outcomes for the same problem. Trying to avoiding this uncertainty related to the store integration process test points identification, in this study are examined the two most recognized method proposed by the academic and industrial world and new ways to think and perform are proposed in order to meet the requirement of a tailorable, efficient and effective tool for planning test activity. Theory of games and Theory of fields are the pillars of the new proposed algorithm.

1.2 Geometry acquisition techniques

Nowadays, the global market is extremely competitive, therefore product enterprises are constantly seeking new ways to shorten lead times for new product developments matching customers' expectations. Product enterprise has invested in CADCAM, rapid prototyping, and a range of new technologies that provide business benefits.

Engineering is the process of designing, manufacturing, assembling, and maintaining products and systems. Two major types of engineering could be identified: forward engineering and reverse engineering, Figure 3.

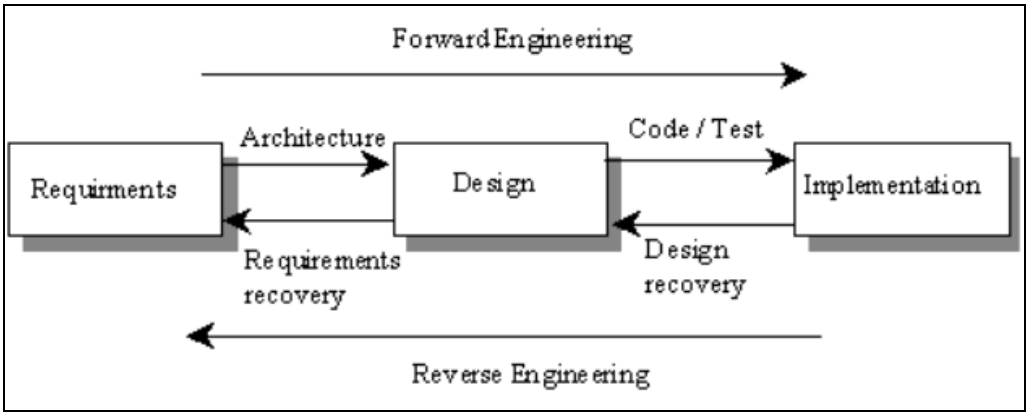

Figure 3: Re-engineering/Model.

Forward engineering is the traditional process of moving from high-level abstractions and logical designs to the physical implementation of a system.

The process of duplicating an existing part, subassembly, or product, without referencing to drawings, documentation, or a computer model is known as reverse engineering. RE is also defined as the process of obtaining a geometric CAD model from 3-D points acquired by scanning/digitizing existing parts/products.

In aeronautics environment it is very important to determine the aim of the CAD generation activity, in fact the required quality of a product, the CAD drawing, is dramatically relevant to determine the success of a computational fluid dynamic analysis or not. Where a precise fine-tuning, asymptotically a zero-error correction, is required, as for the case of a propeller or wing profile, the RE could not be the best fitting method, of course every consideration is related also to the available tools. In fact, the operator judgement and intervention required in order to reproduce the lifting surface starting from the laser scanning acquired cloud of points brings in itself some relevant error; filling the uncertainty means to misrepresent the truth, Figure 4.

However, a reconstruction of the profile via forward engineering, for example interpolating a certain number of the cross section area airfoils, could place the analysis on realm of realism instead of on the plane of pure simulation academic training analysis.

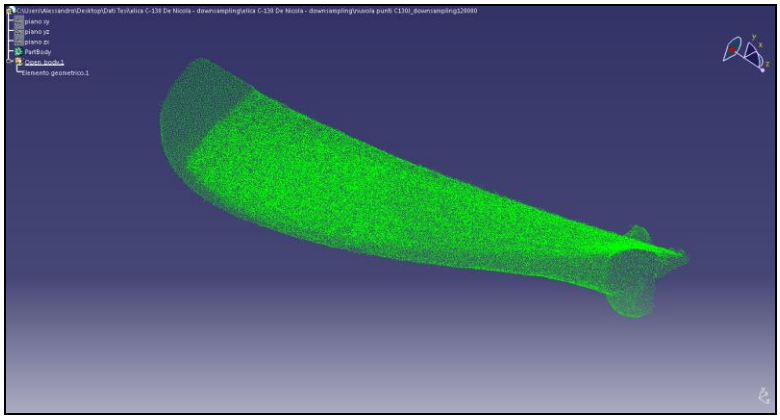

Figure 4: Propeller discrete laser scanned cloud of points.

1.3 Numerical prediction: fluid-structure interaction

In fluid-structure interaction problems, one or more solid structures interact with an internal or surrounding fluid flow. FSI problems play prominent roles in many scientific and engineering fields, yet a comprehensive study of such problems remains a challenge due to their strong nonlinearity and multidisciplinary nature. For most FSI problems, analytical solutions to the model equations are impossible to obtain, whereas laboratory experiments are limited in scope; thus to investigate the fundamental physics involved in the complex interaction between fluids and solids, numerical simulations may be employed.

With recent advances of computer technology, simulations of scientific and engineering systems have become increasingly sophisticated and complicated. To fill the technological gap, an efficient numerical algorithm can be used to investigate in detail the interaction for example between fluid (air) and the motion of the modern jet. Such an investigation is typically multidisciplinary. In this example, the performance of the aircraft is a result of the interaction between air dynamics and structural dynamics. Other FSI applications include, but are not limited to, sedimentation, particle assembly, hydrodynamics, turbulence, complex flows in irregular domains, electro-hydrodynamics, magneto-hydrodynamic flows, biofluid and bio-mechanics (such as cell aggregation and deformation, blood-heart interaction, inner ear fluid dynamics, jellyfish swimming, sperm motility, cilliary beating, etc.), [2].

The numerical procedures to solve these FSI problems may be broadly classified into two approaches: the monolithic approach and the partitioned approach, [3]. It is understood that the distinction between the monolithic and partitioned approaches may be viewed differently by researchers from different fields. In this study, it is intend to define these two approaches from the engineering application point of view. Figure 5 illustrates the solution procedures of the monolithic and partitioned approaches.

The monolithic approach, [4],treats the fluid and structure dynamics in the same mathematical framework to form a single system equation for the entire problem, which is solved simultaneously by a unified algorithm. The interfacial conditions are implicit in the solution procedure. This approach

can potentially achieve better accuracy for a multidisciplinary problem, but it may require substantially more resources and expertise to develop and maintain such a specialized code. In contrast, the partitioned approach treats the fluid and the structure as two computational fields which can be solved separately with their respective mesh discretization and numerical algorithm. The interfacial conditions are used explicitly to communicate information between the fluid and structure solutions.

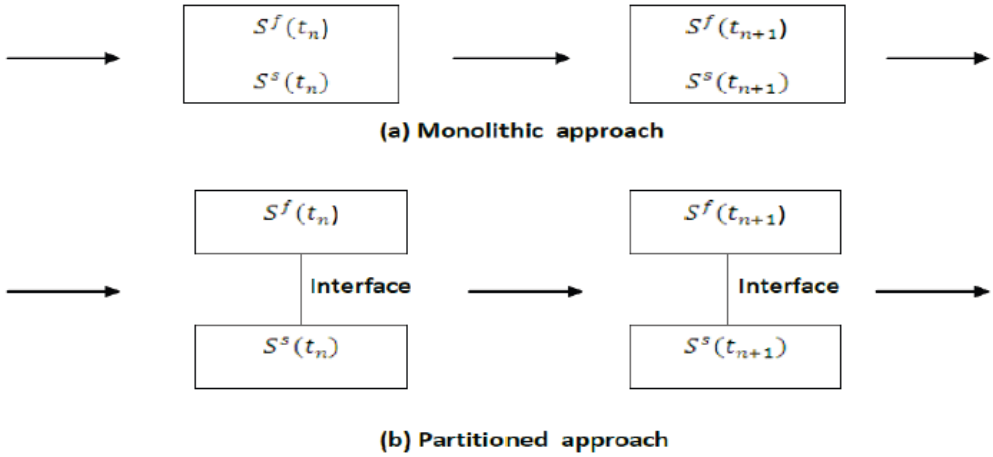

Figure 5: Monolithic and partitioned approches.

A motivation of the later approach is to integrate available disciplinary (i.e., fluidic and structural) algorithms and reduce the code development time by taking advantage of the ”legacy” codes or numerical algorithms that have been validated and used for solving many complicated fluid or structural problems. As a result, a successful partitioned method can solve a FSI problem with sophisticated fluid and structural physics. The challenge of this approach is, however, to coordinate the disciplinary algorithms to achieve accurate and efficient fluid-structure interaction solution with minimal code modification. Particularly, the interface location that divides the fluid and the structure domains is not known a priori and usually changed in time; thus, the partitioned approach requires the tracking of the new interface location and its related quantities, which can be cumbersome and error-prone.

Due to time constraints and in order to reduce the wide scope of the present cycle of study, the only portion of the analysis accomplished is related to the aerodynamic model, also if the foreseen application is for sure oriented to the integration of a structural model into the analysis, looking to the aero loads as input of the latter. At the same time, the deformation of the structure would be the new input for the geometry adaptation of the aero model.

1.4 Model Validation & Flight Test Techniques

After estimating a model, you can validate whether it reproduces the system behaviour within acceptable bounds. Iteration between model refinement and validation is necessary until you find the simplest model that best captures the system dynamics. Flight test is a matter of data gathering, analysis and processing.

Before instrumenting a jet and going in flight to take data, it is important to understand, based on the desired output of the analysis, which data are required and which manoeuvers could allow to gather those useful information. This manoeuvers are generally called flight test techniques and are peculiar for each branch of the flight test. Is it useful a WUT for the evaluation of the aeromechanical integration of a new store on a jet? Why should I perform a Split-S or a Roller-Coaster on an F-35? A Flight Test Engineer/Pilot needs to be able to answer to all this question and, if the case, to propose new techniques to gather the relevant data required by his developmental program.

Once defined the type of manoeuvers required to fill in the blanks of the FTE/P flight cards, it is necessary, most of time, to set up the aircraft with the appropriate FTI.

After the flight, analysing the qualitative comments of the test crew combined with the quantitative data, gathered by the FTE or recorded via FTI/telemetry device, Figure 6, it is possible to validate the model or at least to have the basis for its fine tuning, before being ready for next validation flight.

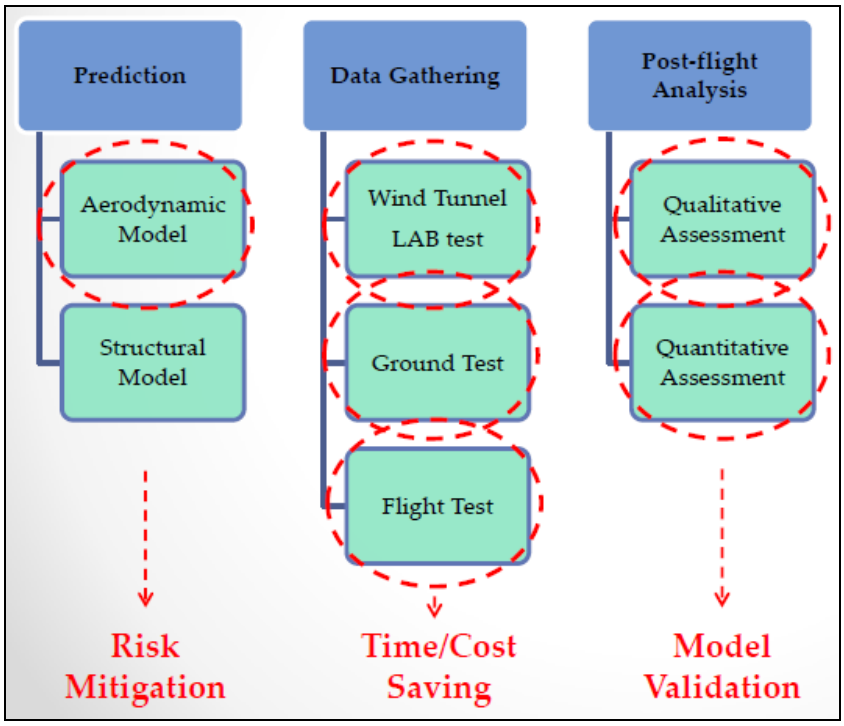

Figure 6: Predict-Test-Validate blown-up model.

CHAPTER 2

TESTING SET-UP: TEST MATRIX IDENTIFICATION

The first optimization step for each new experimental activity is the identification of an effective and efficient test matrix. Which are the significant factors to be analysed and test points to be executed in order to gather the relevant information we are looking for?

It is no cost effective for experiments to be performed in a trial-and-error way; changing one factor at a time. A far more effective method is to apply a computer-enhanced, systematic statistical-based approach to experimentation, one that considers all factors simultaneously and distinguish the main factors of the problem. That approach is commonly called DoE and is a starting point for each project manager approaching a new test activity.

Once defined the main factors, the choice of the number of test points to be performed is the next key step; in some cases, i.e. flutter or envelope expansion testing, the test team deals with unique prototype. For this type of aircraft, limiting the total flight hours of testing is a mandatory requirement not only for the significant cost associated, but also for the consideration of minimizing the risk of failure/loss of the highly valuable asset; in the last decade, a fatal mishap to a fully instrumented F-22 prototype brought to almost one year of delay in the Raptor Development Program and, unfortunately, to the loss of the experimental crew. Cost wise is useful to highlight that the average cost of a 4th/5th generation fighter type aircraft could range between 100 K$ and 500 K$. Therefore, when testing is required in the entire flight envelope, it is essential to find out a way to distribute the test points efficiently in order to gather all the required data, but at the same time saving time and reducing the number of test points. This means that

given some test constraints and key parameters to be evaluated, all efforts should be spent in order to optimize test points distribution, covering the entire envelope following the rules imposed by the objective functions, whose aim is populating the areas where the test execution has a higher priority based on engineering requirements.

Containing the analysis to the store integration activity, historically, two main different approaches have been used to face the test matrix identification problem: the classical method and the economy/zeta method.

In this thesis study two innovative approaches are presented: a non-cooperative game (spatial location) method and an alternative method based on the concept of potential and repulsive fields to optimize and standardize the design of the test matrix in an envelope expansion flight test activity.

All the aforementioned activities have been developed on behalf of and for the actual testing purposes of the Italian Flight Test Wing - RSV.

2.1. Classical approach

Experimental design is a critical tool in the engineering world for improving the execution process. The way to perform DoE is product-oriented. However, a common approach in flight testing is to use OFAT technique to design test matrixes; varying one variable, i.e. Mach number or pressure altitude, and leaving constant all other parameters.

The Classical method used in envelope expansion/store integration testing basically attempts to cover the most part of the flight envelope, exploring all combination of Mach, pressure altitude and AoA, resulting very expensive and time consuming. This approach allows both structural and system engineers to gather all relevant data for their technical clearance and certification process.

shows the complete set of test points (test matrix) that would be tested using a Classical (a.ka. Extensive method) approach for a new store integration, for each possible AoA.

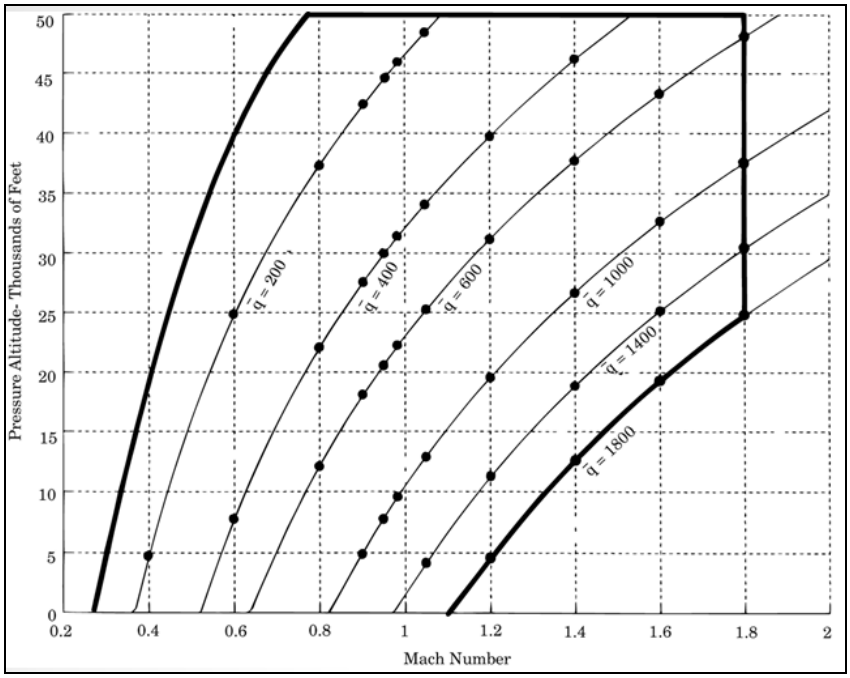

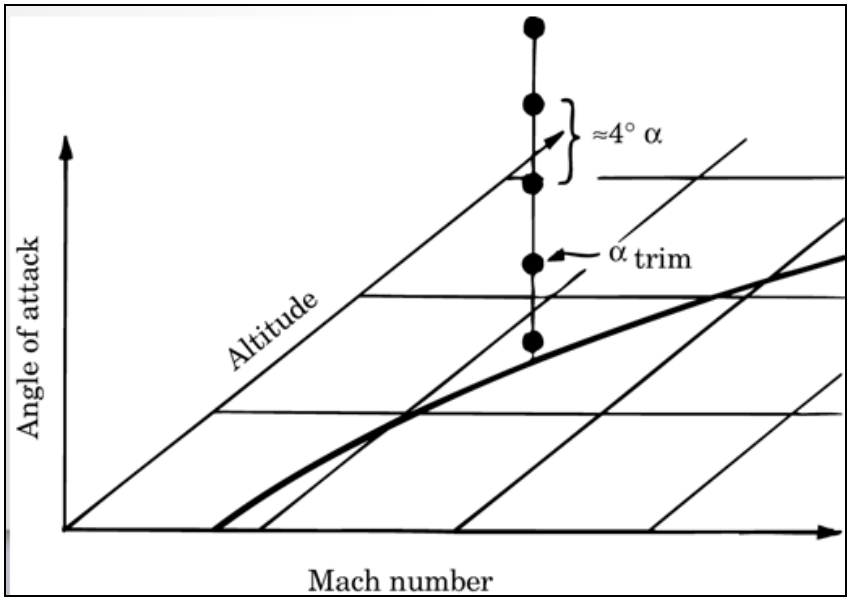

Figure 7: Classical/Extensive approach.

2.2. Economy approach

The other method commonly and often used in the flight test environment is the so called Economy Method, which consists on a choice of a subset of flight conditions starting from the classical method test matrix in accordance with the build-up approach principle in dynamic pressure. It means that only few test points are actually tested, reducing the spectrum of the test activity and assuming that interpolation within pressure altitude bands is a valid approximation in order to estimate the not linear aero-elastic phenomena connected with this kind of analysis.

Of course, the economy method, also called the "zeta" method for the test points execution path described on the flight envelope in accordance to the build-up principle, Figure 8, gives less information than the classical method, but has got the advantage to drastically reduce time and cost associated to the test campaign. Technical risk is almost the same in the two aforementioned methods, however, due to the reduced data and information gathered, the economy method presents some additional programmatic risk.

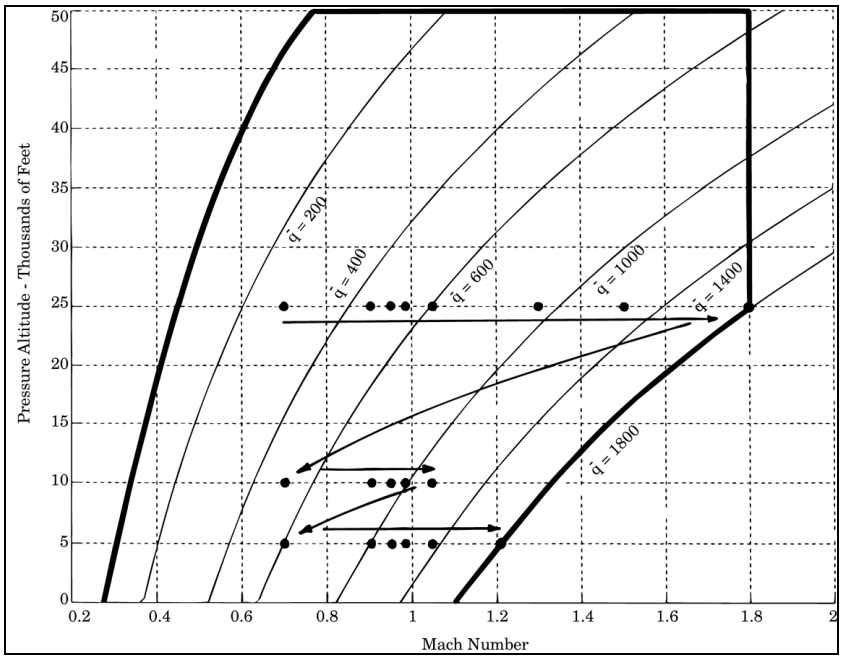

Figure 8: Economy/"Zeta" approach.

2.3. Innovative Approaches

2.3.1 Multiple simultaneous test points location problem

In this paragraph is presented a computational methodology to solve the problem of the proper design of the test matrix for an envelope expansion test campaign, where both flutter, , and systems testing are required (i.e. a new store integration). There are two different stakeholders involved: StE, who want to verify their predictions about the flutter free area, and the SyE, who want to investigate environmental aspects in the entire operational flight envelope.

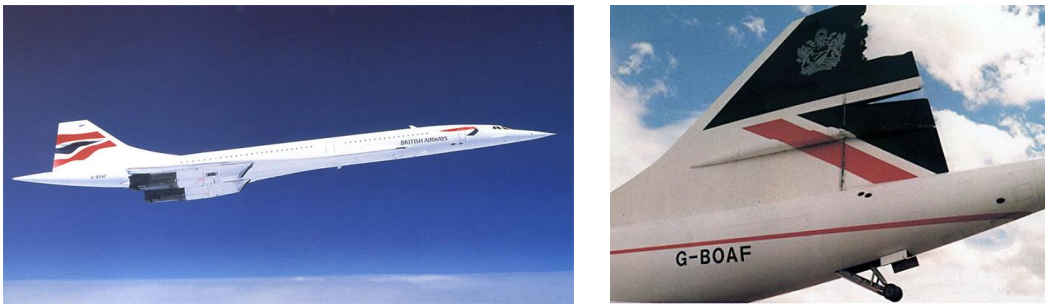

Figure 9: Flutter damage example.

The test matrix, representing the test points distribution in the flight envelope, can be found solving an optimization problem with hard constraints (flight envelope boundaries) and different objective functions for the two stakeholders: the aim of the StE is to optimize distribution in M range; the aim of SyE is to optimize distribution in HC range; both of them want to maximize test points density near maximum VE area. Given the goals of the two stakeholders, the problem is formulated as a potential game, where StE control M distribution and SyE control HC distribution, according to their respective strategies. The two players make their decision about test points location simultaneously, playing a spatial competition game; [5], [6], [7], [8], [9], [10]. A simple Newton-Raphson method is sufficient to numerically solve the single test point location problem; a genetic algorithm is adopted to estimate the Nash

equilibrium solutions to the multiple test points location problem; [11], [12], [13], [14], [15], [16].

2.3.1.1 A location problem: test points identification

In this study has been considered that the requirements of the different engineers categories can be formalized with two different objective functions. The StE, being more interested on combined true airspeed, load factor and compressibility effects on the structures, want to optimize distribution in M range, while SyE, being more focused on environmental effects on the aircraft and store systems, want to optimize distribution in HC range. In addition to the individual objectives, both categories of flight test engineers share a common goal: exploring the entire envelope (thus distributing the test pointe as widely as possible in the flight envelope) and increasing density in the high dynamic pressure area (where aeroelastic and environmental effects are predicted to be more critical). Their requirements can be generalized and tailored to the specific problem, rearranging the same framework proposed, by simply adapting the weights in the objectives functions. Different requirements can be easily achieved: for example, using the same problem formulation an high angle of attack testing can be faced concentrating test points in the low dynamic pressure range. The dichotomy of the requirements can be interpreted as a particular non-cooperative game, a spatial competition, also known as Hotelling competition, [5], [7], [9], where the two groups of engineers represent the two players. The facility is identified with each single test point and the spatial domain corresponds to the flight envelope.

2.3.1.2 Model and results

Let n be a fixed natural number ($n \geq 1$) that is the number of the prescribed flight tests. Γ is a two-player normal form

game $\Gamma=<2;X_1;X_2;f_1;f_2>$ where player 1 is the StE and player 2 is the SyE. The strategy sets X_1, X_2 are real intervals and represent the variable ranges: for each $i \in [1; n]$ ($[1; n] = \{1,\ldots,n\}$), player 1 choses the Mach number M_i in the set $X_1=[M_L;M_U]$ and player 2 the pressure altitude H_i in $X_2=[H_L;H_U]$. The i-th flight test point has coordinates $(M_i;H_i)$ and $(M;H)$ is the $2n$-dimensional vector $(M_1,\ldots M_n, H_1,\ldots H_n)$. The objective functions are real valued functions defined on $X_1^n \times X_2^n$ and defined by the following equations.

$$f_1(M,H)=\sum_{i=1}^{n}\left[\sqrt{\alpha_1(M_i-M_L)^2+\alpha_2(M_i-M_U)^2}+\delta(V_U-V_i)-\min_{j\in[1,n],j\neq i}\sqrt{\frac{(M_i-M_j)^2}{M_U^2}+\frac{(H_i-H_j)^2}{H_U^2}}\right]$$

$$f_1(M,H)=\sum_{i=1}^{n}\left[\sqrt{\beta_1(H_i-H_L)^2+\beta_2(H_i-H_U)^2}+\delta(V_U-V_i)-\min_{j\in[1,n],j\neq i}\sqrt{\frac{(M_i-M_j)^2}{M_U^2}+\frac{(H_i-H_j)^2}{H_U^2}}\right]$$

Where $\alpha_1,\alpha_2,\beta_1,\beta_2,\delta$ are positive numbers, V_U is the maximum equivalent airspeed and $Vi=V_E(M_i,H_i)$ is the equivalent airspeed that is a function of M_i and H_i under the assumption of International Standard Atmosphere, [17]. Here $V_E(M_i,H_i)=aM_i(1-bH_i)^c$ with *a, b, c* real positive constants.

The first term of each objective function represents the position of the points with respect to the lower bound and the upper bound of the variable range, the second term is the distance in terms of equivalent airspeed and the last one considers the opposite distance from the closest test point.

So that each player asks to minimize his own objective function in order to obtain an optimal points distribution: the task is to distribute the points maximizing their dispersion in the flight envelope and in the same time to be close as possible to the right lower corner of the envelope. This corresponds in terms of facility location to a minsum problem, [6], [8].

In this model the optimal flight test distribution is a Nash equilibrium solution of the game Γ, i.e. a vector M,H ∈ $X_1^n \times X_2^n$ such that:

$$f_1(\overline{M},\overline{H}) \le f_1(M,\overline{H}), \forall M \in X_1^n$$
$$f_2(\overline{M},\overline{H}) \le f_2(\overline{M},H), \forall H \in X_2^n$$

In terms of facility location problems, the payoff functions of the flight test location game present a minsum part as well a minmax one, [19], [20].

In order to prove the existence of Nash equilibria of the game Γ, we recall the definition of potential game, a class of games that have pure Nash equilibrium strategies under suitable assumptions on the data.

Let <*A,B,K,L*> be a two-person game with strategy space A for player 1, strategy space B for player 2, and $K: A\times B \to R$, $L: A\times B \to R$ the payoff real valued function of player 1, 2 respectively. If the players 1 and 2 choose $a \in A$ and $b \in B$ respectively, then player 1 obtains a payoff $K(a,b)$ and player 2 obtains $L(a,b)$.

Such a game is called a potential game if there is a potential function $P: A\times B \to R$ such that:

$K(a_2,b)-K(a_1,b)=P(a_2,b)-P(a_1,b), \forall a_1, a_2 \in A$ and $\forall b \in B$,

$L(a,b_2)-L(a,b_1)= P(a,b_2)-P(a,b_1), \forall a \in A$ and $\forall b_1, b_2 \in B$.

Clearly, elements of argmax(P) are Nash equilibria of the game.

The next lemma is useful, [21]: it states that for a two-person potential game the payoff function of player 1 (player 2) can be written as the sum of a potential and a function on

the Cartesian product of the strategy spaces, which only depends on the strategy choice of player 2 (player 1).

Lemma: Let <A,B,K,L> be a potential game with potential P. Then there exist functions $h: A \to R$ *and* $g: B \to R$ *such that:*

K(a,b) = P(a,b)-2g(b),
L(a,b) = P(a,b)-2h(a),
$\forall a \in A$ and $\forall b \in B$.

The following results guarantees that the flight test location game Γ admits at least a Nash equilibrium thanks to the potential structure of the considered game.

Theorem: Γ*=<2;* X^n, Y^n*;* f_1*,* f_2*> where X,Yare real intervals and* f_1*,* f_2 *given as before, is a potential game with potential function:*

$$P(M,H) = \sum_{i=1}^{n} \left[\begin{array}{l} \sqrt{\alpha_1 (M_i - M_L)^2 + \alpha_2 (M_i - M_U)^2} + \sqrt{\beta_1 (H_i - H_L)^2 + \beta_2 (H_i - H_U)^2} + \\ \delta (V_U - V_i) - \min\limits_{j \in [1,n], j \neq i} \sqrt{\dfrac{(M_i - M_j)^2}{M_U^2} + \dfrac{(H_i - H_j)^2}{H_U^2}} \end{array} \right]$$

Then, Γ *admits at least a Nash equilibrium solution.*

Proof. By using previous *Lemma*, the function P is a potential function since the function $f_1(M,H)–P(M,H)$ does not depend on *M* and $f2(M,H)-P(M,H)$ does not depend on *H*. Moreover P admits a minimum point. The problem of the test matrix design is now reduced to the following optimization one: finding a pair $(\overline{M}, \overline{H})$ so that:

$$P(\overline{M}, \overline{H}) = \min_{(M,H) \in X^n \times Y^n} P(M,H)$$

Therefore, based on the aforementioned considerations, from the analysis of the two objective functions representing the pillars of the problem, it turns out that this is a potential game; this reduces its resolution to the determination of the

minimum of the potential function, which represents a Nash Equilibrium (NE) solution, [10][12][15].

A simple Newton-Raphson method is sufficient to numerically solve the single test point location problem; while, a GA[1] needs to be adopted to estimate the Nash equilibrium solutions to the multiple test points location problem. The following Table 1 shows the parameters setup used in order to achieve a fast convergence; this setup refers to GA function setting in MatLab MathWorks software application. After generating the solution of the proposed problem the output was analyzed to evaluate the goodness of the result and robustness of the solution iterating the process applying step by step minor changes to the setup configuration. Furthermore, results validation was accomplished comparing the test cases results with the test matrix structure given by other standard empirical testing method, as the Economy method already mentioned in this study.

Parameter	Set up value
Population size	200
Crossover fraction	0.80
Mutation fraction	0.20
Fitness scaling	Rank
Selection function	Tournament
Crossover mode	Scattered
Mutation mode	Adaptive feasible

Table 1: GA details.

A typical store integration test campaign requires a test matrix dimension ranging from 10, Figure 10, to 30, Figure 11, test points. From a quick analysis of Figure 11 is possible to

[1] Genetic algorithms consist of a heuristic search technique modeled on the principle of evolution with natural selection, by reproduction of the best elements with possible crossover and mutation. Efficient procedure with non smooth data (Di Francesco, De Paolis, D'Argenio, Mallozzi, (2013)).

verify that the initial requirements of the test team have been met by the solution in terms of test points distribution and compliance to the buildup approach philosophy. At higher altitude the test points are more spaced than at low altitude where is possible to appreciate that test conditions range from low to high dynamic pressure portions of the flight envelope.

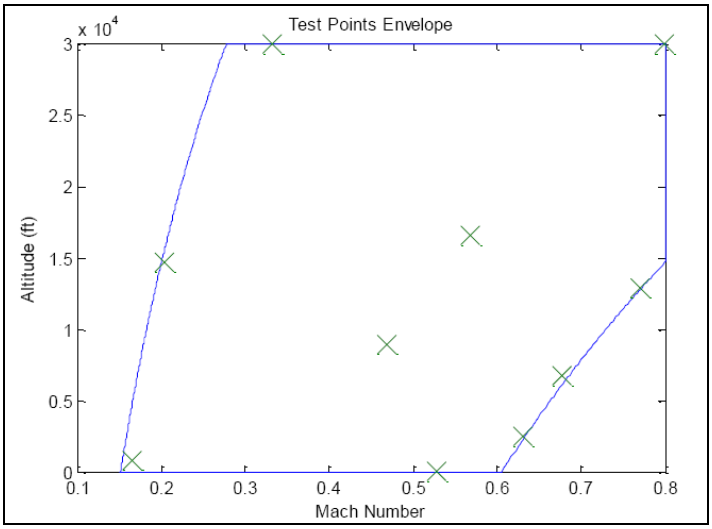

Figure 10: The optimal distribution for 10 flight test points.

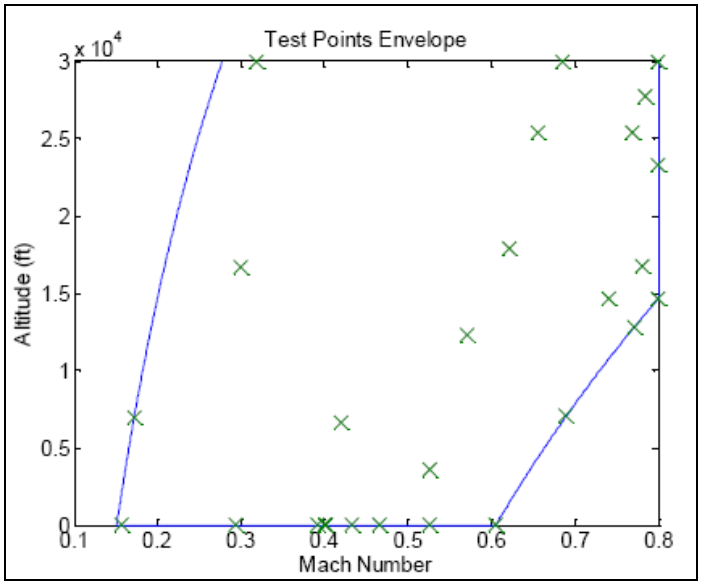

Figure 11: The optimal distribution for 30 flight test points.

2.3.1.3 Conclusions and way-ahead

By means of this tool is possible to approach the optimal simultaneous test points distribution for a test campaign of a new store integration, where optimality is assessed in terms of prescribed objective functions, [11]. Flutter, which represents one of the most dangerous aero-elastic instability (divergent induced oscillations), and systems test can be performed simultaneously in an effective way. All procedures implemented in the algorithm presented and relative results are deemed to be reliable, also compared with studies of previous literature and test philosophy, [12], [16], [18]. One of the subjects that has been the focus of following studies is the definition of new methodologies to translate in math the attractiveness of the portion of the flight envelope with higher dynamic pressure and the opportunity to dynamically relocate the test points, also varying the dimension of the test matrix.

2.3.2 Flight test matrix design and TPs dynamic relocation

In this paragraph a computational methodology for designing an experimental test matrix is presented based on the concept of potential and repulsive fields. The problem consists in the optimal distribution of test points in a two-dimensional domain, pursuant to hard constraints (permitted boundaries of the domain) and soft constraints (minimization of potential). Each test point is assumed to be the source of different fields which expose all other points to repulsive forces, thus accelerations, acting in different directions, [14], [15]. The result of the mutual repulsive forces is a dynamic evolution of the configuration of test points in the domain, which eventually converges to a condition of minimum potential, where forces are balanced. An iterative process is adopted to find a numerical solution where residual accelerations are below a desired threshold, Figure 12. The method has been extended to the additional task of dynamically relocating the remaining test points, after an initial subset has been performed and a need to change (either increase or reduce) the number of test points has arisen. The proposed

technique allows for an easy accomplishment of the task with minor modifications to the algorithm. A large degree of flexibility in the algorithm is allowed to tune the relative weights to attribute to the different requirements. The method proved effective and computationally efficient, exhibiting satisfactory results in both the test matrix design task and the dynamic relocation task.

The idea has been tested against a practical case: the definition of a flight test matrix for the evaluation of the aero-elastic and environmental characteristics of an aircraft. The goal is to distribute flight test points in the flight envelope in such a way to satisfy the requirements of structural engineers, interested in an optimal distribution in terms of airspeed and Mach, and systems engineers, more interested in the altitude and airspeed distribution. The method provides means to combine all objectives in a single test campaign, through an optimization of the test point distribution, being the result of a compromise of all needs.

In the previous paragraph is presented the case of the design of a flight test matrix for a combined aero-elastic and environmental flight test campaign, where the objective was to locate a predefined number of points in the classic Mach-Altitude envelope, in order to simultaneously maximize the mutual distances of test points in the envelope and optimize the distributions of the three major parameters (Mach number, pressure altitude and dynamic pressure, or equivalent airspeed) according to desired engineering requirements. In this paragraph is proposed a different method, which is computationally lighter, and expands the results to the problem of dynamically relocating points at a given stage of the test program, when contingencies require a revision of the amount of the overall number of experiments.

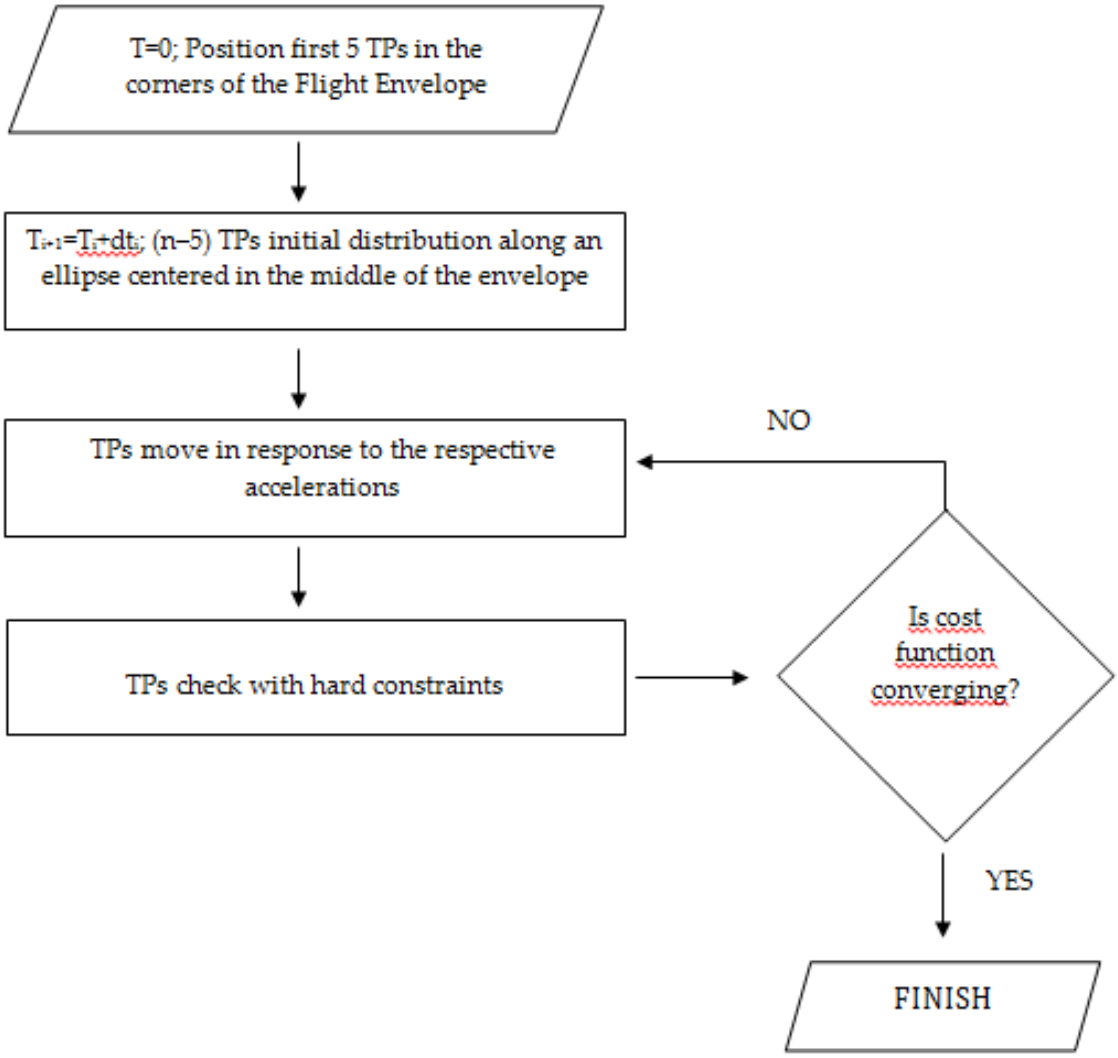

Figure 12: Block diagram of iterative algorithm.

Repulsive forces are similar to those acting between electrical charges having the same sign, except that the intensity decreases with the cubic power of the distance (to reduce the effect of distant points compared to near ones). The acceleration to which a point is subject only depends on its position in the field and the field intensity (same as electric or gravitational fields). To improve convergence, momentum is not preserved from step to step: in other terms the point is allowed to

move according to the acceleration imposed by the fields, but at the next step it is assumed initially at rest and it further evolves only by virtue of the new acceleration produced by the new spatial configuration, regardless of the previous velocity. All points move sequentially and the time step for each point is chosen in such a way that the distance travelled (at the given step) exponentially decreases with elapsed time (to improve convergence) and the point is not allowed to exit the permitted domain (violate the hard constraints).

For the specific problem, three fields are introduced, associated with Mach number, pressure altitude and equivalent airspeed. The intensity of each field is a function of the value of the related parameter at the specific position of the point. Moreover Mach and pressure altitude fields act only along the corresponding direction (Mach and altitude respectively), while airspeed field acts radially in both directions.

Thus the airspeed field plays the dual role of distributing points in airspeed and spreading points over the envelope. Engineering considerations suggest that large Mach number and airspeed and low altitude are more critical for aero-elastic and environmental issues, thus test points are expected to be more concentrated in the bottom right region of the envelope. This is achieved by establishing field intensity laws reflecting this objective: Mach field intensity decreases with Mach number, altitude field intensity increases with altitude and airspeed field intensity decreases with airspeed. The relative importance of different parameters is attributed by properly scaling the intensities of the three fields, [26], [27], [28].

2.3.2.1 The relocation problem

This method has been also extended to the additional task of dynamically relocating the remaining test points, after an initial subset has been performed and a need to change (either increase or reduce) the number of test points has arisen.

Suppose that a test matrix has been designed and a certain amount of test points has been performed according to a predefined execution order. Suppose also that initially unforeseen events (partial test results, budget reviews,

changes of the trial objectives) require a modification of the amount of test points. The relocation problem of the remaining test points (which may be either more or less than the original plan) can be approached similarly to the initial task already described in paragraph 2.3.2. The only difference is that the remaining points must be distributed with an additional hard constraint: the presence in the envelope of the test points already performed along with their respective fields. With this minor adjustment, the same algorithm can be used for the relocation problem.

2.3.2.2 The execution order problem

Once the test matrix is defined, a preliminary chronological order must be established of the test points. To this end several approaches can be followed depending on the particular application. In our example we considered two requirements: safety and efficiency. Given the hazardous nature of flutter (aero-elastic phenomenon) testing, safety is the first and paramount priority. Thus efficiency can be sought only when safety is assured. Assuming that a 20 KEAS margin between test points is a cautious and safe approach to the envelope expansion task, test points are ordered with increasing airspeed; however, if more than a single point meet the 20 KEAS margin criterion, efficiency considerations suggest that points are ordered to best manage energy (either in ascending or descending order).

The two forms of energy attributed to a flight condition represented by a point in the envelope are potential and kinetic energy, leading to the following expression for the specific energy (energy per unit weight):

$$SE = H + \frac{1}{2}\frac{V^2}{g}$$

where H is the pressure altitude, V is the equivalent airspeed and g is the acceleration of gravity. Of course this is just a possible simple criterion to attribute an a priori

execution order. Depending on the complexity of the problem, several additional constraints might apply and the actual execution order might need to be dynamically adjusted while in progress, based on the results gathered from previous points.

However different choices of the execution order do not invalidate the effectiveness of the proposed method for identifying the location of the test points.

2.3.2.3 Algorithm

Let n be a fixed natural number ($n > 5$) that is the number of the prescribed flight tests. Each test point is defined by a pair (M_i,H_i), where i is an integer number, $i \in [1,n]$, M_i and H_i are real numbers chosen in the following sets: $M_i \in [M_L,M_U]$ and $Hi \in [H_L,H_U]$, where the nonnegative constants $0 \le M_L < M_U$ and $0 \le H_L < H_U$ define the bounds of Mach number and altitude choices.

An additional hard constraint on the test points (M_i,H_i) is the condition that the equivalent airspeed is bounded: $V_i \in [V_L;V_U]$ $(0 \le V_L < V_U)$: the equivalent airspeed can be computed as a function of Mi and Hi under the assumption of International Standard Atmosphere, [17].

$$V_i(M_i,H_i) = aM_i(1-bH_i)^C$$

with a, b, c positive real constants.

A graphical depiction of the domain (flight envelope) is shown in Figure 13 where $[M_L,M_U]=[0,1]$ and $[H_L,H_U]=[0,35000]$.

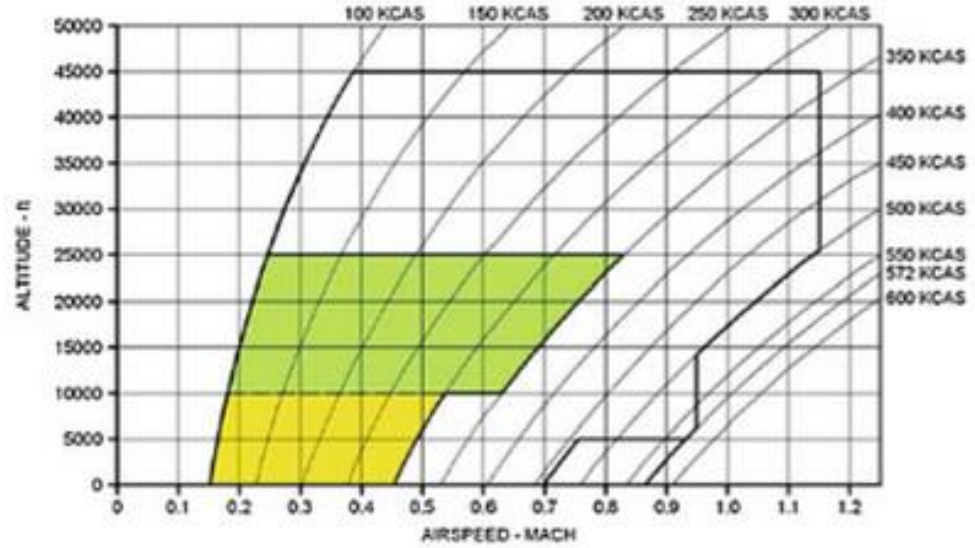

Figure 13: Flight envelope.

Let the first five points stay fixed in the 5 corners of the flight envelope (hard constraint). The remaining *(n-5)* points are free to travel within the permitted envelope; let the initial distribution of those points be according the following:

$$M_i = \frac{M_L + M_U}{2} + \frac{M_U - M_L}{4}\cos\left[\frac{2\pi(i-6)}{n-5}\right] \qquad i \in [6;n]$$

$$H_i = \frac{H_L + H_U}{2} + \frac{H_U - H_L}{4}\sin\left[\frac{2\pi(i-6)}{n-5}\right] \qquad i \in [6;n]$$

Let each test point be the source of three distinct fields, whose intensities are respectively:

$$m_{M_i} = W_M\left(1 + K_M\frac{M_i - M_L}{M_U - M_L}\right)$$

$$m_{H_i} = W_H\left(1 + K_H\frac{H_i - H_L}{H_U - H_L}\right)$$

$$m_{V_i} = W_V\left(1 + K_V\frac{V_i - V_L}{V_U - V_L}\right)$$

where W_M, W_H, W_V are positive real numbers (defining relative weight of the three fields), while K_M, K_H, K_V are real numbers

(prescribing the desired distribution trend of the corresponding parameters). The first two fields act along a single dimension (the respective parameter), while the third field acts radially.

Assuming repulsive forces proportional to the inverse of the cubic distance from the field source, the resulting accelerations (in the two directions: *M* and *H*) to which all points are subjected (except the 5 fixed points) are:

$$a_{M_i} = M_U \left\{ \sum_{\substack{j=1,3 \\ j\in[6,n] \\ j\neq 1}} \frac{m_{M_j}}{\left(\frac{M_i - M_j}{M_U} \right)^3} \right\} + \sum_{\substack{j\in[1,n] \\ j\neq 1}} \frac{m_{V_j} \left(\frac{M_i - M_j}{M_U} \right)}{\left[\left(\frac{M_i - M_j}{M_U} \right)^2 + \left(\frac{H_i - H_j}{H_U} \right)^2 \right]^2}$$

$$a_{H_i} = H_U \left\{ \sum_{\substack{j=1,3 \\ j\in[6,n] \\ j\neq 1}} \frac{m_{H_j}}{\left(\frac{H_i - H_j}{H_U} \right)^3} \right\} + \sum_{\substack{j\in[1,n] \\ j\neq 1}} \frac{m_{V_j} \left(\frac{H_i - H_j}{H_U} \right)}{\left[\left(\frac{M_i - M_j}{M_U} \right)^2 + \left(\frac{H_i - H_j}{H_U} \right)^2 \right]^2}$$

where the first fixed point *(j=1)* is at the bottom left corner of the envelope (M_L,H_L) and the third fixed point *(j=3)* is at the top right corner of the envelope (M_U,H_U). The points are then allowed to move sequentially in the envelope in response to the respective accelerations.

At each iteration the time step is chosen such that displacements are progressively smaller and smaller (as the distribution converges toward the optimal solution) while the Mach and altitude hard constraints are not violated.

The displacements consequent to the accelerations acting during the time step are computed as:

$$dM_i = \frac{1}{2} a_{M_i} dt^2$$

$$dH_i = \frac{1}{2} a_{H_i} dt^2$$

thus ignoring any velocity gathered in the previous time steps, in order to facilitate convergence. Here

$$dt = \min\left\{ dt_{\min}; \sqrt{\frac{2dM_{\max}}{\left|a_{M_i}\right|}}; \sqrt{\frac{2dH_{\max}}{\left|a_{H_i}\right|}} \right\}$$

where $dt_{min} = 0.01/n$ and

$$dM_{\max} = \begin{cases} \min\left\{ \frac{M_U - M_i}{2}; \frac{M_U - M_L}{2} e^{-\frac{t}{10}} \right\} & if \quad a_{M_i} > 0 \\ \min\left\{ \frac{M_i - M_L}{2}; \frac{M_U - M_L}{2} e^{-\frac{t}{10}} \right\} & if \quad a_{M_i} \le 0 \end{cases}$$

$$dH_{\max} = \begin{cases} \min\left\{ \frac{H_U - H_i}{2}; \frac{H_U - H_L}{2} e^{-\frac{t}{10}} \right\} & if \quad a_{H_i} > 0 \\ \min\left\{ \frac{H_i - H_L}{2}; \frac{H_U - H_L}{2} e^{-\frac{t}{10}} \right\} & if \quad a_{H_i} \le 0 \end{cases}$$

The displacements thus computed do not guarantee adherence to the last hard constraint: airspeed within the two permitted boundaries. An additional check must be performed: if airspeed limits are exceeded with the computed time step and accelerations, then the new position is set at 90% of the airspeed limits (moving the point along the direction of the acceleration). Then acceleration is set to zero, because points constrained on the border are assumed to be subjected to a reaction force (acceleration) equal and opposite to the force (acceleration) which tends to push them out of the envelope.

Define:

$$dM_{V_{\max}} = 0.9\frac{V_U - V_i}{\left(\frac{dV}{dM}\right)_i + \left(\frac{dV}{dH}\right)_i\left(\frac{dH}{dM}\right)_i}$$

$$dM_{V_{\min}} = 0.9\frac{V_L - V_i}{\left(\frac{dV}{dM}\right)_i + \left(\frac{dV}{dH}\right)_i\left(\frac{dH}{dM}\right)_i}$$

where

$$\left(\frac{dV}{dM}\right)_i = a\left(1 - bH_i\right)^c$$

$$\left(\frac{dV}{dH}\right)_i = -abcM_i\left(1 - bH_i\right)^{c-1}$$

$$\left(\frac{dH}{dM}\right)_i = \frac{dH_i}{dM_i}$$

Then

$$if \quad dM_i < dM_{V_{\min}} \; we \quad let \begin{cases} dM_i = dM_{V_{\max}} \\ dH_i = dM_{V_{\max}}\left(\frac{dH}{dM}\right)_i \\ a_{M_i} = a_{H_i} = 0 \end{cases}$$

and

$$if \quad dM_i < dM_{V_{\min}} \; we \quad let \begin{cases} dM_i = dM_{V_{\min}} \\ dH_i = dM_{V_{\min}}\left(\frac{dH}{dM}\right)_i \\ a_{M_i} = a_{H_i} = 0 \end{cases}$$

Finally the position is updated according to the calculated displacements, the field intensities are updated pursuant with the new configuration:

$$M_i^{k+1} = M_i^k + dM_i$$
$$H_i^{k+1} = H_i^k + dH_i$$
$$t^{k+1} = t^k + dt$$

Weights m_{Mi}, m_{Hi}, m_{Vi} are also updated at each iteration and we assume that the EAS weight decreases with time: initially points must be quickly spread over the envelope and the weight is large, then the weight must decay with time to the desired final value. More precisely we let:

$$m_{V_i}^{k+1} = W_V e^{-\frac{t^k}{10}}\left(1 + K_V \frac{V_i^k - V_L}{V_U - V_L}\right)$$

The process is reiterated until a convergence cost function decays below a predetermined threshold. The convergence cost function is a measure of the residual accelerations to which the test points are subject, thus the potential energy of the configuration:

$$J(M,H) = \sum_{i=1}^{n}\left[\left(\frac{a_{M_i}}{M_U}\right)^2 + \left(\frac{a_{H_i}}{H_U}\right)^2\right]$$

with $(M,H)=(M_1,...,M_n,H_1,...,H_n)$. Convergence is reached when J is less than a predefined value (dependent on the number of points).

2.3.2.4 A case study results

A case study with $n=25$ planned TPs is presented. The flight envelope bounds being:

$[M_L, M_U]=[0.1, 0.8]$; $[H_L, H_U]=[0, 3\times10^4]$

weights and scaling parameters:

$W_M=1$, $K_M=-0.95$;

$W_H=2$, $K_H=100$;

$W_V=500$, $K_V=-0.8$.

and the constants are

$a=1116.46;\ b=6.87\times10^{-6};\ c=2.62$

Results for a 25 TPs location problem are shown in Figure 14.

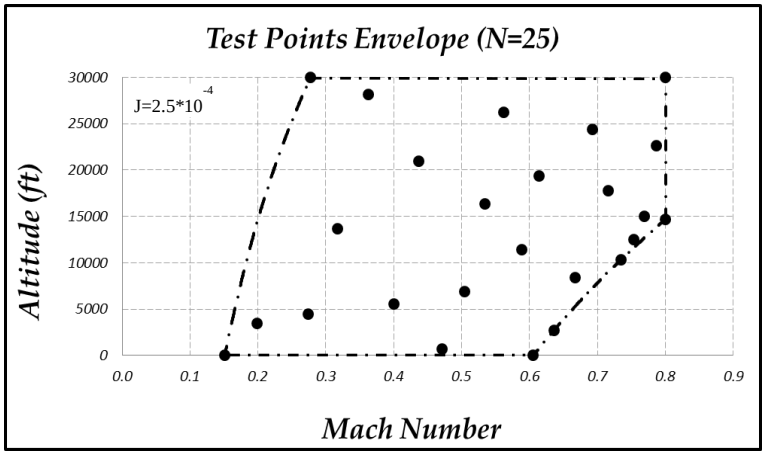

Figure 14: The optimal distribution for 25 TPs.

Relocation problem #1: points addition. When 15 TPs have already been performed, the test management decides to increase the number of tests from 25 to 30 (for an overall number of 30 TPs): in the new configuration the added test points are denoted with white circles. In this case the final point distribution, Figure 15, can be defined as a sub-optimal distribution compared to the case where thirty test points are located in one step, Figure 16, without the constraint of the 15 points already located in the flight envelope. It is possible to observe the different distribution in the two cases.

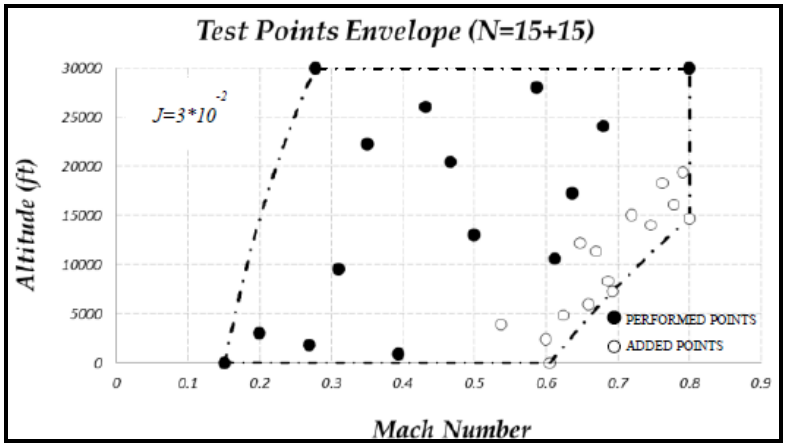

Figure 15: 25 initial TPs: 15 performed + (10 planned + 5 extra TPs).

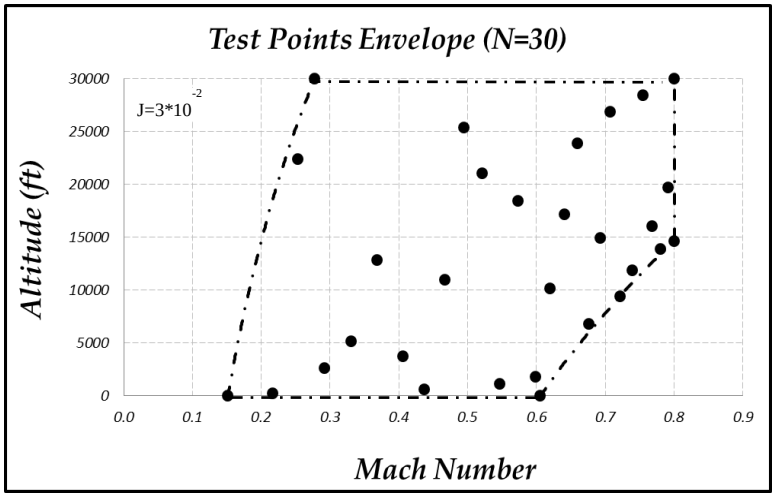

Figure 16: The optimal distribution for 30 test points.

Relocation problem #2: points subtraction. In this case, when the 15 TPs have already been performed, the test management decides to decrease the number of TPs from 25 to 20 (for an overall number of 20 TPs). Also in this case the final point distribution, Figure 17, can be defined as a sub-optimal distribution compared to the optimal case distribution, Figure 18.

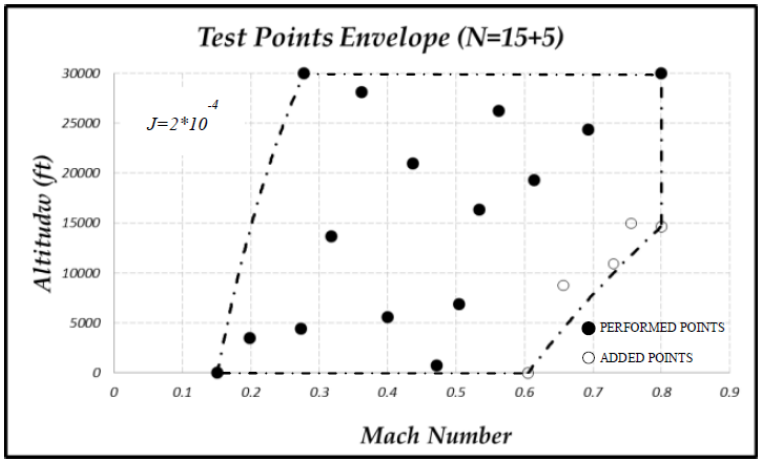

Figure 17: 30 initial TPs: 15 performed+(15 planned+5 subtracted TPs).

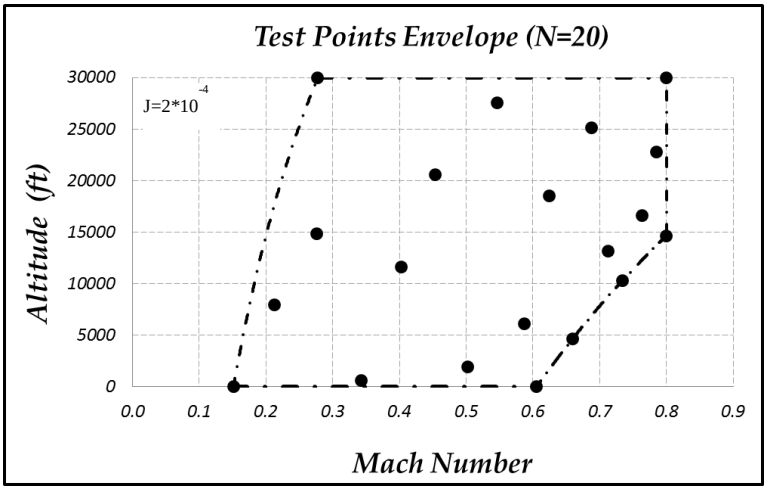

Figure 18: The optimal distribution for 20 TPs.

2.3.2.5 Conclusions

An optimization method based on the concept of fields has been proposed for the identification of a two-dimensional test matrix. The experimental TPs distribution was optimized according to tunable soft constraints and hard constraints. The method has been tested against a practical case: the simultaneous evaluation of aero-elastic and environmental

characteristics of an aircraft. The method proved effective and computationally efficient: all the configurations tested came to a convergence in short time and the outcome was satisfactory.

The method was extended to the additional problem of relocating part of the test points after the execution of an initial subset of experiments and following the decision of the test management to change the number of experiments. The results were satisfactory also for this additional task.

The proposed technique allows for an easy accomplishment of the task with minor modifications to the algorithm. A large degree of flexibility in the algorithm is allowed to tune the relative weights to attribute to the different requirements. The method proved effective and computationally efficient, exhibiting satisfactory results in both the test matrix design task and the dynamic relocation task.

CHAPTER 3

TECHNIQUES FOR TEST ITEM GEOMETRY ACQUISITION

As already mentioned, two major geometry acquisition/generation techniques have been explored ride along the optimization process analysis: forward engineering and reverse engineering. The latter has been deemed useless for CFD purposes when approaching a lifting surface, however, still valuable when evaluating the velocity/pressure field around and hunk body. Generally this is the case for example of a reconnaissance pod to be integrated under a wing or of the acquisition of the geometry of an entire aircraft, where geometry generation from the scratch could results in a very time consuming and cumbersome work.

In the following paragraphs are presented both cases: the geometry generation of a rockets launcher integrated underwing a 3rd generation jet aircraft and used for CFD analysis (starting from paper drawings - forward engineering), and the geometry acquisition of an entire external surface of a 3rd generation attack jet (using laser scanning techniques – reverse engineering). Furthermore, the latter method has been used also for the geometry acquisition of a 4th/5th generation, ot presented for lack of security clearance, however also in this case the proposed sequence of events/procedure has been deemed satisfactory. Reverse engineering well apply to rough CFD preliminary prediction and also to other kind of task, i.e. target positioning and trajectory reconstruction for store separation task.

All the aforementioned activities have been developed on behalf of and for the actual testing purposes of the Italian Flight Test Wing - RSV.

3.1 Forward Engineering technique

Computer Aided Design is defined as the use of information technology in the design process. A CAD system consists of information technology hardware, specialized software and peripherals, which in certain applications are quite specialized. The core of a CAD system is the software, which makes use of graphics for product representation; databases for storing the product model and drives the peripherals for product presentation. Its use does not change the nature of the design process but as the name states it aids the product designer. The designer is the main actor in the process, in all phases from problem identification to the implementation phase. The role of the CAD is in aiding him by providing:

- Accurately generated and easily modifiable graphical representation of the product. The user can nearly view the actual product on screen, make any modifications to it, and present his/her ideas on screen without any prototype, especially during the early stages of the design process.
- Perform complex design analysis in short time.

The technique initiated in the MIT from Ian Sutherland, when the first system the Sketch- pad was created within the SAGE research project. The automotive and aerospace industries were the first users and the forerunners of development of CAD technology. The first system were very expensive, the computer graphics technology was not so advanced at that time and using the system required specialized HW and SW which was provided mainly by the CAD vendors. The first CAD systems were mainframe computer supported systems, while today the technology is for networked but stand-alone operating workstations (UNIX or WINDOWS based systems). AUTODESK was the first vendor to offer a personal computer based CAD system the AUTOCAD (early ‘80s). Nowadays, WINDOWS is the main operating system for CAD systems. The first applications were for 2D-Drafting and the systems were also capable of performing only 2D modelling. Even today 2D-drafting is still the main area of application (in terms of number of workplaces). Later, (mid-‘80s),

following the progress in 3D modelling technology and the growth in the IT HW, 3D modelling systems are becoming very popular. 3D modelling at the beginning were wire frame based. Aerospace and automotive industries were using surface modelling systems for exact representation of the body of the product. At the same time solid modelling was recognised as the only system, which could provide an unambiguous representation of the product, but it was lacking adequate support for complex parts representations. Nowadays, we are experiencing a merge of solid and surface modelling technology. Most solid modelling systems are capable of modelling most of industrial products. Systems sold today are characterised as NURBS based systems, employing solid modelling technology, and they are parametric and feature based systems.

Originally CAD technique was aiming at automating a number of tasks a designer is performing and in particular the modelling of the product. Today CAD systems are covering most of the activities in the design cycle, they are recording all product data, and they are used as a platform for collaboration between remotely placed design teams. CAD systems have the ability to provide a digital prototype of the product at early stages of the design process, which can be used, for testing and evaluation. Many people from various departments can share it, they can express their opinion for the product at early stages, in order to complete the design in less time and with the least mistakes. Most researchers accept that having the digital prototype in early stages allows more effort to be spent on the definition stage (early stage) of the design process and not in redesigning an already completed design.

Development trends of CAD systems Development of CAD systems, in principal measure, is directed on following issues:

- advanced surface modelling tools (surface styling, tools for surface continuity analysis, free-form surfaces modelling);
- functional modelling (consideration of functional aspects of CAD model by designer not for determine of features sequence in design-history tree;
- design based on knowledge-based engineering;

- development of expert tools for example for detecting and solving problems in sketches, dimensions and features on the part level or mates on the assembly level;
- development of specialized tools for converting existing 2D drawings to 3D models;
- possibility of publication and presentation of product as a virtual 3D model (i.e. virtual reality, Internet 3D presentation formats, advanced rendering and animation);
- trends to consolidation tools for scanning and processing "point clouds" with popular CAD systems.

3.1.1 A powerful CAD software example: CATIA

CATIA is a multiplatform CAD/CAM/CAE commercial SW suite developed by the French company Dassault Systemes, written in the C++ programming language. Commonly referred to as a 3D Product Lifecycle Management software suite, CATIA supports multiple stages of product development, from conceptualization, design, manufacturing and engineering. CATIA facilitates collaborative engineering across disciplines, including surfacing & shape design, mechanical engineering, equipment and systems engineering. CATIA provides a suite of surfacing, reverse engineering, and visualization solutions to create, modify, and validate complex innovative shapes. From subdivision, styling, and Class A surfaces to mechanical functional surfaces. CATIA enables the creation of 3D parts, from 3D sketches, sheet-metal, composites, molded, forged or tooling parts up to the definition of mechanical assemblies. It provides tools to complete product definition, including functional tolerances, as well as kinematics definition. CATIA started as an in-house development in 1977 by French aircraft manufacturer Avions Marcel Dassault, at that time customer of the CAD/CAM CAD software to develop Dassault's Mirage fighter jet, then was adopted in the aerospace, automotive, shipbuilding, and other industries. In 1984, the Boeing Company had chosen CATIA V3 as its main 3D CAD tool, becoming its largest customer. In 1988, CATIA V3 was ported from mainframe

computers to UNIX. In 1990, General Dynamics Electric Boat Corp chose CATIA as its main 3D CAD tool, to design the U.S. Navy's Virginia class submarine.

CATIA can be applied to a wide variety of industries, from aerospace and defence, automotive, and industrial equipment, to high tech, shipbuilding, consumer goods, plant design, consumer packaged goods, life sciences, architecture and construction, process power and petroleum, and services. CATIA V4, CATIA V5 are one the dominant systems. The Boeing Company used CATIA V3 to develop its 777 airliner, and used CATIA V5 for the 787 series aircraft. The development of the Indian Light Combat Aircraft has been using CATIA V5. Chinese Xian JH-7A is the first aircraft developed by CATIA V5, when the design was completed on September 26, 2000. European aerospace giant Airbus has been using CATIA since 2001, Figure 19. Canadian aircraft maker Bombardier Aerospace has done all of its aircraft design on CATIA. The Brazilian aircraft company, EMBRAER, use CATIA V4 and V5 to build all airplanes. The Anglo/Italian Helicopter company, AgustaWestland, use CATIA V4 and V5 to design their full range of aircraft. The Eurofighter Thyphoon has been designed using both CATIA V4 and V5. The main supplier of helicopters to the U.S Military forces, Sikorsky Aircraft Corp., uses CATIA as well. Bell Helicopter, the creator of the Bell Boeing V-22 Osprey, has used CATIA V4, V5, and now V6, [25].

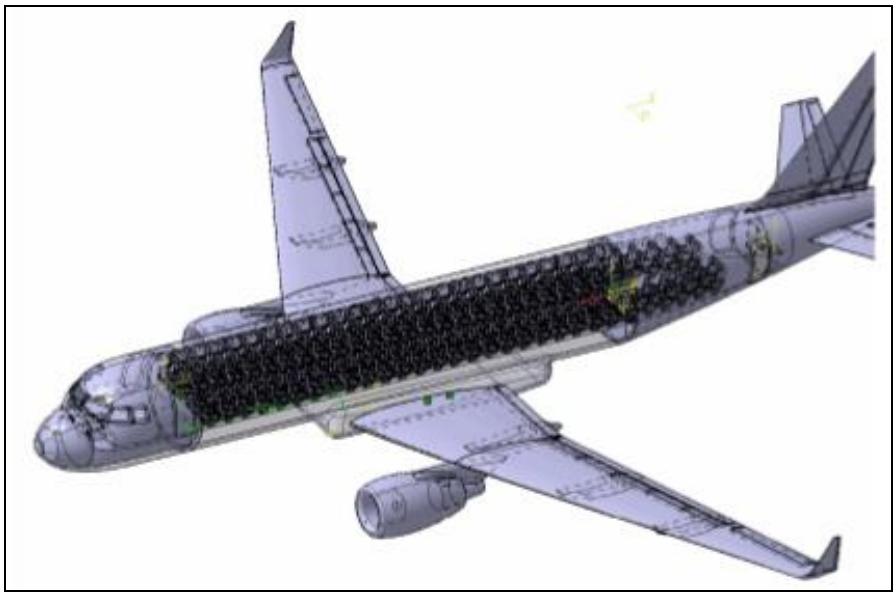

Figure 19: Airbus A-320 (self-made) - CATIA V5.

3.1.2 Rockets Launcher integration on a 3rd generation fighter A/C

The weapon integrated under the fighter type A/C was an ARL capable to carry and to launch 2,75" (70mm) caliber rockets type, powered with MK-4/40 or MK-66 motors types and provided with standard practice and war-heads, Figure 20.

Figure 20: ARL.

The pay load of the ARL was constituted by six rockets, that could be fired in single shot or in ripple sequence, according to the setting of the Intervalometer/Weapon Management System installed on-board. The ARL is the extended version of a previous seven tubes aircraft rockets launcher model made by the same company and it has been designed and developed to allow also installation and firing of laser guided rockets, Figure 21.

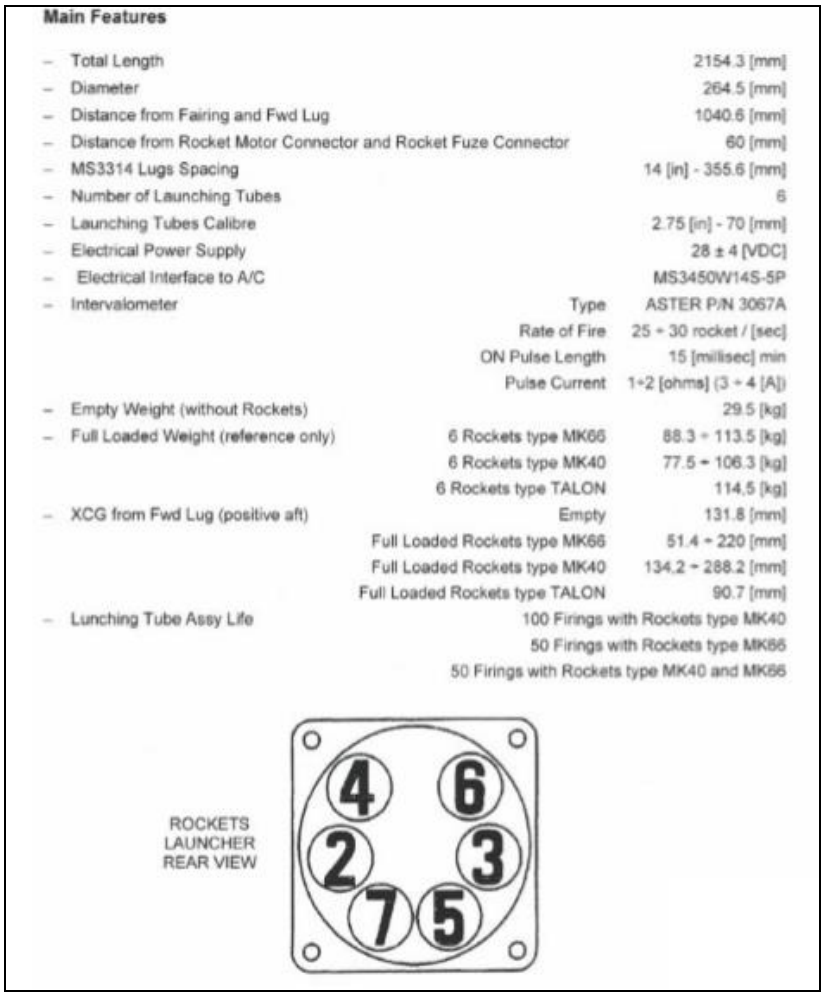

Figure 21: ARL technical data and firing sequence.

The ARL was compliant with military normative and it had got provisions for installation of two suspension lugs spaced 14" (355,6 mm. To assure the stability of the launcher during captive carriage, a preload was applied, by the swaybraces of the aircraft bomb-rack, on the upper reinforced plate of the launcher itself. The rockets were housed in the relevant launching tubes and locked by the retaining systems (DREAM). The ARL structure was composed of the following main subassemblies that could be easily assembled and disassembled for maintenance and/or repair operations:

– Mainframe Assy

The Launcher main structure assembly consisted mainly of aluminium alloy components properly reinforced in the central section, in order to support the reactions of the bomb-rack swaybraces and the handling. The main components with a brief description were the following:

Frame - Aluminium alloy extruded shape, properly shaped to withstand the reactions coming through the bomb-rack swaybraces It embodies two threaded bushing to retaining the two 14" spaced standard lugs

Supports - two casting components properly shaped in order to link the Inner Flanges and a well as the Frame to the Skin. They are spaced and sized to withstand the reactions coming from the bomb-rack swaybraces

Inner-flange - Aluminium alloy plates properly machined and shaped with the main function to withstand the shear load due to tubes and rockets mass These flanges (2 off) are linked to the Flanges by means of screws.

Rear-flange - Aluminium alloy plate properly machined and shaped with the main function to connect the tubes to the skin by means of the DREAM assy detent. This flange reacts the axial loads acting on rockets.

Skin - External surface of the launcher that withstands the aerodynamic loads and protects the inner components. It was riveted to the Frame and to the Flanges in such a way that the launcher itself could be considered as a structural beam. At the back and front end of the Skin a Ring Fairing was riveted to locally increase the stiffness of the Skin itself.

– B. Fairing Assy

The Fairing Assy closed the front of the launcher: item bodies a flange and it was connected to the Main Frame Assy by mean of seven screws, which allowed easy assembly-disassembly operation. The main functionality of the Fairing Assy was to reduce the aerodynamic drag of the launcher and to support the launching tubes withstanding the rockets blast during firings.

– Tube Assy

The six launching Tube Assy were housed in appropriate holes of the Inner Flanges and they were indirectly linked to the Rear Flange by their detent mechanisms DREAM). Each Tube Assy was provided with the following main components:
Tube - Aluminium alloy tubes designed with the function to house and to guide the rockets during carriage and launch phases.
DREAM - DREAM assembly was the mechanism used to retain either the MK4/40 and MK66 rocket as well as to provide the firing signal to the rocket motor when required. It consisted mainly of the following: A steel hook that provided the mechanical engagement of the rocket till the gas pressure generated during firing acted rotating the back lever and then unlocking the hook itself; three electrical contacts providing electrical interface with the Launcher main Flange and with the rockets, one for MK4/40 type and one for MK66 type. The DREAM was fitted to the Tube by means of screws and interfaces the Rear Flange of the Launcher with two screws and an electrical connection.

– D. Rear panel Assya

Positioned on the back side of the aft 14" lug, it was accommodated the intervalometer and the ground safety device. The safety device included a switch which, once the safety pin was inserted, inhibited the electrical circuit avoiding the communication between A/C and the intervalometer. A reset indicator showed when the intervalometer was in the reset condition.

3.1.2.1 Geometry for CFD analysis

An effective CFD analysis starts with good CAD techniques both in terms of model integrity and proper creation of the flow region. The first step is to design the CAD model for the flow analysis. This means modelling the flow geometry and optimizing the model for simulation. How to reach this objective?

Production-level geometry can contain gaps, interferences, fasteners, and very small features. These features are often necessary for manufacturing, but can add unnecessary complexity for simulation. To save time and computer resources, eliminate these features if they are too small to affect the results of the simulation. For large assemblies, consider analysing only critical portions of the design. This can accelerate the analysis process. In some cases, it is faster to create a new, simpler version of your design to focus on the key areas of study. Relevant steps for geometry preparation, should always be the following:

- Eliminate gaps that prevent void filling. These include clearances between parts, sheet metal reliefs, and fastener holes;
- Eliminate fasteners that do not impact flow or heat transfer. Reduce very large assemblies to include only relevant components;
- Eliminate interferences, i.e. press-fits and improper mates.
- Eliminate very small features that do not affect the analysis results.

3.1.2.2 Rockets launcher CAD via a Bottom-Up strategy

Provided technical data and blueprints of the test item it is possible to get a CAD representation through the process depicted in Figure 22.

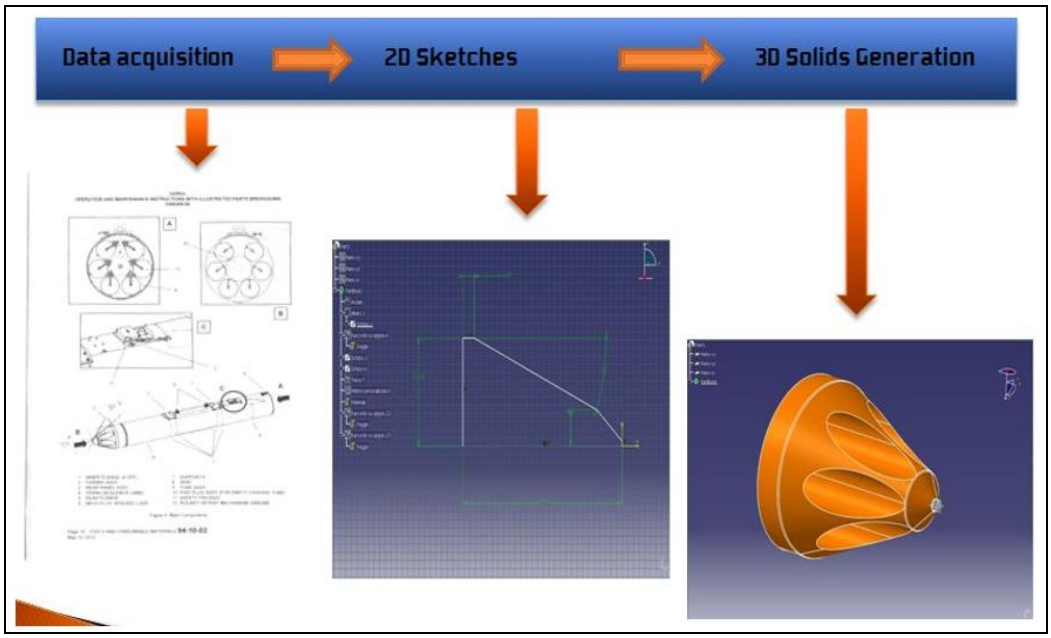

Figure 22: Standard CAD approach.

It is useful for drawing parts made by different and numerous pieces to use the so called *Bottom-Up approach*.

Bottom-up assembly modelling is a part-centric modelling method where the assembly design is started with a principal structural or functional element, and individual parts are designed in relative isolation from the overall assembly. Component parts and sub-assemblies are defined as the process moves up towards the top-level assembly. Working with the CATIA V5 the bottom-up assembly is the most preferred approach for creating assembly models. In this approach, the components are created in the Part Design workbench as **.CATPart* file. Then the product **.CATProduct* file is started and all the previously created components are inserted and placed in it using the tools provided in the Assembly Design workbench. After inserting each component, constraints are applied to position them properly in the 3D space with respect to other components, Figure 23. Adopting the bottom-up approach gives the user the opportunity to pay more attention to the details of the components as they are designed individually. This approach is preferred for large assemblies, especially those having intricate individual components.

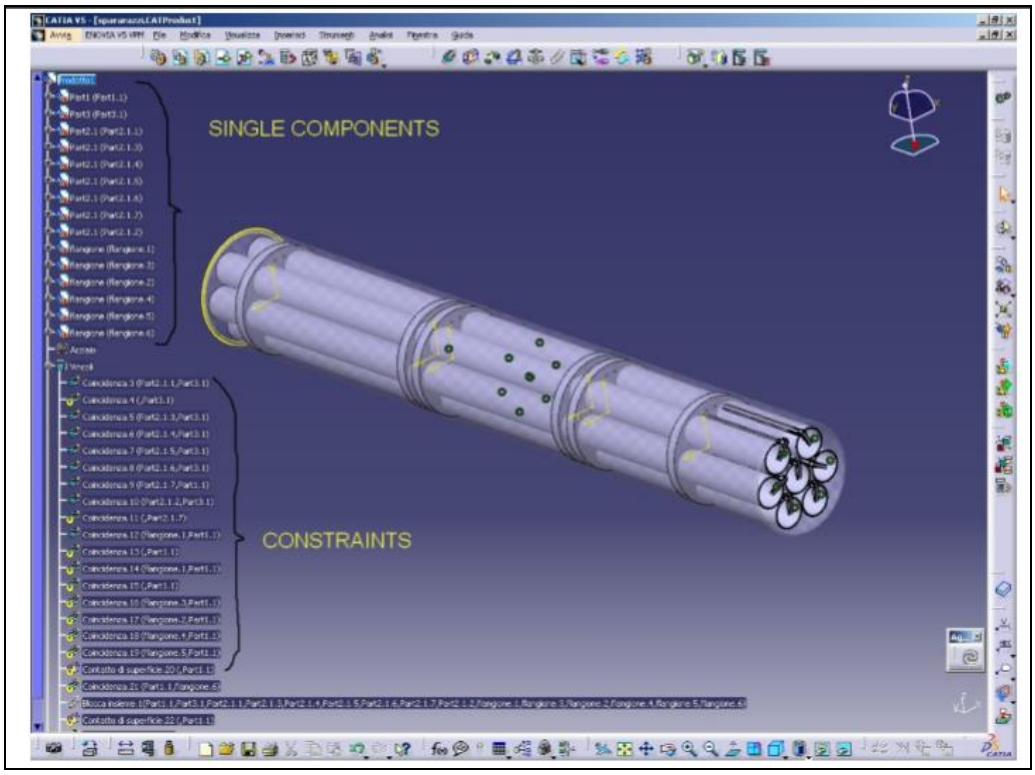

Figure 23: Product Assembly screen shot.

3.1.2.2.1 Creating the ARL parts

For creating the ARL 3D model the entire Assy has been divided in several single components, each one of them has been draw as separated part:

- Skin;
- Launching tubes;
- Flanges;
- Fairing.

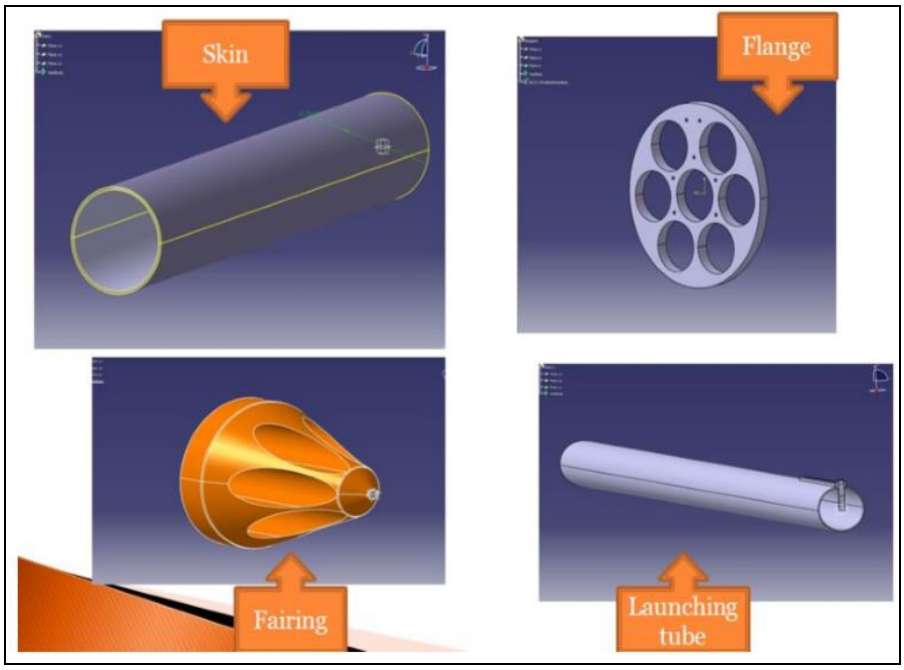

Figure 24: ARL main components.

As already stated before, for the CFD analysis it is not needed the perfect replication of the actual test item, it is better to have a CFD-suitable CAD, therefore the following idealization/simplification of the model parts has been applied.

Skin. The external part of the ARL has been idealized as a 264mm diameter cylinder with a thickness of 7mm and a 1878mm length. The 3D model has been extruded from 264mm circle as a "Thin Pad" of 7mm thickness. Edges have been soften with the "Edge Fillets" command.

Tubes. Made by a 1871mm and 2mm thick "Thin Pad". It has been connected with a very simplified version of the missiles detention system made with the "Multipad" command.

Flanges. A 125mm radius cylinder 30mm depth with seven circular "pockets". Pockets have been disposed with the "Matrix" Feature according with the data sheets configuration.

Fairing. Created starting from a poor detailed polygonal sketch. Then it has been used the "Shaft" feature to create a Rotation Solid, Figure 25. Firing holes have been created thanks to a pockets matrix starting from the base of the object. Sharp edges have been soften with various radius.

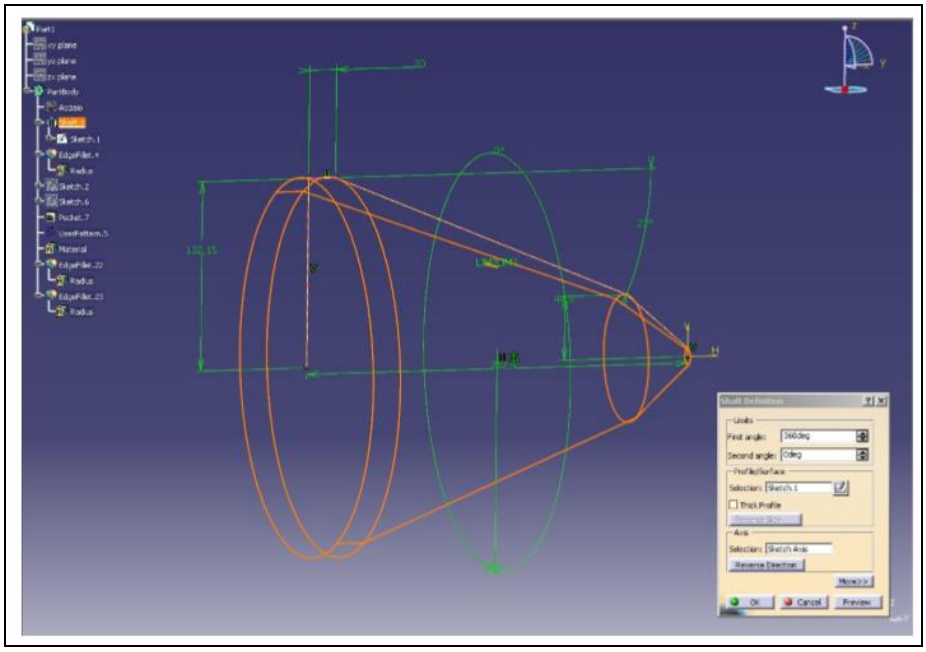

Figure 25: Shaft feature.

3.1.2.2.2 Assembling

After creating every-single components it was necessary to put together the entire set. In this second step, called Assembly, they have been used "Assembling features" as:

Coincidence constraints: are used to align elements. Depending on the selected elements, it is possible to obtain concentricity, coaxiality or complanarity;

Surface contact: make two planar faces touch each other;

Offset: it is used to fix the distance between two different components faces;

Angle: creates angular constraints between two selected surfaces;

Fix: Fixing a component means preventing this component from moving from its parents during the update operation.
Re-use pattern: with this command is possible to re-use a previous sketch or set of fixed points (i.e a disposal matrix) to arrange parts.

Figure 26: CATIA V5 Assembly features.

The starting point was the assembling of the launching tubes, creating one of them and then adding it 6 times in the *.*CatProduct*. They have been disposed in the 3D using a sketched user pattern (*matrix*) as show in Figure 27.

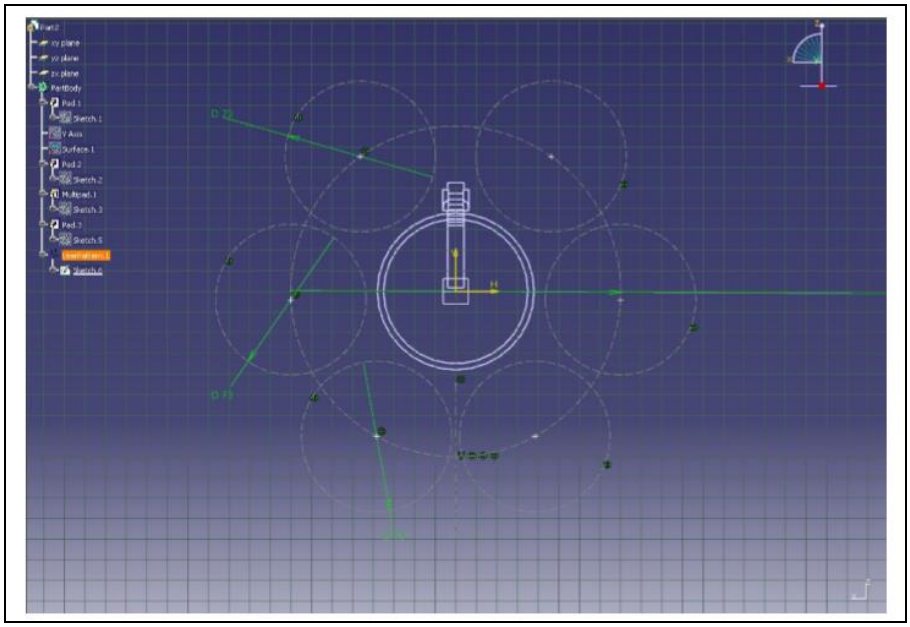

Figure 27: User-pattern used for launching tubes disposal.

Then they have been rotated on their axes to respect the original alignment (*angle constraints*). The second step was to assembly support flanges on the tubes system. After importing 6 times the flange, previously made, it was needed to apply *coincidence constraints* between flanges and the central

launching tube. Finally skin model was imported and set up with the other elements with *coincidence and surface contact constraints* with the flanges. The final result is showed in Figure 28. Figure 29 e Figure 30 show the rear view and inner section of the ARL CAD.

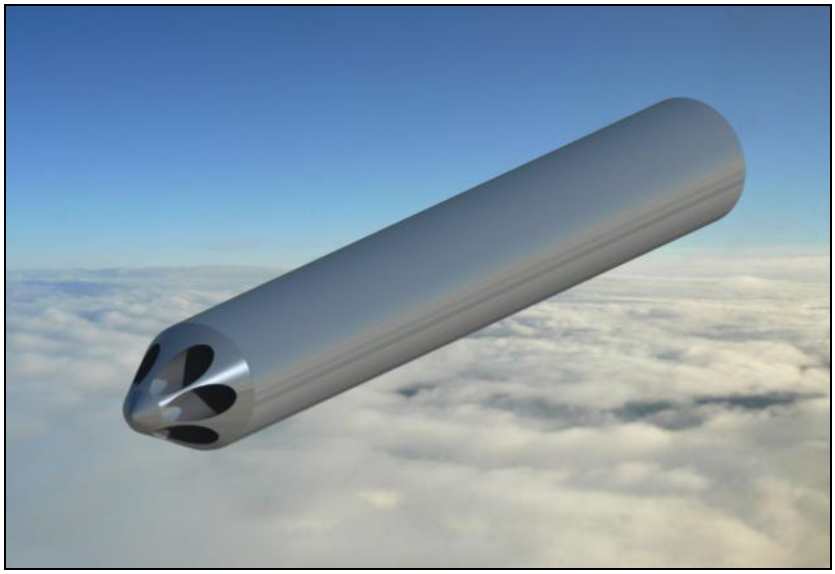

Figure 28: ARL CAD.

Figure 29: ARL CAD rear view.

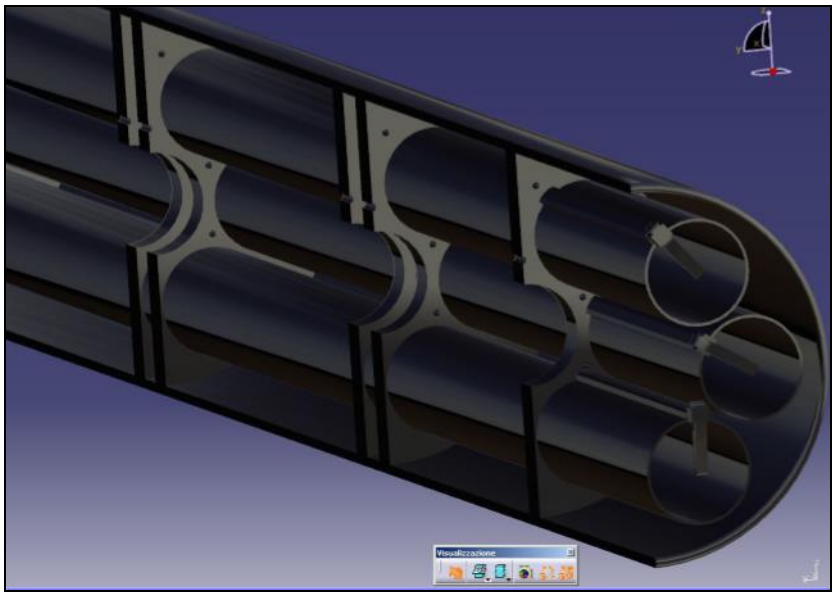

Figure 30: ARL CAD inner section.

Third step was to import the fairing CAD and add it properly to the assy thanks to *contact constraint* as well as *coincidence*.

Furthermore, it was created also a holes/pockets-less version of the ARL to "simulate" the rockets full loaded ARL, Figure 31.

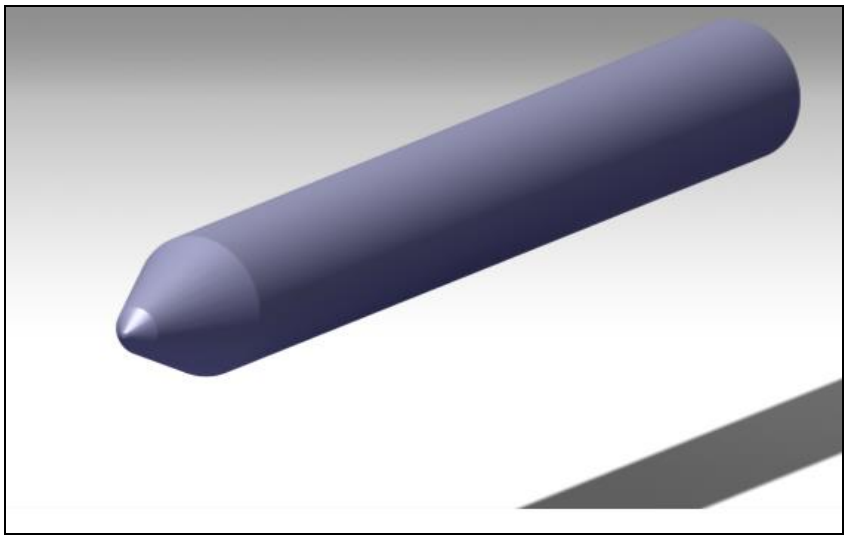

Figure 31: Rockets full loaded ARL CAD.

The same step-process described in details for the rockets launcher has been applied to the wing, pylon, fuel tank and wing tip shooter geometry generation. The following Figure 32, Figure 33 show the final CAD (CFD-suitable) for the geometry representation of the full loaded wing of the 3rd generation fighter type aircraft under analysis.

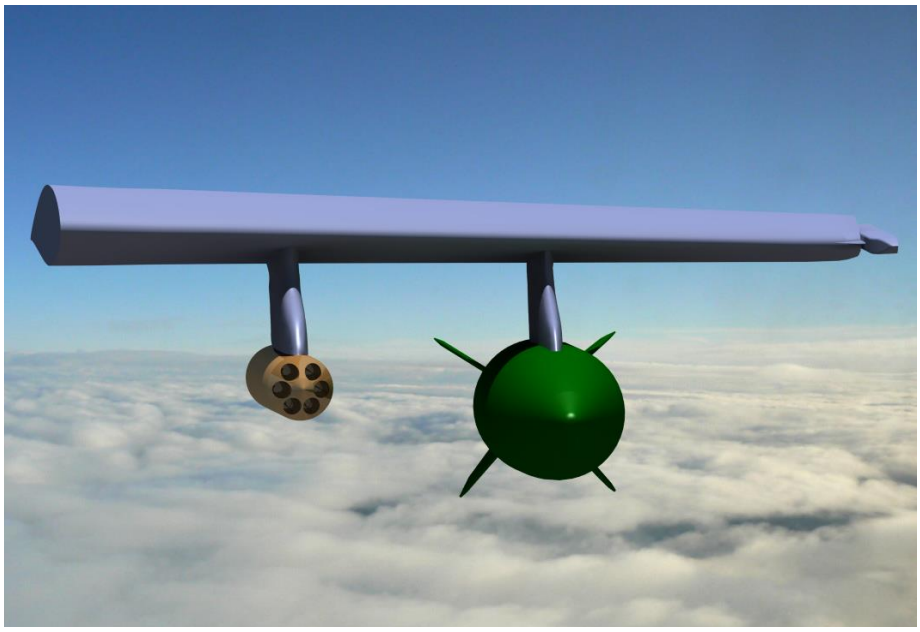

Figure 32: Full loaded wing.

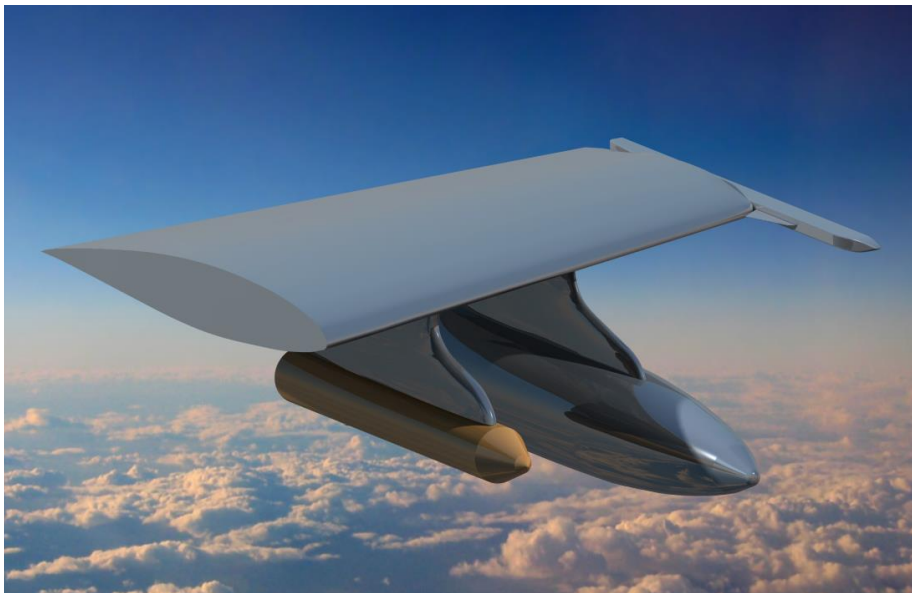

Figure 33: Full loaded wing - ARL fully-closed version.

3.2 Reverse Engineering technique

Reverse engineering could be defined as the process of obtaining a geometric CAD model from 3-D points acquired by scanning/digitizing existing parts/products. The process of digitally capturing the physical entities of a component, referred to as RE, is often defined by researchers with respect to their specific task. Many authors described RE as, "the basic concept of producing a part based on an original or physical model without the use of an engineering drawing" or as the "process of retrieving new geometry from a manufactured part by digitizing and modifying an existing CAD model".

RE is widely used for various reasons. First of all, by reverse engineering a part, we can obtain the CAD model of a part that is no longer manufactured by its manufacturer or for which only traditional blueprints exist. Also, there are cases where the original CAD model no longer corresponds to the physical part that was manufactured because of subsequent undocumented modifications that were made after the initial design stage. In the case study presented at the end of this chapter, RSV applied RE technique in order to acquire an entire A/C geometry not

available by drawings, in order to modify the geometry and use it for subsequent CFD analysis.

The generic process of RE is a three-phase process, Figure 34: scanning, point processing, and application-specific geometric model development.

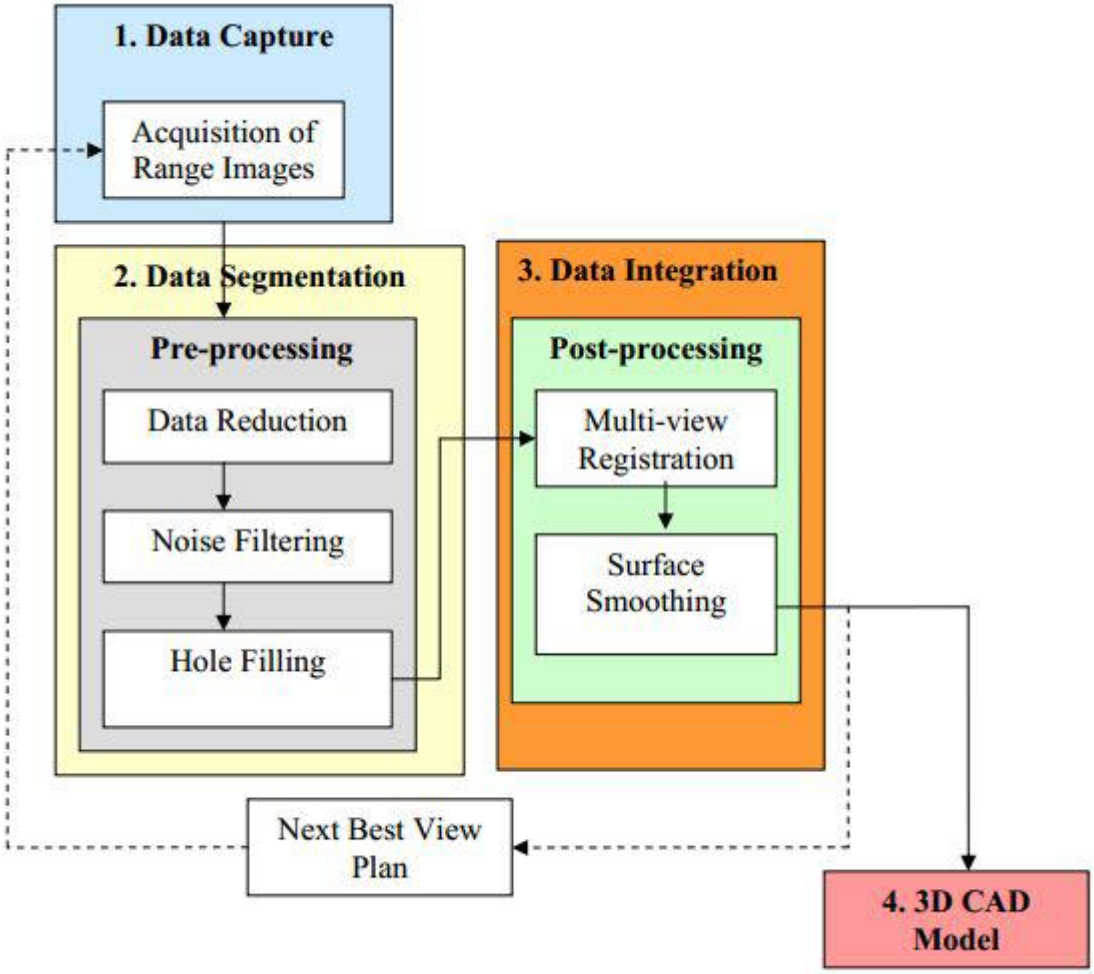

Figure 34: RE process flow chart.

3.1.1 1st phase: Scanning Techniques

This phase is involved with the scanning strategy selecting the correct scanning technique, preparing the part to be scanned, and performing the actual scanning to capture information that describes

all geometric features of the part such as steps, slots, pockets, and holes.

Three-dimensional scanners are employed to scan the part geometry, producing clouds of points, which define the surface geometry. There are two distinct types of scanners, contact and non-contact, Figure 35.

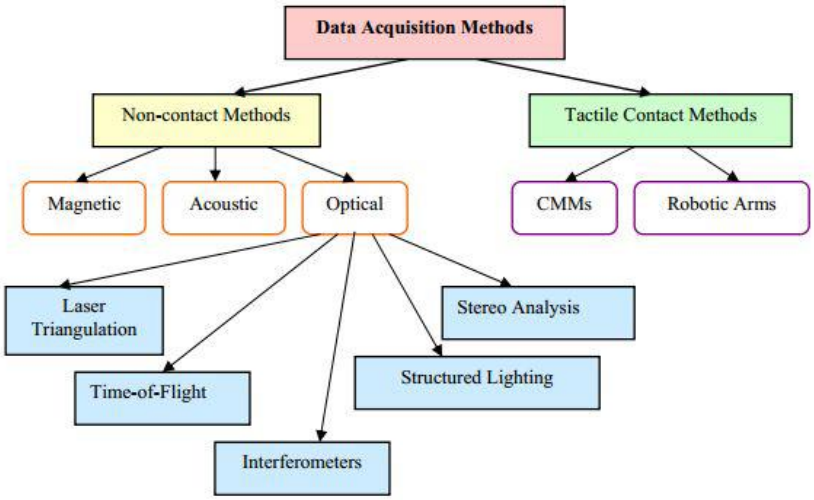

Figure 35: Contact and non-contact RE methods.

3.1.1.1 Contact and non-contact devices

Tactile or contact methods represent a popular approach to shape capture. The two most commonly known forms are CMMs and mechanical or robotic arms with a touch probe sensing device. CMMs are often used when high precision is required, in facts they are very accurate (with a tolerance range of +0.01 to +0.02 mm). Unfortunately there are disadvantages when using a CMM or robotic arm to model surfaces of parts: CMMs having contact to the surface of an object can damage the object if the surface texture is soft, holes can be inflicted on the surface. CMMs also show difficulties in measuring parts with free form surfaces. The part might have indentations that are too small. Flexibility of parts makes it very difficult to contact the surface with a touch probe without creating an

indentation that detracts from the accuracy of the measurements. For CMMs, geometric complexity increases the number of points required for accurate measurements. The time needed to capture points one by one can range from days to weeks for complicated parts. There are also external factors that affect the accuracy of a CMM. The main ones are temperature, vibration and humidity.

A variety of non-contact scanning technologies available on the market capture data with no physical part contact. Non-contact devices use lasers, optics, and charge-coupled device sensors to capture point data. Although these devices capture large amounts of data in a relatively short space of time, there are a number of issues related to this scanning technology. The accuracy is surely poorer than CMMs, usually the typical tolerance of non-contact scanning is within ±0.025 to ±0.2 mm and some non-contact systems have problems generating data describing surfaces, which are parallel to the axis of the laser. Moreover non-contact devices employ light within the data capture process: this creates problems when the light impinges on shiny surfaces, and hence some surfaces must be prepared with a temporary coating of fine powder before scanning. These issues restrict the use of remote sensing devices to areas in engineering, where the accuracy of the information generated is secondary to the speed of data capture. However, as research and laser development in optical technology continue, the accuracy of the commercially available non-contact scanning device is beginning to improve. In is possible to visualize a CMM device and an optical scanner.

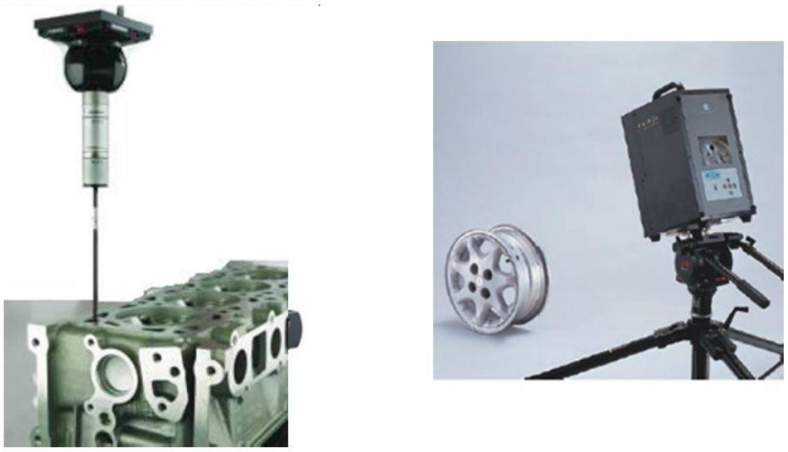

Figure 36: CMM device example and optical scanner.

3.1.1.2 Non-contact methods: optical scanner device

Optical methods of shape capture are probably the broadest and growing in popularity over contact methods. This is because they have relatively fast acquisition rates. There are five main categories of optical methods: laser triangulation, TOF, interferometers, structured lighting and stereo analysis; the most used methods being: laser, TOF, structured lightening and stereo.

Laser Triangulation is a method, which uses location and angles between light sources and photo sensing devices to deduce position, Figure 37. A high-energy light source is focused and projected at a pre-specified angle at the surface of interest. A photosensitive device, usually a video camera, senses the reflection of the surface and then by using geometric triangulation from the known angle and distances, the position of a surface point relative to a reference plane can be calculated.

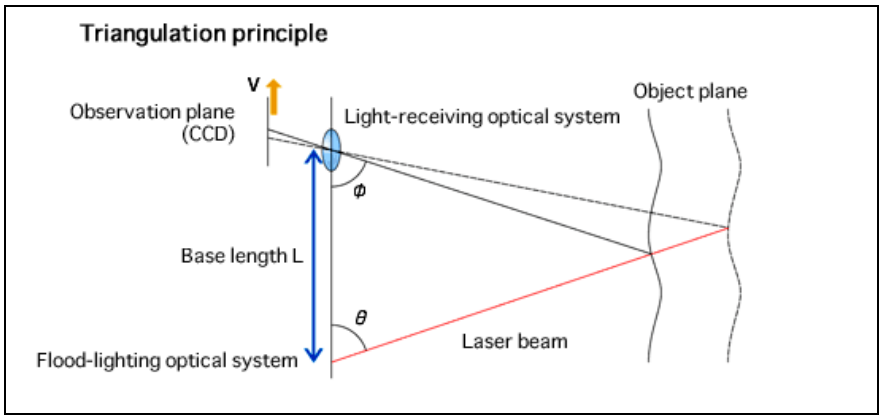

Figure 37: Triangulation.

The light source and the camera can be mounted on a traveling platform which then produces multiple scans of the surface. These scans are therefore relative measurements of the surface of interest. Various different high energy light sources are used, but lasers are the most common. Triangulation can acquire data at very fast rates. The accuracy is determined by the resolution of the photosensitive device and the distance between the surface and the scanner.

TOF method uses the principle of measuring the amount of time (t) that a light pulse (i.e. laser electromagnetic radiation) takes to travel to the object and return. Because the speed of light (C) is known, it is possible to determine the distance travelled. The distance (D) of the object from the laser would then be equal to approximately one half of the distance the laser pulse traveled: D = C × t/2. Figure 38 illustrates in block diagram form how a TOF laser scanner works. For all practical purposes, the angle θ is very small and thus has no effect on the accuracy of the TOF distance measurement. The high velocity of light allows TOF scanners to make hundreds, or even thousands of measurements per second. The advantage of TOF techniques is that they can digitize large, distant objects such as buildings and bridges. The accuracy of RE hardware based on TOF is reasonable and approximately between a few millimeters and two or three centimeters for long range scanners. The accuracy depends on the pulse width of the laser, the speed of the detector, and the timing resolution; the shorter the pulse and the

faster the detector, the higher the accuracy of the measurement. The main disadvantage is that TOF scanners are large and do not capture an object's texture, only its geometry. They are not practical for fast digitization of small and medium-sized objects. Moreover, it takes time to complete the digitization process because the object has to be swept during scanning.

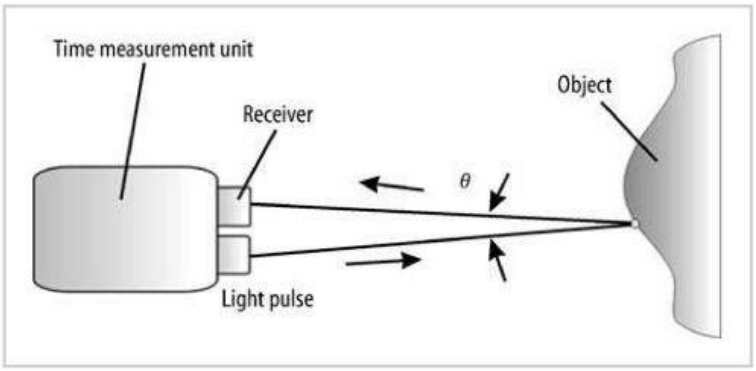

Figure 38: TOF system.

Structured lighting involves projecting patterns of light upon a surface of interest and capturing an image of the resulting pattern as reflected by the surface. The image must then be analyzed to determine coordinates of data points on the surface. A popular method of structured lighting is shadow Moire, Figure 39,where an interference pattern is projected onto a surface producing lighted contour lines. These contour lines are captured in an image and are analysed to determine distances between the lines. This distance is proportional to the height of the surface at the point of interest and so the coordinates of surface points can be deduced. Structured lighting can acquire large amounts of data with a single image frame, but the analysis to determine positions of data can be rather complex.

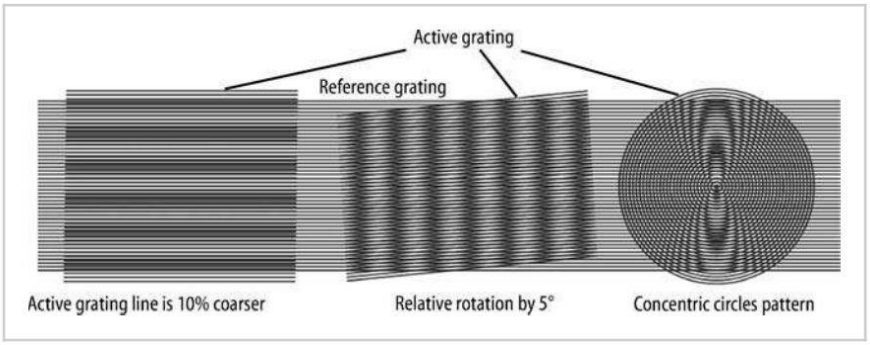

Figure 39: Moirè finges.

Stereo image analysis is similar to structured lighting methods in that frames are analysed to determine coordinate data. However, the analysis does not rely on projected patterns. Instead, typically, stereo pairs are used to provide enough information to determine height and coordinate position. This method is often referred to as a passive method since no structured lighting is used. Active methods are distinguished from passive methods in that artificial light is used in the acquisition of data. Correlation of image pairs and landmarks within the images are big difficulties with this method and this is why active methods are preferred. Another stereo image analysis approach deals with lighting models, where an image is compared to a 3D model. The model is modified until the shaded images match the real images of the object of interest. Finally, intensity patterns within images can be used to determine coordinate information.

3.1.2 2nd phase: Point-Processing

Finally, the output of modern 3D digitization systems is large quantities of points in a unit of time, at the end of the process the result obtained is a dense set of spatial coordinates (real points), the so called Points Cloud, Figure 40.

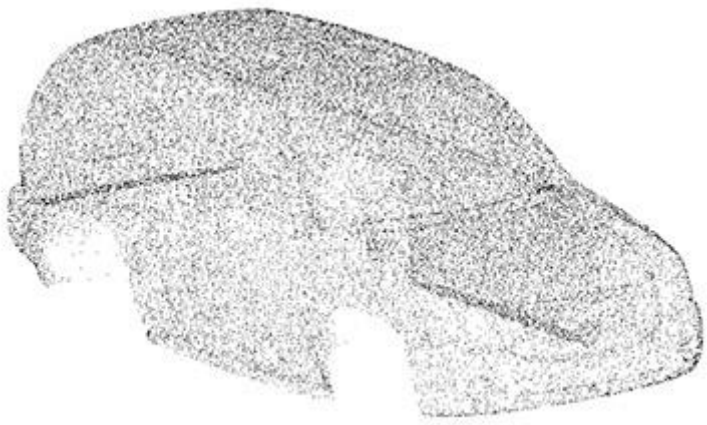

Figure 40: A car points cloud.

However, the huge number of point data, generated in the course of 3D digitization, can become a serious practical problem, later on, when the CAD model is generated. In addition, the 3D digitization process is very often plagued by measuring errors, which can be attributed to the very nature of measuring systems, various characteristics of the digitized objects and subjective errors by the operator, which also contribute to problems in the CAD model generation process. Although most scanners allow scanning an object from different angles with certain provided degrees of freedom, multiple scans of the object are required to capture the entire geometry of an object or to avoid any occlusions (undercuts). Relevant problems caused by erroneous point data and a huge number of point data as the result of 3D digitization are: deviations in shape of the resulting CAD model as compared to the original physical object, and impeded work with software applications for CAD model generation. Moreover the process of surface model generation can be significantly slowed down, and in some extreme cases even brought to a complete halt, despite the high processing power of modern computers. Considering all this, one can conclude that the data pre-processing stage, which includes error filtering, smoothing and reduction of point data, is very important and almost unavoidable in every RE-system.

3.1.2.1 Data reduction and Filtering (Pre-Processing)

The 3D digitization most often results in numerous unwanted points. These points frequently belong to objects which surround the object being digitized, such as fixtures, measurement table, or some other part of the assembly to which the digitized part belongs. However, in the case of non-contact methods, such as the laser triangulation, those points can originate from objects located further away. To some extent, the unwanted points can also be the result of measurement errors (due to operator errors, system-specific errors and/or errors due to specific nature of the digitized object, some external disturbance i.e., vibrations), etc. Those points (which are called "noise") have to be eliminated in order to maintain quality of surface reconstruction.

Noise reduction tools are used for both manually and automatically removing the noise in scanned data. With automatic approaches, the noise removal operation determines where the points should lie, then moves them to these locations based on statistical information about the point data. If the point set represents a free-form or organic shape, the operation reduces the noise with respect to surface curvature. When working with a mechanical or prismatic shape, the operation helps keep features such as edges and sharp corners. The redundancy reduction tool is used to

reduce the number of points in the point cloud when points are too close to one another or overlap.

Sampling algorithms are a useful way to get a more refined points cloud. The sampling function is used to minimize the number of points in the point cloud data

and to make the data well-structured so that it is easier to handle. There are three sampling methods: curvature, random, and uniform; they are based on a curvature, random, and proportional basis. In curvature sampling, fewer points are deleted in a region of high curvature than in a low curvature region to maintain the accuracy of the curvature. Random sampling is a random sampling of points within a specified region or over the entire model, based on the percentage of total points that need to be reduced. Uniform

sampling, Figure 41, uniformly reduces the number of points in a point set; it subdivides the model space into equally sized cubic cells and deletes all but one point from each cell.

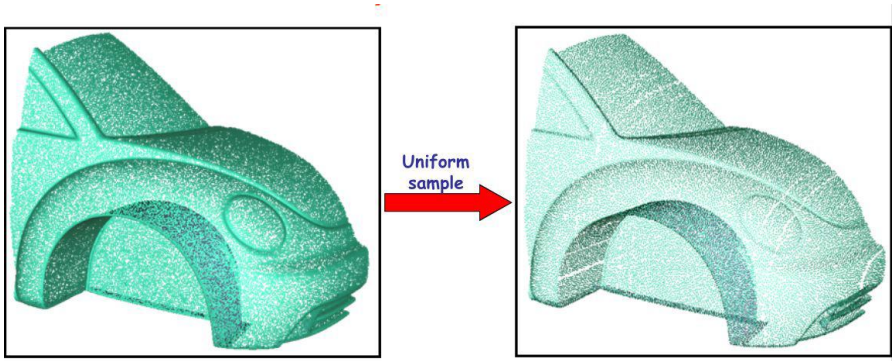

Figure 41: Uniform sampling.

Another problem is restoration of missing data (holes). It is partly necessary due to the above-mentioned inaccessibility and occlusion problems. Moreover, because of the nature of optical and even tactile scanning, the data close to sharp edges is also fairly unreliable. Finally there are situations where only parts of a certain surface can be measured, there are missing parts or parts obscured by other elements, but we need to reconstruct the whole surface from just the visible parts. So various "holes filling" algorithms can be implemented trying to solve this missing points problem.

3.1.2.2 Generation of the polygonal surface

It is the core part of almost all reconstruction programs. A triangulation converts the given set of points into a consistent polygonal model also called "meshes". This operation partitions the input data into simplices and usually generates vertices, edges and faces (representing the analysed surface) that meet only at shared edges. Finite element methods are used to discretize the measured domain by dividing it into many small 'elements', typically triangles or quadrilaterals in two dimensions and tetrahedra in three dimensions, Figure 42. An optimal triangulation is defined measuring angles, edge lengths, height or area of the elements while the error of the finite element approximations is usually related to

the minimum angle of the elements. The vertices of the triangulation can be exactly the input points or extra points, called Steiner points, which are inserted to create a more optimal mesh. Triangulation can be performed in 2D or in 3D, according to the geometry of the input data. Triangles are a default standard as a surface primitive for a variety of reasons, but mainly they simplify computer visualizations because they have guaranteed convexity and thus are useful as a first-order approximation of an object.

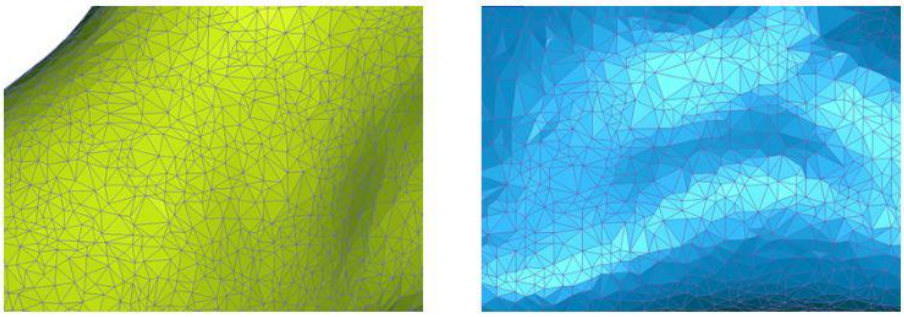

Figure 42: Polygonal meshes.

In 2D Triangulation the input domain is a polygonal region of the plane and, as result, triangles that intersect only at shared edges and vertices are generated. A well-known construction method is the Delaunay triangulation (DT) that simultaneously optimize several quality measures as angles, edge lengths, height or area of the elements.

3D Triangulation is called tetrahedralization or tetrahedrization. A tetrahedralization is a partition of the input domain into a collection of tetrahedra that meet only at shared faces (vertices, edges or triangles). Tetrahedralization results are much more complicated than a 2D triangulation.

3.1.2.3 Surfaces Fitting

Once we have a first approximation of the object from mesh reconstruction, the final stage of the process is to generate higher order descriptions that are more appropriate for CAD applications. In few cases, a triangle mesh itself is sufficient as the final product

but most commonly parametric representations such as NURBS are necessary, Figure 43. NURBS are an accurate way to define free-form curves and surfaces and are useful for the following reasons:

- they offer one common mathematical form for both standard analytical shapes and free-form shapes;
- they provide the flexibility to design a large variety of shapes;
- they reduce the memory consumption when storing shapes (compared to simpler methods);
- they can be evaluated reasonably fast by numerically stable and accurate algorithms;
- they are invariant under affine as well as perspective transformations;
- they are generalizations of non-rational B-splines and non-rational and rational Bézier curves and surfaces.

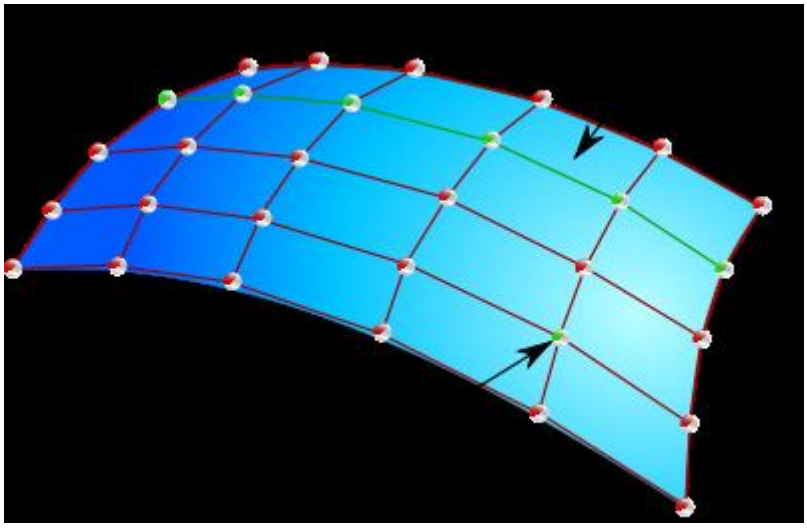

Figure 43: NURBS example.

3.1.2.4 Post-Processing

The created polygons usually need some refinements to correct imperfections or errors in the surface. These operations (mainly manually) vary from single triangles editing to surface corrections:

- edges correction: faces can be split (divided in two parts), moved to another location or contracted;

- triangles insertion: holes can be filled constructing polygonal structures that respect the surrounding area; incomplete meshes can also be repaired with radial basis function or with volumetric approach;
- polygons editing: the number of polygons can be reduced, preserving the shape of the object or fixing the boundary points. The polygonal model can also be improved adding new vertices and adjusting the coordinates of existing vertices. Moreover spikes can be removed with smooth functions.

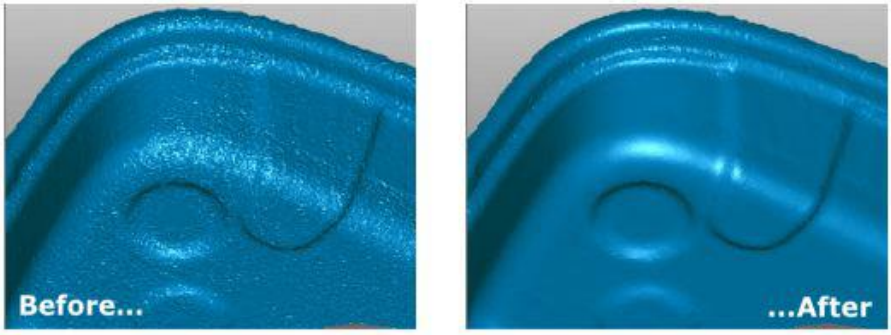

Figure 44: Edges/spikes smoothing polygonal model.

3.1.3 3rd phase: generating the CAD

The generation of CAD models from point data is probably the most complex activity within RE because powerful surface fitting algorithms are required to generate surfaces that accurately represent the three-dimensional information described within the point cloud data sets. Most CAD systems are not designed to display and process large amounts of point data; as a result new RE modules or discrete software packages are generally needed for point processing. Generating surface data from point cloud data sets is still a very subjective process, although feature-based algorithms are now emerging and enabling engineers to interact with the point cloud data to produce complete solid models for current CAD environments. The output of this phase is a geometric model in one of the proprietary formats such as IGES, VDA, STL, DXF, OBJ,

VRML, ISO G Code, etc. A list of the most important and powerful RE software for CAD generation is showed in .

Company	Relevant products	Web address
Parametric Technology Corporation	ProEngineer Interactive surface design, ProEngineer reverse engineering, CAD/CAM products	www.ptc.com
Dassault Systems/IBM	CATIA reverse engineering 2 (RE2), CATIA digitized shape editor 2 (DSE), Solidworks, CAD/CAM products	www.3ds.com or www.ibm.com
UGS	NX Imageware, eM-probe CAD, CAD/CAM products	www.ugs.com
Delcam	CopyCAD, powerINSPECT, CAD/CAM products software	www.delcam.com
INUS Technology Inc	Rapidform XO, scan workbench, polygon workbench, curve workbench, surface workbench, inspection workbench, feature workbench, inspect workbench, etc.	www.rapidform.com
HiRes Inc	Reverse engineering software modules to integrate with major CAD vendors' suites	www.reverse-it.com
Geomagic Inc	Inspection, reverse engineering and surfacing software	www.geomagic.com
Revware Inc	Reverse engineering software for use with Solidworks	www.revworks.com
Innovmetric	Integrated point cloud manipulation, surfacing, inspection and reverse engineering suite	www.innovmetric.com
Robert McNeel & Associates	Rhinoceros NURBS modeling software with reverse engineering and rapid prototyping interfaces	www.rhino3d.com

Figure 45: List of commercial RE SW.

3.1.4 A case-study: RE CAD generation

In this paragraph is pictorially presented a case study referred to a 3rd generation fighter type A/C geometry acquisition, following the schematic process proposed in Figure 46, which represents the sum up of the previous paragraphs.

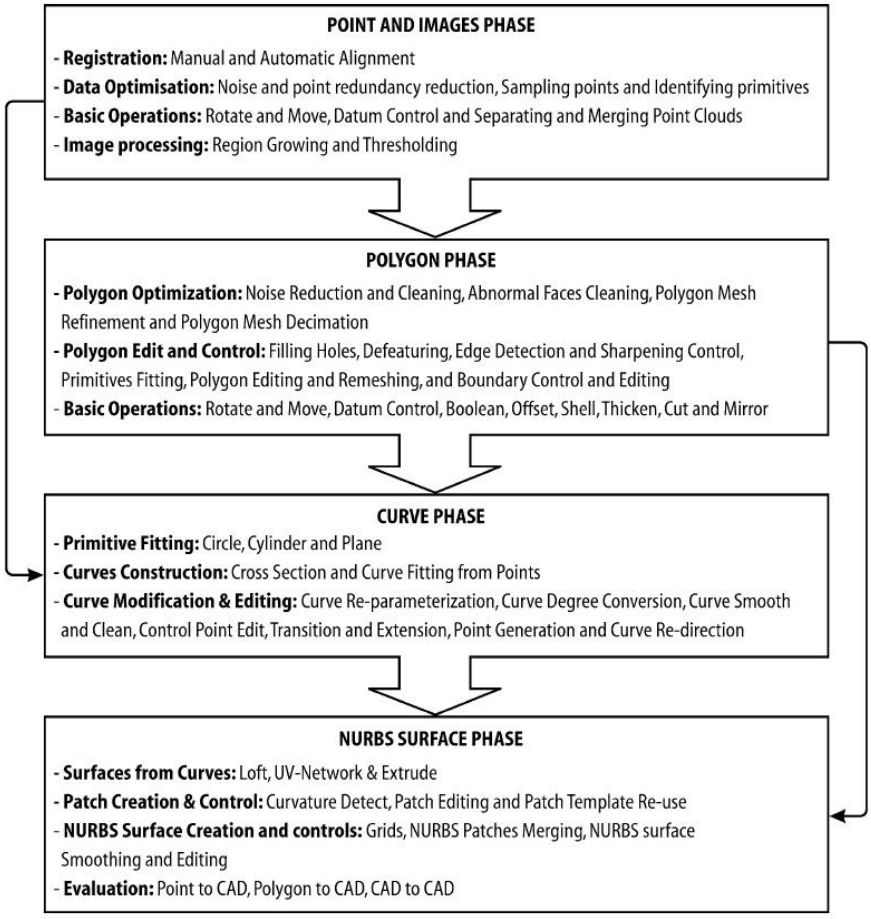

Figure 46: RE data processing chain.

All the geometries were generated using the TOF acquisition RE technique explained. The geometries were acquired using a high-resolution time of flight laser scanner, FARO CAM 2 Photon 80, Figure 47.

Figure 47: Laser scanner FARO CAM 2 Photon 80.

The following sequence represents the flow of the actions performed:

- Laser scanning of the test item, Figure 48;

Figure 48: Laser scanned test item.

- Cloud Clean-up (through Faro Scene SW), getting reed of useless surface as hangar/tarmac/etc…, Figure 49;

Figure 49: Cloud clean-up.

– Reference system setting, putting all scanned images in the same reference system - the A/C body axes. Faro Scene SW is able to give a feedback about the three rotations angles and its position, that is assumed as the origin of its reference system, within another preplanned reference system. The process consists on a roto-translation of axes according to the following simple rules:

$$\begin{bmatrix} X \\ Y \\ Z \end{bmatrix}_{P,II} = \begin{bmatrix} X_0 \\ Y_0 \\ Z_0 \end{bmatrix} + \lambda \mathbf{R} \begin{bmatrix} X \\ Y \\ Z \end{bmatrix}_{P,I}$$

$$\mathbf{R_X}(R_X) = \begin{bmatrix} 1 & 0 & 0 \\ 0 & \cos R_x & \sin R_x \\ 0 & -\sin R_x & \cos R_x \end{bmatrix}$$

$$\mathbf{R_Y}(R_Y) = \begin{bmatrix} \cos R_Y & 0 & -\sin R_Y \\ 0 & 1 & 0 \\ \sin R_Y & 0 & \cos R_Y \end{bmatrix}$$

$$\mathbf{R}_Z(R_Z) = \begin{bmatrix} \cos R_z & \sin R_z & 0 \\ -\sin R_z & \cos R_z & 0 \\ 0 & 0 & 1 \end{bmatrix}$$

In the subject case the scale factor $\lambda=1$ and the rotation matrix $R=R_Z R_Y R_X$

- Wrap and wrap clean-up (through Geomagic 11 SW), creating a multi-triangles surface having the vertices on the cloud points and getting reed of holes, singularities, etc…, Figure 50;

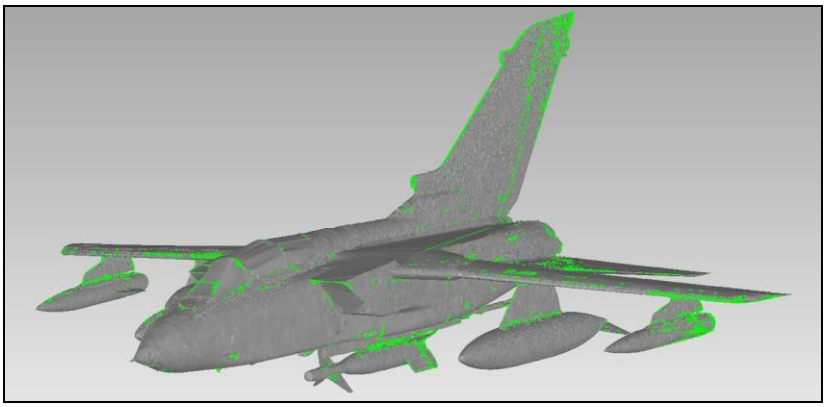

Figure 50: Wrap.

- Patching (through Geomagic 11 SW), creating the shape skeleton; red colored lines indicates a customization is required in order to overcome a computational problem, generally strong changes of normal vector to the surface, Figure 51;

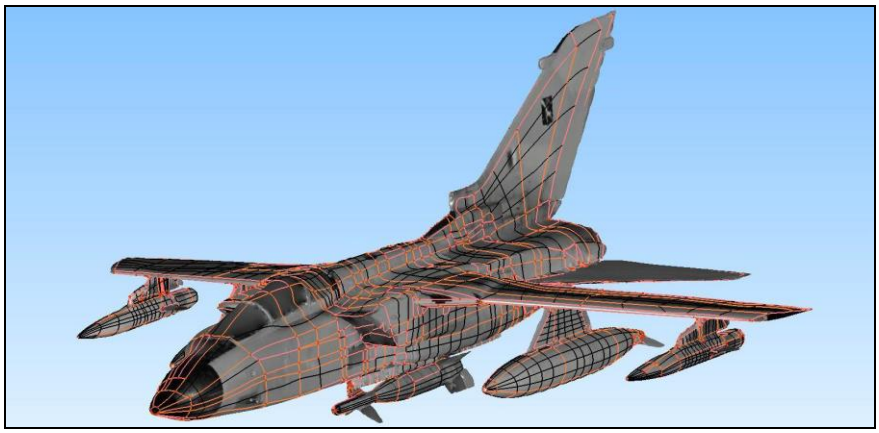

Figure 51: Patching.

– NURBS (through Geomagic 11 SW), creating the final shape in CAD format (.step, .dxf), .

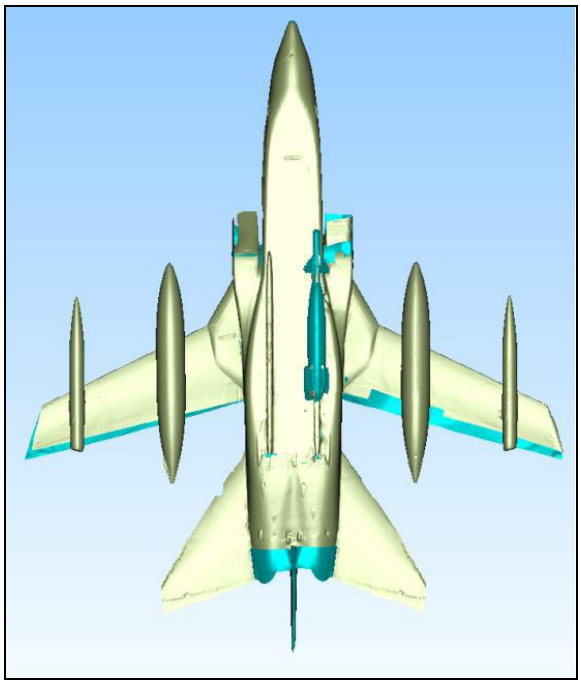

Figure 52: NURBS 1/2.

Figure 53: NURBS 2/2.

CHAPTER 4

MODELLING AND SIMULATION FOR STORE INTEGRATION: CFD ANALYSIS

Aircraft Store compatibility is of major importance to the aircraft and weapon designer. Weapon system compatibility and aircraft performance are directly affected by the problems associated with store integration and separation. Improved weapon integration can improve the air vehicle effectiveness by orders of magnitude.

The aerodynamic problems associated with the carriage of stores and their release from military aircraft are numerous and very complex, making this a most difficult task for the aircraft designer. Improvements in the integration process can lead to significant reductions in the air vehicle development costs.

However, the general understanding about the modern warfare is accustomed to focus on the weapons and its capabilities mostly, considering that the weapon is a substantive system; the people involved in integration business are profoundly aware that the weapon and the launch aircraft forms a complex system together in which the performance of each individual component depends on the performance of the other one. The weapon can only achieve its designated performance, if the transactions on the launch aircraft required for the integration are done accurately.

The integration of weapons on aircraft requires evaluation of multiple topics related to different disciplines such as aerodynamics, structures, avionics/software maintenance, electro-magnetic interactions, flight test instrumentation, ground and flight tests. In addition to compatibility concerns, the release of a weapon creates issues such as the ability of the specific store to achieve safe separation and the ability of the aircraft structure to withstand the imparted loads during the

ejection of store from pylon or launching phase in the presence of aircraft flow field. The number of subjects to cover is increased when the requirements for all the phases of integration process are considered, therefore, the necessity for an optimized test management.

Analyses and simulations are used for a variety of purposes including program reviews, airworthiness release, safety-of-flight, and full integration activities. The selection of analyses and simulation requirements is highly tailorable to the nature, complexity and risk of the new or modified weapon.

M&S has always played a key role in flight testing. Nowadays, due to the economic constraints, the importance of M&S is increasing. M&S should be an essential part but it cannot replace flight testing because of an high number of uncertainties and tolerances.

In particular, the focus of this study is on analytic simulation for solving aerodynamic flow-field to support aircraft/store integration and separation flight test activities.

4.1 Aerodynamic analysis for store integration problem

Physical shape and mechanical interfaces of stores should be designed according to the limitations and requirements of the carrying platforms. Hence, the limits of the physical parameters such as length, width, wing span, chord and diameter of the store should be determined during the preliminary design stages of the development projects. For this purpose 3D models of aircraft that have the capability of simulating the moving parts should be prepared and limits of the design space should be determined by using this model. This model may also be used to determine mechanical interface requirements and limitations.

Platform/store compatibility studies cannot be realized with the lack of computational analyses in a budget optimized development project. According to computational analysis results, critical flight and release conditions can be determined and wind tunnel test program can be shortened. In this way, the wind tunnel testing is used only for accurate predictions of flight clearances which are considered as critical according to analysis results. With the coupling of these two methods flight test matrix can be minimized too.

In the 60's, some of CFD codes started to provide trajectory solutions for the stores in the effect of carrier platform flow field. However, at that time, since the computational power was not sufficient for such large problems, techniques were limited to some linear theories and panel methods. With the improvements in the computational field, the capabilities and accuracy of the codes were also advancing. Higher order panel methods, Euler solvers and finally fully unsteady Navier-Stokes solvers were developed and applied to separation problems with the improvements in the computation power. Nowadays, a separation problem may be solved with a fully unsteady N-S solver in a couple of hours with the help of high-performance parallel computing facilities.

Nowadays, drag index, aerodynamic flight loads and effects on aircraft performance and separation characteristics of stores can be analysed via computational fluid dynamics analysis tools.

Aerodynamic loads on a store during carriage stage differ from free flight loads. Moreover, these loads may result in a performance defect in carrying platform. Hence, change in the aerodynamic characteristics of store should be analysed and effect of aerodynamic loads on the platform performance should be considered for the carriage envelope. At the end of these analyses, carriage envelope of platform for the analysed specific loading conditions should be clearly defined.

Determination of drag index is of critical importance and is one of the measures of store effect on fuel consumption for the given loading configuration of carrying platform. Increase in the total drag of the carrying platform with a new integration shall be calculated for the most flown conditions for accurate mission planning. Calculation methodology of drag index value of a store for different platforms may vary according to platform cruise Mach number, angle of attack and other platform related physical reference values.

As already mentioned in chapter 1, the weapons integration problem is completed by analysing also the structural model, the FSI and the safe separation phase; however for lack of time in this study the structural model, the FSI and the safe separation prediction have been neglected and are not subject of this study. However, the ground/flight test and data gathering/analysis of the safe separation phase have been conducted for an

activity related to a multiple weapons integration on a 3rd generation fighter type A/C (both pit drop and in-flight safe separation).

Prediction phase focus has been oriented on the aerodynamic model useful for performance and flying qualities evaluation. The aerodynamic loads, output of the aero-model, will be used as input together with the GVT modal basis for the structural model and FSI analysis in a future research program.

4.2 CFD Simulation

CFD is the branch of fluid dynamics providing a cost-effective means of simulating real flows by the numerical solution of the governing equations. The governing equations for Newtonian fluid dynamics, namely the Navier-Stokes equations, have been known for over 150 years. Computational techniques replace the governing partial differential equations with systems of algebraic equations that are much easier to solve using computers.

The basic concept of CFD methods is to find flow field characteristic parameters at a large number of points in the system. These point are usually connected together in what is called numerical grid or mesh. The system of differential equations representing the flow is converted, using some procedure, to a system of algebraic equations representing the interdependency of the flow at those points and their neighbouring points.

The resulting system of algebraic equations, which can be linear or non-linear, is usually large and requires a digital computer to solve. In essence, we end-up with a system with the unknowns being the flow quantities at the grid points. Solution of this system results in the knowledge off these quantities at the grid points, [22].

With the development of fast and validated numerical procures, and the continuous increase in computer speed and availability of cheap memory, larger and larger problems are being solved using CFD methods at cheaper cost and quicker turnaround times. In many design and analysis applications, CFD methods are quickly replacing experimental and analytical methods. CFD simulations also enable flow solutions at the true scale of the engineering systems with the actual operating conditions, while experimental measurements mostly require either scaling up or down. In most cases, realistic conditions cannot be economically represented and thus results need

to be extrapolated. This problem does not exist in CFD simulations. CFD methods are now widely used in most aerospace applications for the purpose of predicting component performance and as an integral part of the design cycle.

Wind tunnel tests require substantial scaling which leads to some difficulties of matching the important flow parameters. Attempting to model the correct Mach number, the Reynolds number will be substantially lower than the full scale Reynolds number leading to errors in the modelled shear stress and other flow features. It is also very expensive to replicate altitude conditions within a wind tunnel. Full scale flight tests are extremely expensive and risky. For these reasons, CFD provides a useful tool in predicting the performance of the airframe components under various conditions and this leads to substantial cuts in the time and cost of the design process.

In this process the meshing strategy is paramount for the correct set up before running the fluid dynamic solver.

4.2.1 Meshing strategy

In order to solve the aerodynamic flow field around a geometry of interest, first of all it is necessary to discretize the domain in which solve the system of algebraic equations.

A mesh is a discretization of a geometric domain into small simple shapes, such as triangles or quadrilaterals in two dimensions and tetrahedral or hexahedra in three. Meshes are essential in the numerical solution of partial differential equation arising in physical simulation. In fact, CFD uses a series of cells (referred to as control volumes), elements and nodes that combined form the so called mesh. It is at each of these node locations, that CFD calculates the fundamental equations of fluid dynamics. The shape of the cells greatly impacts the accuracy of the solution due to discretization errors, therefore the meshing stage is one of the most crucial stages in the problem simulation.

There are 3 types of meshing predominately used in CFD:

- *structured meshing*: all interior vertices are topologically alike (typically quadrilaterals and hexahedra), Figure 54;

- *unstructured meshing*: vertices may have arbitrarily varying local neighbourhood (typically triangles and tetrahedra), Figure 54;
- *block-structured or hybrid meshing*: formed by a number of small structured meshes combined in an overall unstructured pattern.

In general, structured meshes offer simplicity and easy data access, while unstructured meshes offer more convenient mesh adapt capability and a better fit to complicated domains. High-quality hybrid meshes enjoy the advantages of both approaches.

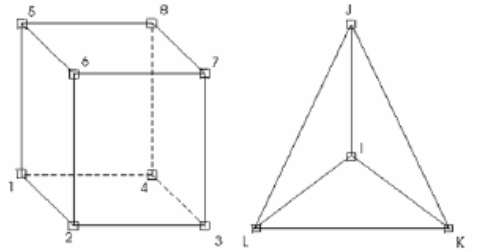

Figure 54: Hexahedral/tetrahedral for structured/unstructured mesh.

Each method has advantages and disadvantages and it is imperative that the CFD user understands which meshing type is applicable for the given problem. Table 2 and Table 3 summarize advantages and disadvantages of structured and unstructured mesh.

Structured Mesh	
Strengths	**Weakness**
• High degree of user control. Mesh can be accurately designed to user's requirements. • Hexahedral cells are very efficient at filling space, support a high amount of skewness and stretching before affecting solution. • Grid is flow aligned which helps the solver converge. • Post-processing is easier due to the logical grid spacing act as excellent reference points for examining the flow field.	• Excessive time spent producing the mesh compared to unstructured mesh • Some geometries don't allow structured topology due to the high skewness angles and stretch of cells that are required.

Table 2: Structured mesh: strengths and weaknesses.

Unstructured Mesh	
Strengths	**Weakness**
• Automated grid generation allows much less effort by user to define mesh.	• Lack of user control – mesh may not be defined as well as the user may like in certain areas.
• Well suited to inexperienced users	• Tetrahedral elements do not twist or stretch well, which will severely impact accuracy of results.
• Will generate a valid mesh for most geometries	• Require excellent CAD surfaces. Small mistakes in the geometry can lead to large meshing problems.

Table 3: Unstructured mesh: strengths and weaknesses.

Mesh generation, in most cases is the timeliest task in the CFD simulation and can be quit challenging to generate a mesh that accurately defines the problem, especially for complicated geometries.

For the objective of this study, as presented in the following chapter, structured and hybrid meshes have been used to perform CFD calculations and comparisons.

4.2.1.1 Unstructured Grid Generation

Unstructured grids have become very popular in recent years, due both to the influence of the finite-element method and to the increase in the power of computers.

Unstructured grids and unstructured solvers have successfully demonstrated their capabilities to handle complex geometries in the demanding field of aerospace applications (an area dominated for many years by structured grids). The most flexible and automatic grid generation codes create unstructured grids. They are well suited to point-wise adaptive refinement and to moving mesh methods.

It is difficult to achieve good performance on unstructured grids, more memory is required and it is quite hard to apply certain fast algorithms such as implicit methods and multigrid. Attaining performance on vector, parallel and cache based computer architectures

is not easy for solvers using unstructured grids because these machines prefer that operations be performed on data that is stored locally in memory. On an unstructured grid the data belonging to the neighbour of a point may be stored a long distance away. Moreover, triangular and tetrahedral meshes inherently require more elements and more computations per grid point; in three dimensions, there are some five to six times more tetrahedra per grid point than on a corresponding mesh of hexahedra. The creation of better-quality grids for hyperbolic problems and forming highly stretched elements in boundary layers continue to be active areas of research.

Figure 55 shows a 3D unstructured grid around an A/C for use in a viscous flow calculations.

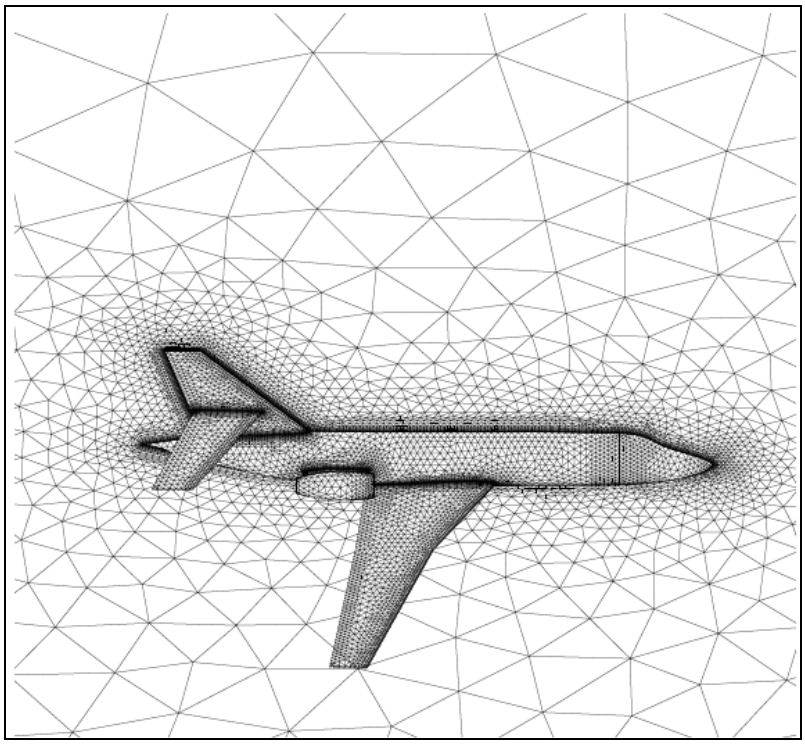

Figure 55: 3D unstructured grid for viscous flow computation.

4.2.1.2 Structured Meshing

Structured meshes offer simplicity and efficiency. A structured mesh requires significantly less memory than an unstructured mesh with the same number of elements (a factor of three less). Moreover a structured mesh can also save time.

On the other hand, it can be difficult or impossible to compute a structured mesh for a complicated geometric domain. Furthermore, a structured mesh may require many more elements than an unstructured mesh for the same problem, because elements in a structured mesh cannot grade in size as rapidly. These two difficulties can be solved by hybrid structured/unstructured approach, which decomposes a complicated domain into blocks supporting structured grids.

As mentioned previously a structured mesh uses hexahedron shaped elements to create the mesh used to simulate the problem. However, difficulty with a structured mesh comes from trying to adapt a hexagon shaped element to a curved or complex shape and can result in a poor quality cells.

Figure 56 shows an example of 2D unstructured grid around an airfoil with flap and slat.

Figure 56: Example of structured grid.

4.2.1.3 Hybrid Meshing

As previously anticipated, a hybrid mesh consist of a union between structured and unstructured mesh.

In particular, when you want to resolve a viscous boundary layer, it is possible to use viscous hybrid meshes that use a layer of prism elements along the wall, with tetrahedral elements in the bulk flow region. The prismatic cells allow you to resolve the normal gradients associated with boundary layers with fewer cells. The resulting mesh is referred to as a "viscous" hybrid mesh. You can create a viscous hybrid mesh by growing prisms from the faces on the surface mesh. High quality prism elements are created near the boundary and tetrahedral elements in the rest of the domain. Automatic proximity detection and height adjustment while growing prisms in a narrow gap are also supported.

Compared to all-tetrahedral meshes, viscous hybrid meshes result in dramatic savings, with far fewer elements required to accurately resolve boundary layers and give good near-wall prediction of shear stress, heat transfer, and flow separation. Figure 57 shows an example of 2D hybrid grid around an airfoil.

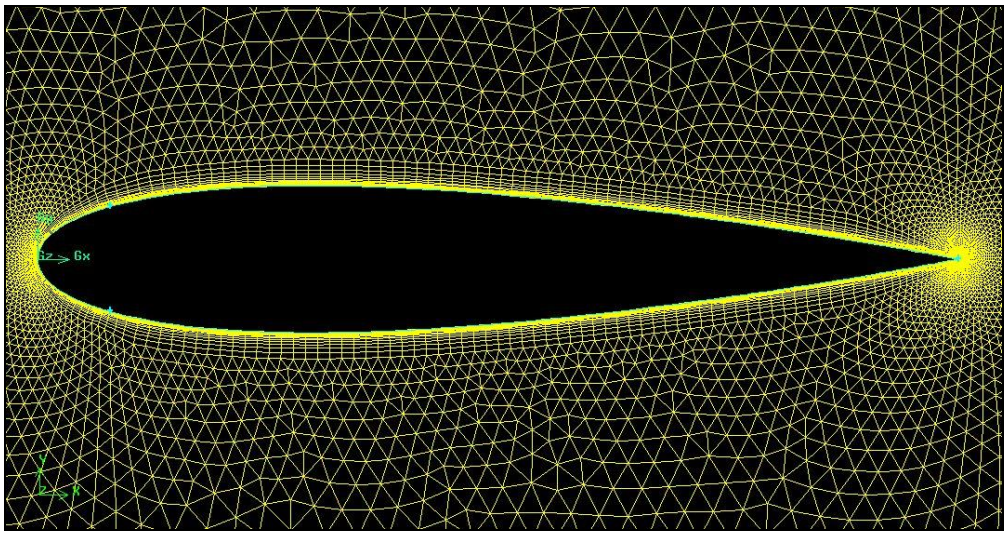

Figure 57: Example of hybrid viscous grid.

4.2.1.4 Mesh quality

The quality of the mesh is determined by the shape of the individual cells. The shape of the elements in a mesh have a pronounced effect on numerical methods. If the quality of one cell is poor it can cause inaccurate results or convergence failure. Key factors that affect the quality of the cells are skewness and aspect ratio.

Skewness

For quad elements, the skew is obtained by first connecting the midpoints of each side with the midpoint of the opposite side. The angle α is the smaller of the two angles, Figure 58. The result is usually normalized by dividing α by 180 degrees.

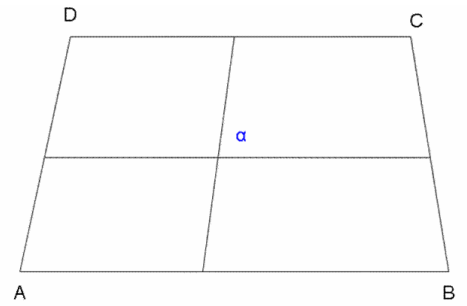

Figure 58: Skewness definition (quadrilateral element).

For triangular elements, the skewness is the ratio of the difference between the optimal cell size and the actual cell size to the optimal cell size, Figure 59.

$$Skewness = \frac{optimal\ cell\ size\ -\ cell\ size}{optimal\ cell\ size}$$

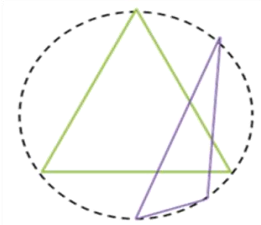

Figure 59: Skewness definition (triangular element).

Aspect Ratio

The aspect ratio is determined by the size of the minimum element edge divided by the size of the maximum element edge. In general, elements of large aspect ratio are bad. Large aspect ratio lead to poorly

conditioned matrices, worsening the speed and accuracy of linear solver. Speed degrades before accuracy. In Figure 60 the aspect ratio is determined by A divided by B.

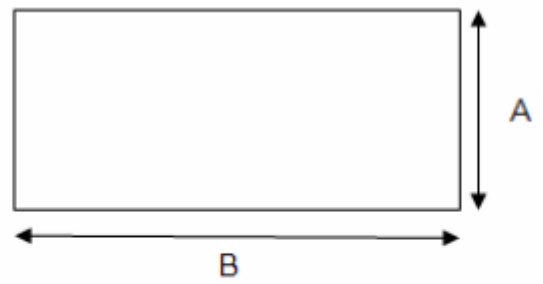

Figure 60: Element aspect ratio determination

Sometimes, however, elements of large aspect ratio are good. If the solution to the differential equation is anisotropic, meaning that its second derivative varies greatly with direction, then properly aligned high-aspect-ratio elements give a very efficient mesh. Fluid flow problems, especially full Navier-Stokes simulation are strongly anisotropic. For example, in aerodynamic simulations ideal aspect ratio may reach 10,000 along the surface of the aircraft. Quadrilateral and hexahedral meshes have an advantage in accuracy over triangular and tetrahedral meshes for control-volume formulations of the problems, as they allow faces of elements in the boundary layer to be either almost parallel or almost orthogonal to the surface.
Simulations with shock fronts – for example supersonic air flow over a wing – are also strongly anisotropic. In this case, however, the locations and directions for high-aspect-ratio elements cannot be predicted in advance. The need to adapt to the changing condition now tilts the balance in favour of triangles and tetrahedra.

CHAPTER 5

ADVANCED RECONNAISSANCE POD INTEGRATION ON A 5TH GENERATION FIGHTER TYPE AIRCRAFT

In this chapter is presented a case study relative to a flight test campaign which looked like a graduation exercise at the moment the task was assigned to the RSV, ride along the described process of the application of the predict-test-validate philosophy to the store integration field.

ItAF Headquarters operational need and technical requirement was to integrate an advanced reconnaissance pod on a 5th generation fighter type aircraft within a time frame of two months, therefore RSV tasked its Aeromechanical Branch of the Technical Department in order to perform a computational aerodynamic prediction to support the aeromechanical integration activity, containing time and associated costs. Time constraints drove towards a clearance by read-across using experimental data gathered during previous certification process of a «*similar*» pod.

Therefore, the aim of the activity was to compare the aerodynamic characteristics of the new pod to a previous one already cleared on the same aircraft fleet, given verified inertial and structural similarity. Shows the external difference in shape between the two pods.

Verifying the aforementioned aerodynamic similarity without involving extensive flight test activity was a must, to save time and to reduce costs. A two steps approach was required by the Certification Authority to verify, initially, the performance data compatibility in terms of aerodynamic coefficients of the old pod with the new one, in order to allow performance flight manual data

interchangeability (a quantitative comparison was required); afterwards, a qualitative assessment was conducted to verify the absence of unsteadiness induced by the introduction in the external structure of the new pod of an auxiliary antenna case.

Figure 61: New and old pods comparison.

Overall, the test team had to deal with the following main technical issues to be evaluated in order to confirm that the new pod was suitable for the operational goal:

- Form, Fit, Function, the basic mechanical interface compatibility check;
- Avionics assessment: Human Machine Interface, Electro-Magnetic Compatibility, Software integration;
- Structural Loads and Environmental evaluation, both static and dynamic;
- Flight Control System Store Management: was it the FCS capable to manage the different inertial properties of the new pod without any re-engineering (SW update or mechanical parts re-design)?;
- Performance definition - Declaration of Acceptable Degradation - 5%, [35], [36], [37];
- Flying/Handling Qualities Assessment.

The first three areas are not object of the present study, which will focus on the last two topics, giving a glace to the forth one.

Table 4 shows as the inertial (especially mass) difference resulted within the Upload Mass Properties of the A/C accounting also for the Avionics ballast (± 46 Kg), therefore the new pod installation was deemed to be compliant with the inertial similarity requirement and the FCS capable to manage the inertial differences without any required modification or update.

Parameter	NEW pod	OLD pod
Weight [Kg]	215 ± 10	203 ± 5
Center of Gravity distance from front end [mm]	1062 ± 76	1062 ± 76
I_{xx} [Kgm²]	4.7 ± 0.5	4.7 ± 0.5
I_{yy} [Kgm²]	80 ± 8	80 ± 8
I_{zz} [Kgm²]	80 ± 8	80 ± 8

Table 4: Inertial properties comparison - old/new pods.

5.1 CFD prediction

5.1.1 Configuration set-up: CAD generation

Before starting the fluid-dynamic analysis, it was necessary to generate two CAD drawings of the two pods, generated in CATIA V5 and imported in ANSYS DesignModeler as ".stp" files; the one of the old pod was fine-tuned starting from a CAD not suitable for fluid dynamic analysis (presence of discontinuities), Figure 62, while the new pod drawing was generated from the scratch, Figure 63. As showed in Figure 62 and Figure 63, the main difference of the external structure between the two pods was the presence in the new pod of an auxiliary antenna unit case; the effect of this external case on the aerodynamics characteristics of the new pod was the main subject of the present study.

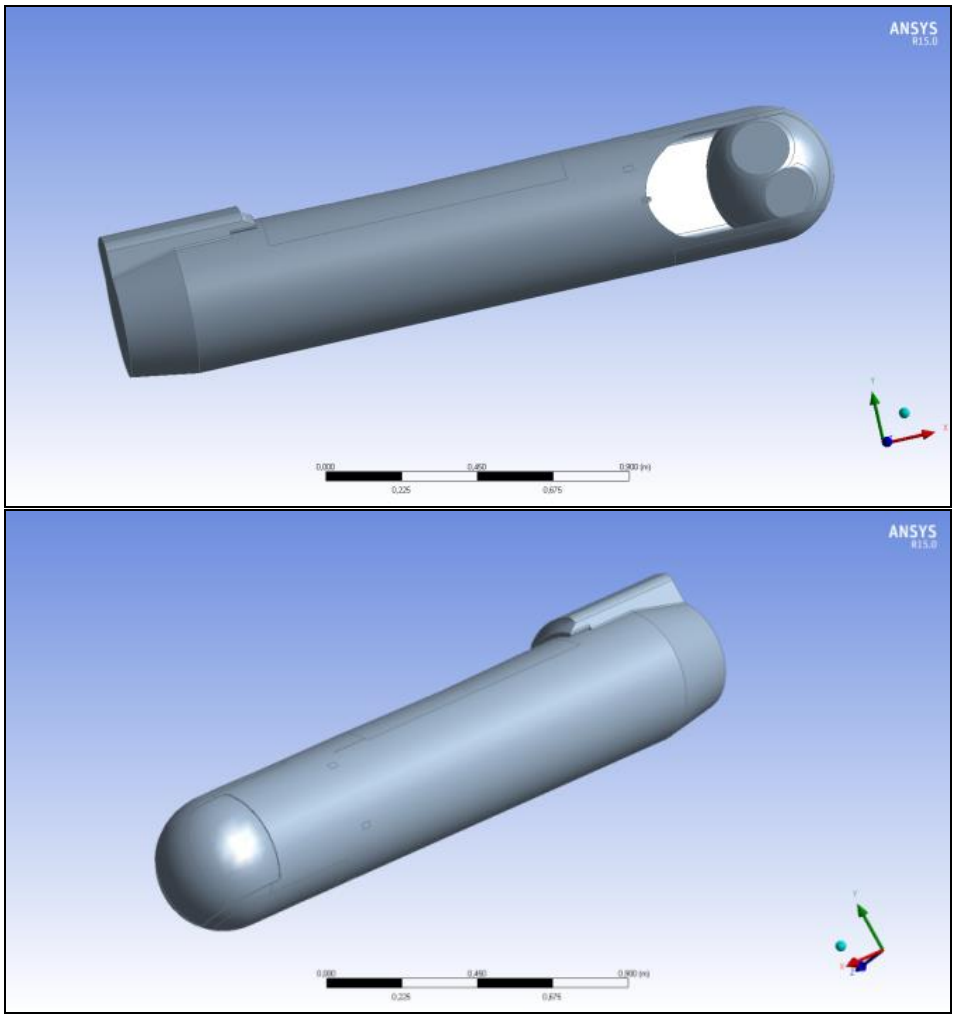

Figure 62: Old pod CAD drawings.

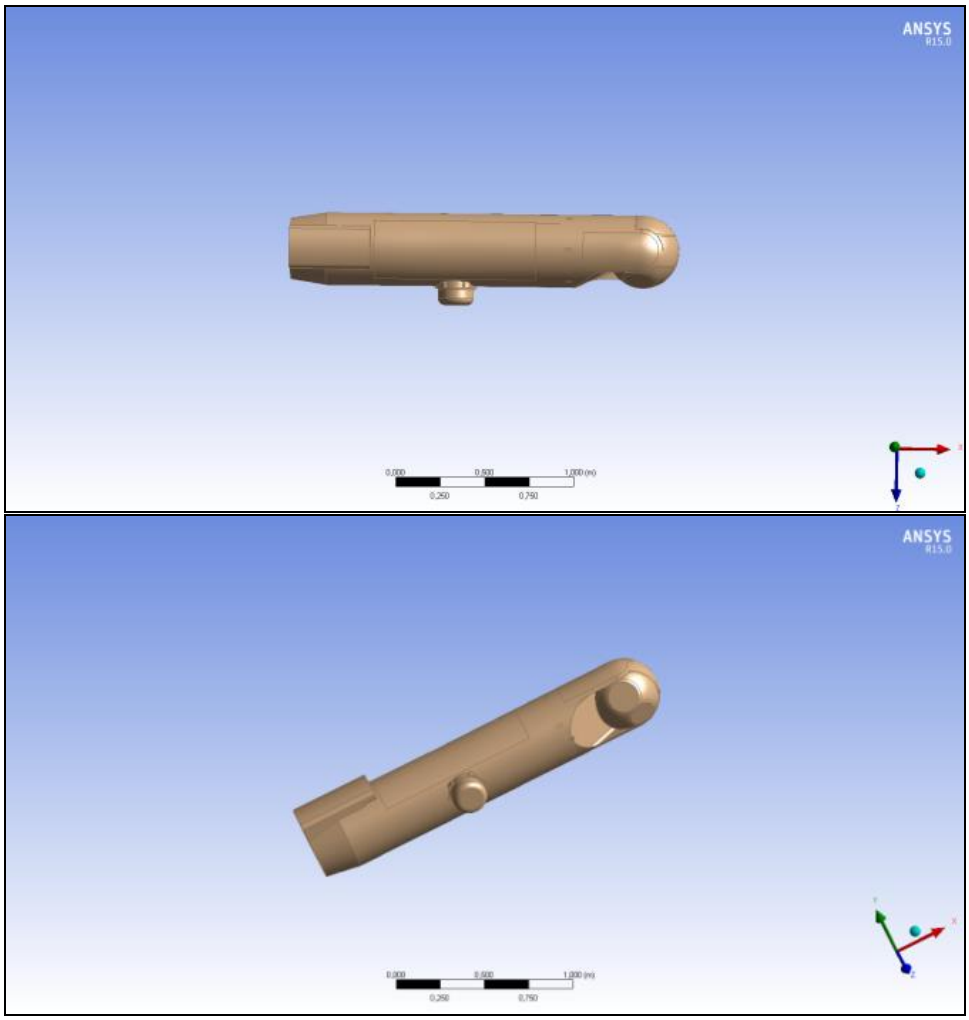

Figure 63: New pod CAD drawings.

5.1.2 Mesh generation

The meshes were generated using the ANSYS Meshing tool, obtaining fair values of skewness for viscous hybrid meshes (≤0.92) and commendable values of Y+ (≤ 0.35), inferring proper discretization of the boundary layers. Number of total cells was about 1.7 M and the boundary layer grids had a number of stratifications of about 30.

Figures 3 shows the grid for the old pod simulation, while show the new pod grid and a detail of the boundary layer discretization.

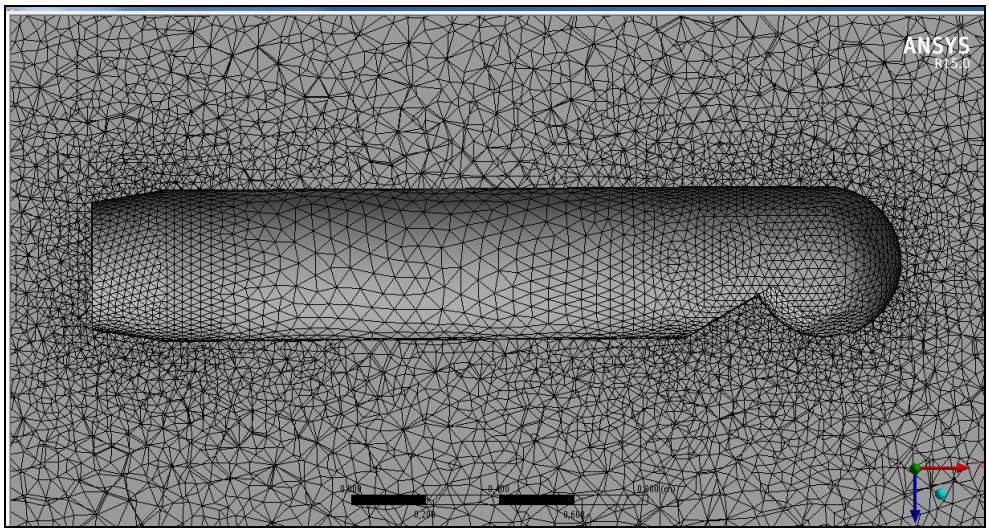

Figure 64: Old pod mesh.

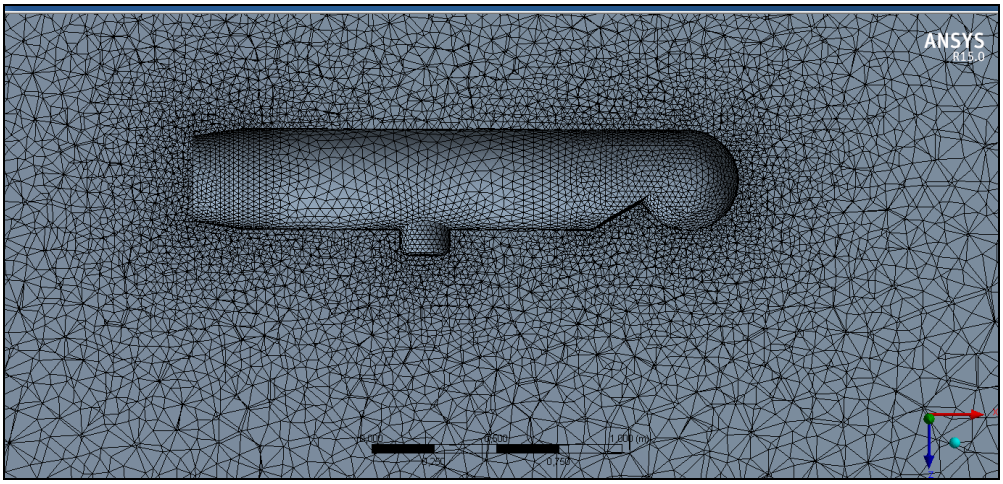

Figure 65: New pod mesh.

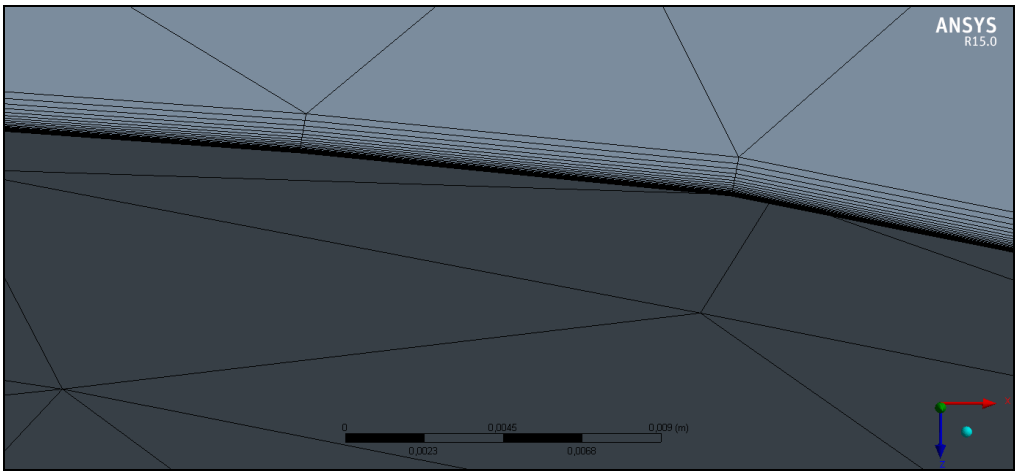

Figure 66: New pod mesh boundary layer.

5.1.3 Prediction method check

Before starting the computational activity on the new pod, a pre-check was conducted on the old pod in order to evaluate the goodness of the CFD model method ([30], [31], [32]) and in case to validate the model generated in ANSYS Fluent. Therefore, a comparison was conducted at Mach number equal to 0.60, 0.80 and 1.20, AoS equal to 0° for a range of total AoA or α_t[2] at sea level in ISA[3] conditions.

The two method under evaluation were respectively the computational fluid dynamic method (ANSYS Fluent) and a semi-empirical Dornier method, [29]. The benchmark for the preliminary validation were data gathered during a laboratory test campaign conducted in wind tunnel.

[2] Total Angle of Attack is the AoA which consider the deflection introduced by the AoS.

[3] ISA = International Standard Atmosphere; it is an atmospheric model of how the pressure, temperature, density, and viscosity of the Earth's atmosphere change over a wide range of altitudes or elevations. It has been established to provide a common reference for temperature and pressure and consists of tables of values at various altitudes, plus some formulas by which those values were derived. The International Organization for Standardization (ISO) publishes the ISA as an international standard, ISO 2533:1975.

As shown in Figure 67, Figure 68 and Figure 69 the results (for the case of Mach=1.20) obtained calculating the aerodynamic coefficients with ANSYS Fluent matched the Wind Tunnel Test Data better than the predictions obtained using a semi-empirical method; presenting a maximum deviation of the 8% instead of the 10% obtained with the semi-empirical method. Therefore, ANSYS Fluent was deemed to be the best option for aerodynamics coefficient prediction in the entire operational envelope of the new pod, with the declared purpose to reduce the number of required experimental test flights, that equals to time and money saving.

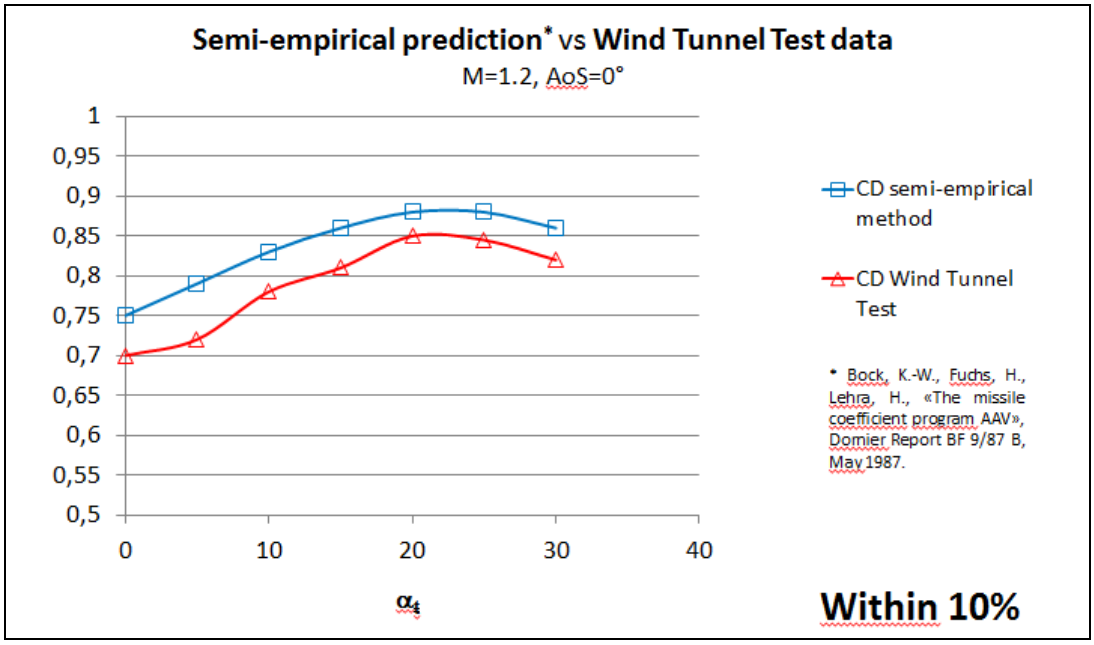

Figure 67: Old pod data comparison: semi-empirical vs WTT data.

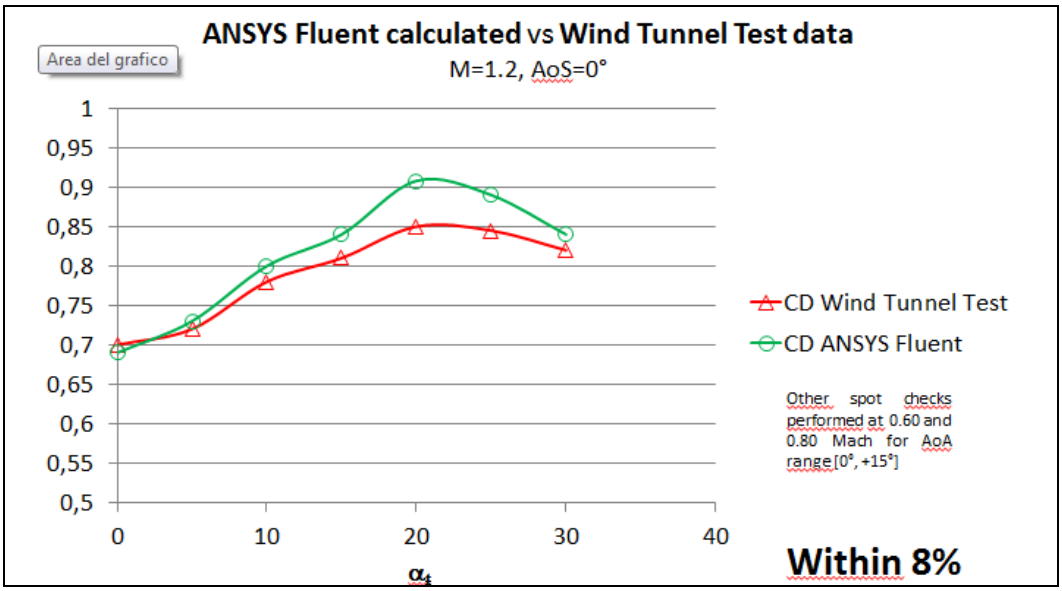

Figure 68: Old pod data comparison: ANSYS Fluent vs WTT data.

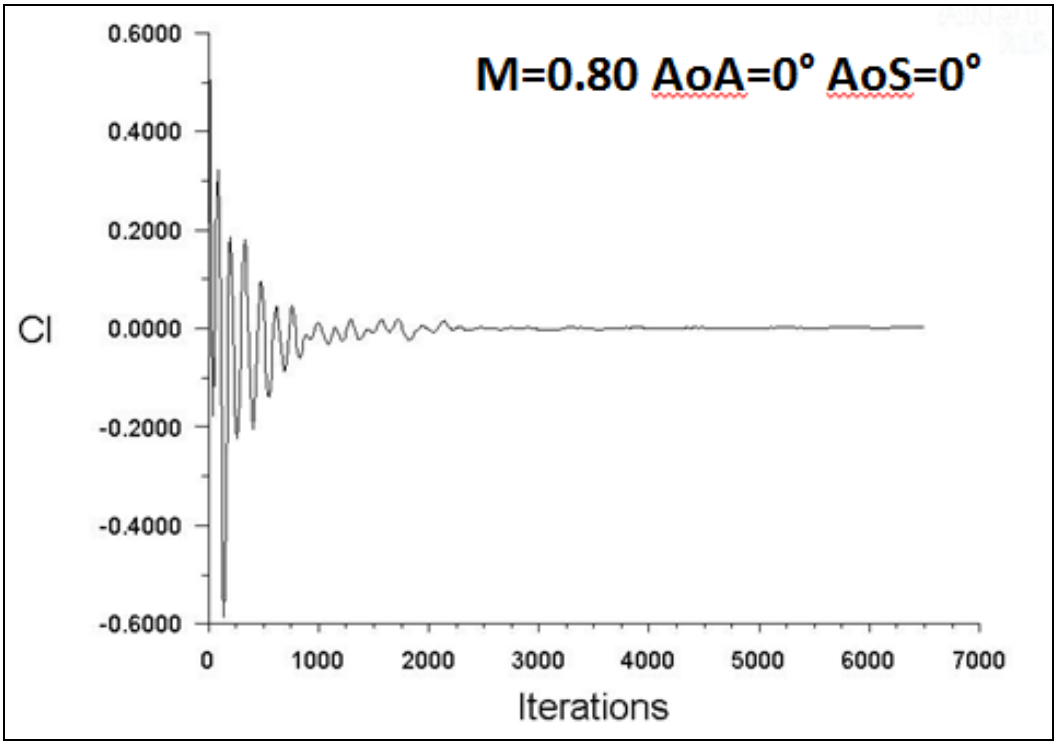

Figure 69: Old pod Lift Coefficient ~0.0.

5.1.4 New pod performance evaluation

The performance evaluation consisted in the comparison between the two following configurations:

- Configuration A = Aircraft + OLD pod;
- Configuration B = Aircraft + NEW pod.

The approach was based on the assumption that a variation of the total asset C_D, drag coefficient, between the two aforementioned configurations, A and B, not higher than a 5% could be considered sufficient to allow the read-across of the performance data without involving additional flight test for performance data gathering purposes.

In order to speed up the computational phase the requirement was translated at store system level:

$$\frac{\Delta C_{D_{pod}} S_{pod}}{C_{D_{old\ pod}} S_{pod} + C_{D_{vel}} S_{vel}} \leq 5\%$$

The reference area in the computational process for the two pods was assumed to be the same.

For the new pod the aerodynamic coefficient, C_L, the associated pressure distribution and velocity field were analysed in the entire operational envelope showing full compliance with the performance requirement (difference between the two pods not higher than 5%). As an example of the relevant calculated data, Figure 70, Figure 71 and Figure 72 show the drag coefficient, the lift coefficient and the polar of the new pod at Mach number equal to 0.60 and AoS= 0° for a range of total AoA [-30°; 30°], at sea level in ISA conditions.

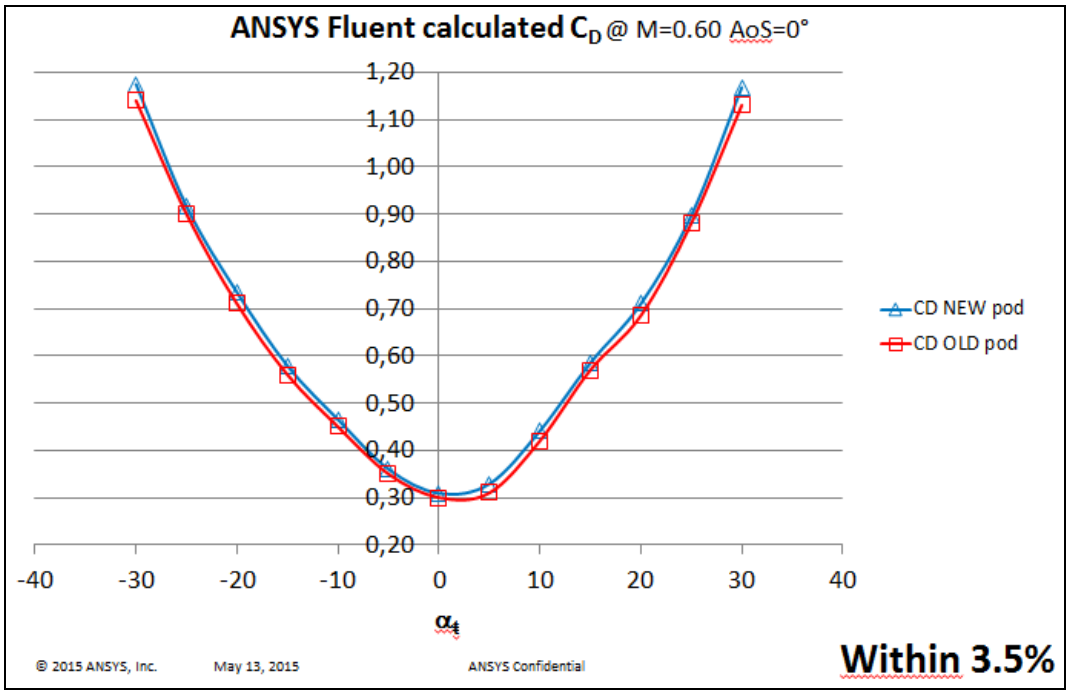

Figure 70: New/Old pods Drag Coefficients.

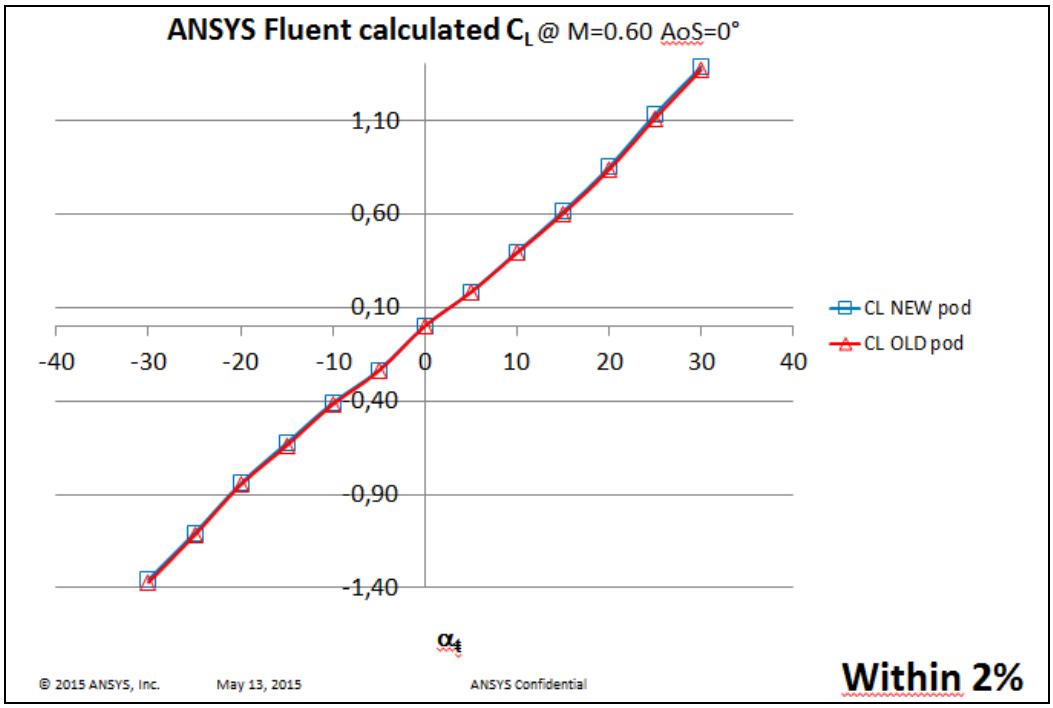

Figure 71: New/Old pods Lift Coefficients.

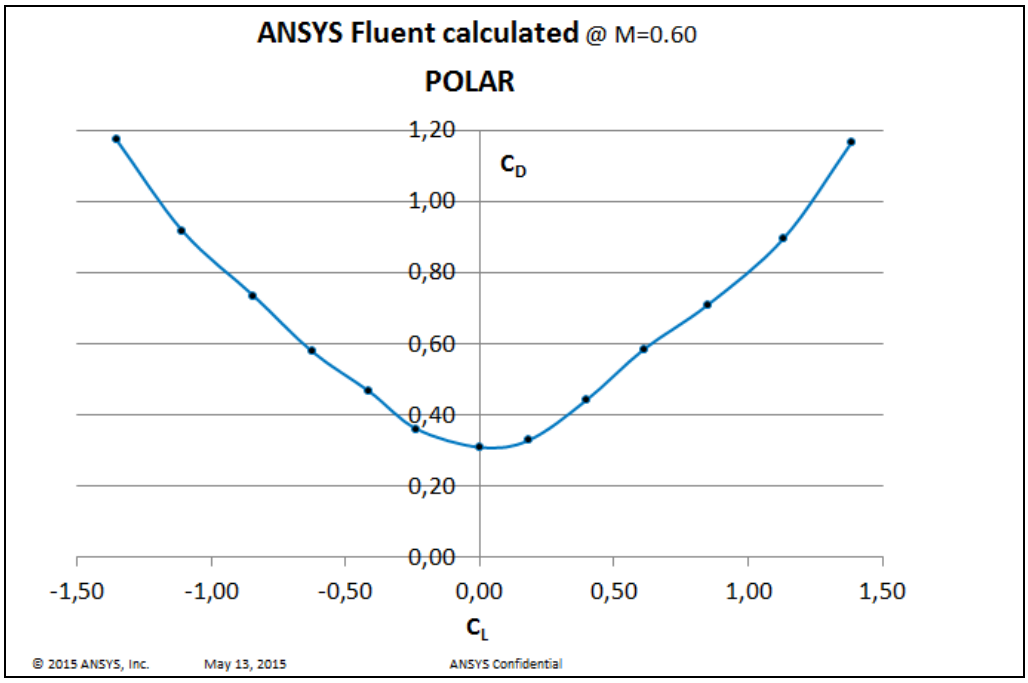

Figure 72: New pod Drag Polar.

In

Figure 73 is shown the trend assumed by the drag and lift coefficient of the new pod with Mach variation; it is interesting to remark the drag coefficient trend presents, as expected, an exponential increase passing through the transonic area, [38]. The lift coefficient is almost zero, slightly negative, probably due to the asymmetric combined effect of the pod air intake and Auxiliary Antenna Unit AAU in the lower portion of new pod.

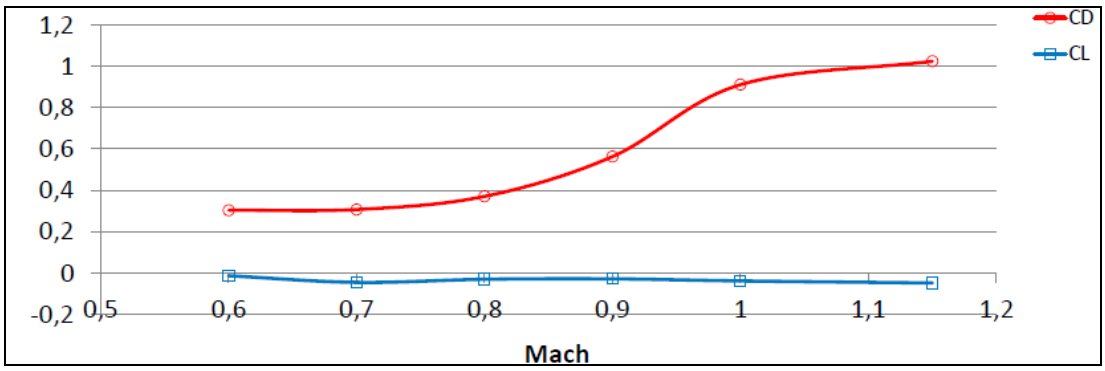

Figure 73: New pod C_L e C_D variation with Mach.

However, in order to validate also the new pod ANSYS model, not having any wind tunnel test data and looking for a more realistic reference, ten test flights were performed (actually only 3 were completely dedicated to performance evaluation). Figure 74 shows the test points executed.

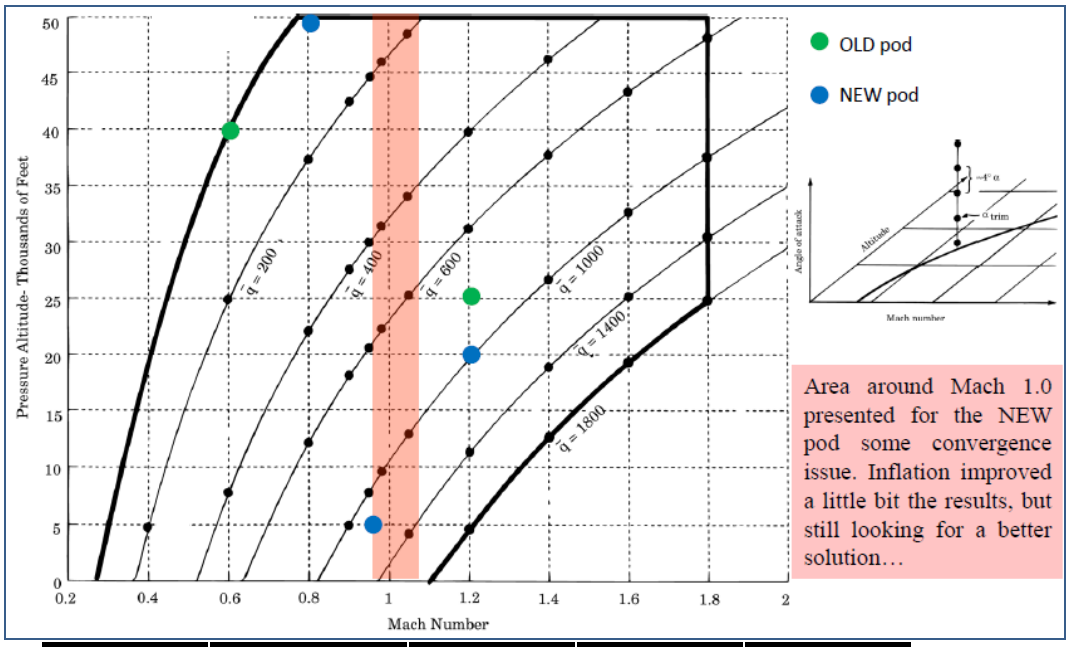

Mach	Pressure Altitude [Kft PA]	AoA [deg]	AoS [deg]	Test Item
0.60	40	10	0	OLD pod
1.20	25	0	0	OLD pod
0.80	45	15	23	NEW pod
0.95	5	0	10	NEW pod
1.20	20	20	0	NEW pod

Figure 74: Flight test spot checks.

Some minor convergence issues were faced in the transonic and sonic area, partially solved via inflation, however further

investigation is still required in order to discriminate the problem trying to understand if there was a calculation issue, an FTI issue or a combination of them. This was a kind of expected computational drawback, in fact when the flow conditions are considered "benign or moderate", CFD analysis can predict the aerodynamic flow field with good accuracy. These conditions are typically the low to medium AoA or AoS and the low subsonic or lower supersonic Mach numbers.

Once significant flow separation is present, or at high transonic Mach numbers (approximately 0.90 to 1.10) where very strong shocks are present, discrepancies with test data are likely to be prominent. In typical CFD codes used for full aircraft configuration analysis, turbulence is generally modelled to some approximation in order to provide a reasonably sized problem. The various turbulence models do a fairly good job for small area of separated flow, [33]. Once the separation becomes significant, with large areas of stagnated and recirculating flow, these models generally break down. The result is the under or over-prediction of the separated regions, with the attendant inaccuracies in the surface pressure distribution and integrated forces and moments. When very strong shocks are present, first the shock strength and location are usually poorly predicted, and then the resulting flow separation and recirculation regions are accordingly not accurately predicted. When applying CFD under these conditions, great caution should be taken unless there are test data to either validate the results, or to calibrate the errors of the computations. Even under benign flow conditions, CFD can still be misleading when applied to certain regions of the aircraft shapes flow field. For example, applying CFD in a boat-tail region, perhaps in an aft-facing step area or in area of the exhaust nozzle, significant flow separation can exist even for benign flow conditions. Drag calculations for a configuration with aft-facing steps will likely be inaccurate. Configurations with landing gear in the flow

stream are similarly troublesome. Landing gear are often complex shapes, both difficult to model in the computational grid, and difficult to compute for the CFD flow solver. It is often desired to evaluate the increment of drag with landing gear down versus landing gear retracted, and thus the temptation to use CFD methods to evaluate this early in the design stage. Again, caution should be exercised in these areas of interest unless wind tunnel data is available to calibrate and correct the results. For the reasons, determining the flow for an aircraft/store combination can be extremely difficult.

Performance wise overall results of the test flight phase demonstrated a good matching between new pod prediction (calculated data via ANSYS Fluent) and data gathered in flight, no more than 7% off including the area around Mach=1.0; less than 5% excluding that area. Furthermore, a very good matching between new pod prediction and old pod prediction ≤ 5%, in all simulated flight conditions in the entire operational flight envelope. As anticipated above, it is still pending a verification around the M=1.0 area in order to understand if there was a calculation issue, an FTI issue or a combination of them.

Therefore, being the performance of the new pod within the required tolerances (≤ 5%), a Declaration of Acceptable Performance Degradation was released by the Certification Authority and the following data were read across from previous cleared old pod:

- Fuel consumption charts (cruise, climb in MAX continuous/MAX REHEAT);
- Takeoff-Landing performance (airspeed, distance);
- Specific Excess Power charts;
- Time to climb charts;
- Dive recovery parameter.

5.1.5 New pod flying qualities evaluation

Further analysis was conducted in order to eventually confirm the predicted minor effects that the introduction of the AAU should have had on the Flying Qualities of the total asset (aircraft + new pod). The aim of the analysis was to ensure that the introduction of the AAU would have not generated any unsteadiness, as for example the presence of any unsteady vortex downstream. No significant differences were noticed between steady and unsteady flow calculation.

The most relevant result of the flying qualities qualitative assessment phase was that no unsteadiness was introduced by the AAU for AoS ϵ [0; 23°], therefore reduced number of additional test flights were required for lateral-directional dynamics characterization.

However, for further information, as graduation exercise and for structural verification purposes, the following subset of flight test manoeuvers in the corners of the new pod operating envelope were performed:

- Steady Heading Side Slips, in order to evaluate the aircraft static stability;
- Rudder doublets, in order to evaluate the aircraft dynamic stability;
- Scissors, bank-to-bank, rolling pull-out and push-over, for parameter identification purposes;
- Zero error/boundaries avoidance point tracking and off-set landing to verify the aircraft + pod operational suitability.

As a side-result, which came out ride along the evaluation, it was noticed that increasing Mach number there was the presence of a vorticity area underneath the new pod in the sensors area, having actually a positive stabilizing effect on the airflow, Figure 75; this phenomenon, however, had a decreasing beneficial effect increasing "pilot's pedal feeding" or in a less test environment jargon "increasing the angle of sideslip".

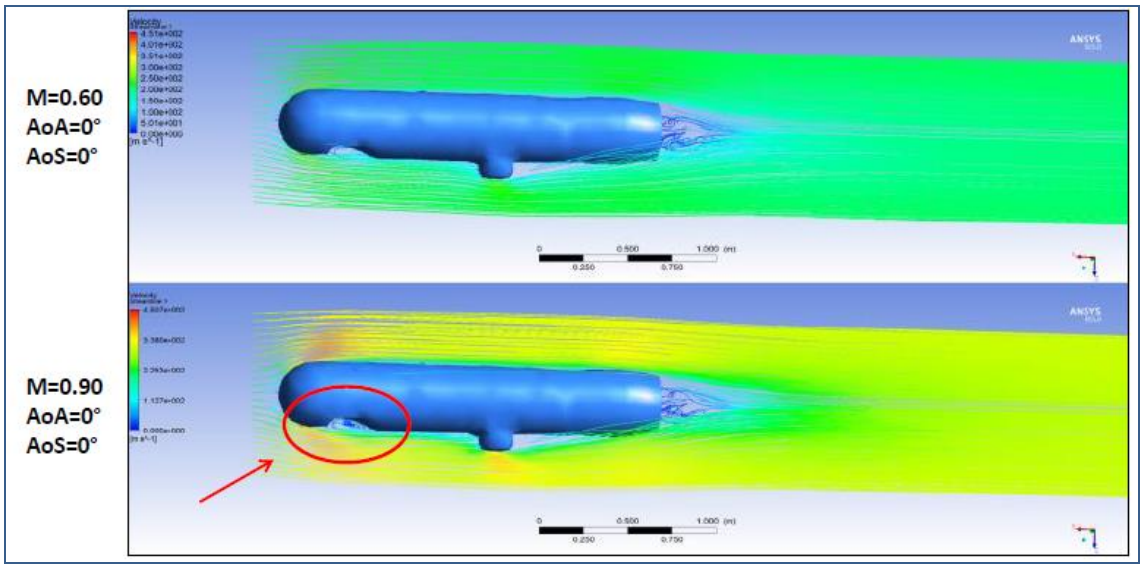

Figure 75: Vorticity in the sensor areas at high Mach number.

Additional simulations were performed in order to evaluate the quantitative effect of the sideslip angle on the aerodynamic coefficients, also for structural verification purposes (of particular interest was the side-force C_Y). In Figure 76 are shown the lift, drag and side-force coefficients at Mach number equal to 0.60 and AoA= 0° for a range of AoS [0°; 23°], at sea level in ISA conditions.

In this conditions the drag coefficient showed small variations, less than 10%, while the lift coefficient increased with a second order polynomial trend and the side-force coefficient with a first order polynomial trend with the increasing angle of sideslip.

AoS [deg]	C_L	C_D	C_Y
0	-0.009	0.3102	0
5	-0,016	0,2749	0,1418
10	0,044	0,2810	0,3635
15	0,196	0,3149	0,6572
23	0,857	0,3398	1,3046

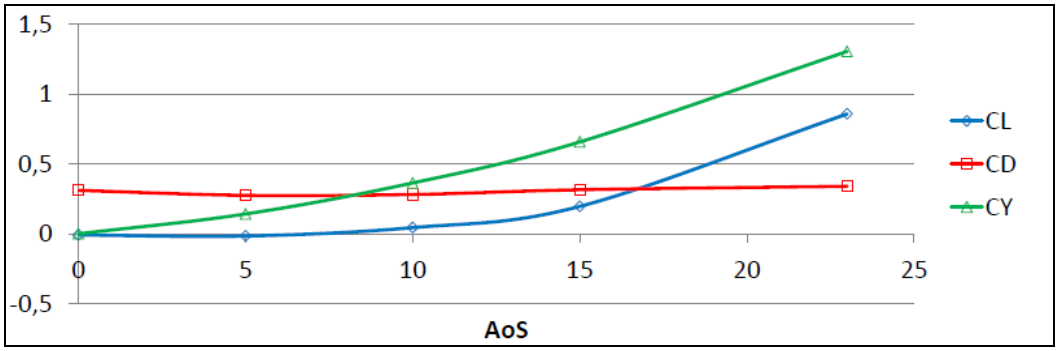

Figure 76: Sideslip angle effects on aerodynamic coefficients.

5.1.6 Conclusions

Overall, it was demonstrated a good match between semi-empirical, ANSYS Fluent and Wind Tunnel Test data for the old pod. Flight test confirmed the goodness of the computational results obtained via ANSYS Fluent simulation, except for the area around Mach 1.0, however, data in that area of the flight envelope were deemed to be still acceptable also if not satisfactory, for the new pod.

The main goal, to achieve an operational capability reducing the number of required experimental flights and associated time and costs, was completed achieved. The Operational Clearance, partially by read across, was released within 36 days, the goal was less than 60, and 10 successful flights (more than 20 flight hours).

Customer satisfaction was achieved.

For sake of clarity it is maybe relevant to highlight that all data presented in this study have been scaled and offset for military security or company intellectual properties reasons.

5.2 A new flight test technique - "Modified WUT".

Ride along the execution of the aforementioned task, the possibility to develop and test a new FTT arisen. The innovative test matrix identification methodology proposed in this study gave the opportunity to perform TPs in flight using a more efficient and effective FTT, that was called "Modified-WUT".

The original WUT manoeuver is a NASA (National Aeronautics and Space Administration) FTT pictorially represented in Figure 77 and described as follows, [34]:

"The windup turn starts from a flight condition slightly higher in altitude than the trim point. (This allows the average altitude of the manoeuver to be close to the trim altitude.)

The pilot begins a level turn, but allows the bank angle to continue to increase beyond that needed for a level turn. As the nose begins to drop due to the increasing bank angle, the pilot begins to slowly increase the angle of attack in a manner which will keep the speed from increasing. In a tricky balancing act, the pilot continues to increase the bank angle while simultaneously increasing the pitch stick force and angle of attack in a manner which will hold the speed constant until the airplane achieves a stall or reaches a g limit. If speed begins to slow, the pilot will increase the bank angle and slow the rate of stick force increase. If speed begins to build the pilot will shallow the bank angle and increase the rate of force increase.

The ideal windup turn is a descending spiral that becomes increasingly tighter and steeper as the g is increased. The values of bank angle required to achieve the test point are not critical to the stick force per g results of the test, but are critical to the establishment of constant speed during the test.

At the end of the manoeuver the airplane is usually in a very steep nose down attitude with quite high bank angles. A fighter will usually end up inverted and in a near vertical dive.

First an initial "hands-off trim shot", followed by a climb to slightly higher altitude. A smooth increase in g and angle of attack results from the smooth

application of increasing stick force. Bank angle is also increased to maintain constant speed as closely as possible. As the angle of attack approaches the stall, buffet can be observed in the accelerometer (g measurement). Following the stall a recovery to level flight is accomplished.
The windup turn is a challenging task for the test pilot. It must be practiced until a smooth increase in g and stick force are achieved with little change in airspeed. It is a relatively gentle manoeuver in a cargo class airplane (1 to 3 g) but more severe for a fighter (1 to 7 g)."

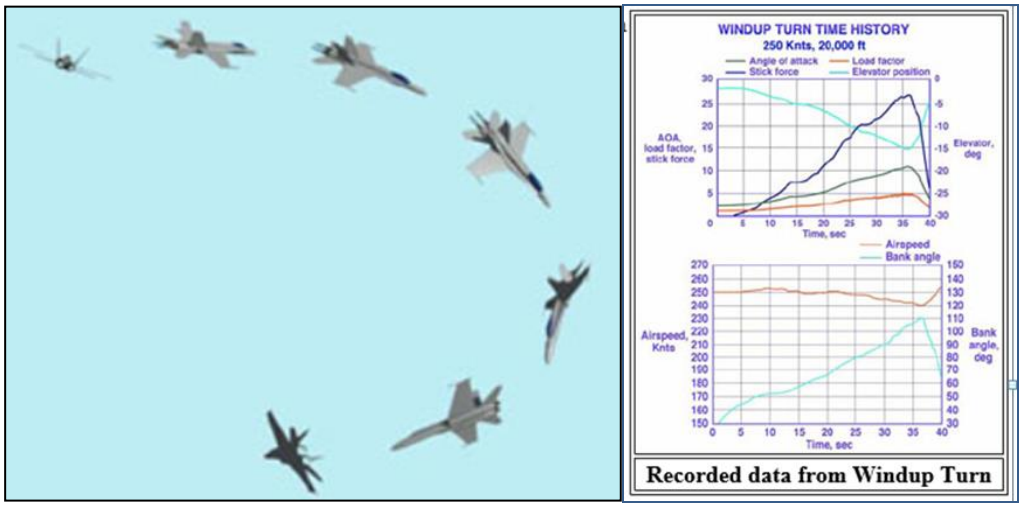

Figure 77: NASA classical (original) WUT FTT.

The Modified-WUT, proposed and tested by the test team, consists in allowing the test pilot to modify during the execution of a classical WUT not only AoA and load factor, but also flown airspeed/Mach number according to a schedule inspired to the efficiency criterion and build-up philosophy as dictated by the test matrix.

The latter being identified via the "Multiple simultaneous test points location method" or the "Flight test matrix design and TPs dynamic relocation method" presented in chapter 2.

Figure 77 shows a possible and actually accomplished execution of 7 different TPs during the same Modified WUT, dramatically reducing time and fuel consumption with reference to the classical 7-step WUT for 7 TPs data gathering activity.

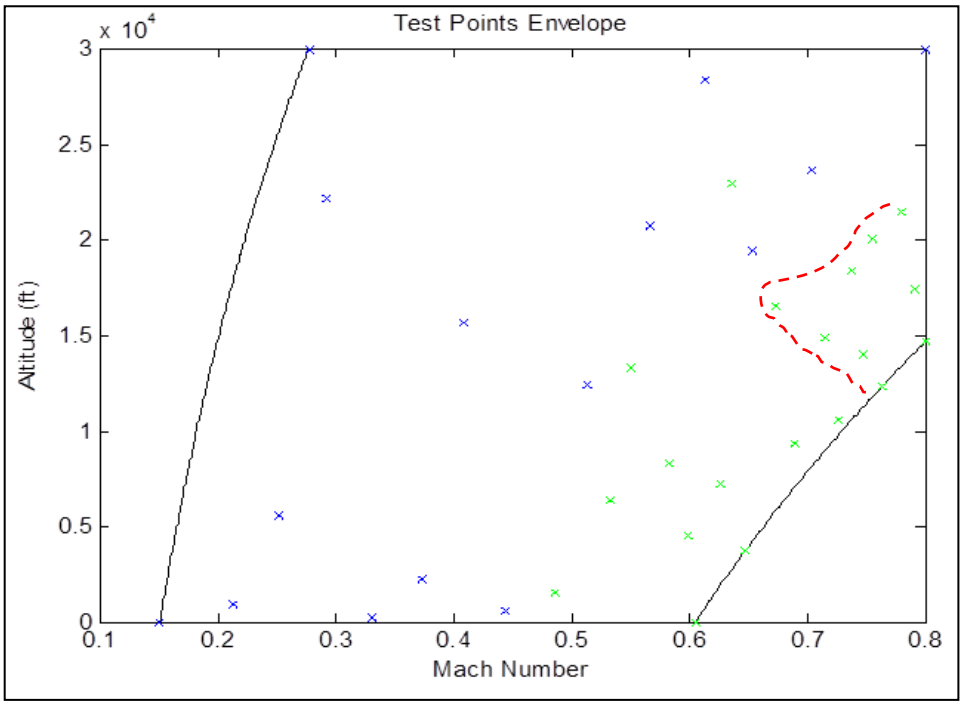

Figure 78: Modified WUT FTT.

CHAPTER 6

VALIDATION DATA GATHERING: TRAJECTORY RECONSTRUCTION CASE STUDY

6.1 A/C/store integration and separation: CFD model validation

Any time a new aircraft is introduced into service, or an old aircraft undergoes substantial modifications or needs to be certified to carry and employ new stores, the store separation engineer is faced with a decision about how much effort will be required to provide an airworthiness certification for the aircraft and stores. Generally, there are three approaches that have been used: wind tunnel testing, CFD analyses and Flight Testing.

During the last thirty years there have been considerable advances in all three areas.

In the early days, store separation was conducted in a hit or miss fashion: the stores would be dropped from the aircraft at gradually increasing speeds until the store came closer to or sometimes actually hit the aircraft. In some cases, this led to loss of aircraft, and has made test pilots reluctant to participate in store separation flight test programs.

During the 60's, the CTS method for store separation wind tunnel testing was developed. The CTS provided a considerable improvement over the hit

or miss method, and became widely used in aircraft/store integration programs prior to flight testing. However, it was not utilized in an integrated approach.

During the late 70's and early 80's, Computational Aerodynamics had finally matured to the point of providing a solution for a store in an aircraft flow field. However, instead of leading to a renaissance in store separation methodology, it mostly led to an ongoing argument among the three groups. The CFD community claimed they could replace the wind tunnel, the wind tunnel engineers said the CFD was unaware of the complexity of the problem, and the flight test engineers said neither group could provide them with the necessary data to conduct a successful flight test program.

Since the time that CFD was first capable of representing the geometric complexity of an attack aircraft with external stores, there has been the desire to replace/reduce the need for wind tunnel testing. The three detriments for full utilization of CFD for this purpose were computational speed, computer resources and accuracy of the solution.

The most critical feature that determines a store separation trajectory are the carriage moments, which are principally caused by the aircraft flow field. For this reason, the first step in separation analysis is to estimate the region of the flight envelope that might have the worst carriage moments. This is done by deriving an estimate of the aircraft flow field. The primary analytical tool for this purpose to evaluate the aircraft aerodynamics in the early 80's was the linear potential flow technique.

From 90's the US Air Force and Navy have made an incredible effort to validate and accelerate the insertion of CFD methods into the store certification process. Nowadays it seems that CFD for external stores has reached a mature phase. The US Air Force, Army and Navy have long-term, proven CFD modelling and simulation experience and software development expertise that has supported advanced weapon development and integration. Each uses unique CFD codes to augment traditional sources of engineering data such as flight and wind tunnel testing.

The flight test process is the most expensive part of store separation testing, and thus can lead to the most overall savings.

An Integrated Test and Evaluation approach to store separation seems to be most reasonable: CFD produces first predictions, then wind tunnel data

add a preliminary refinement to the model. Pit drop and flight test spot checks could validate the refined model or help to fine tune iteratively the prediction CFD model, [23].

6.2 Pit drop testing

Pit drop testing, Figure 79, is one of the essential pre-flight test procedures that allow monitoring functionality of lanyard, separation characteristics and arming system. This type of testing, allows engineers to perform a preliminary validation of the prediction model (aerodynamic model) and to evaluate how:

- aircraft is physically affected by release of store;
- store on-board computer works;
- store components are affected by mechanical shock loads.

Especially following data are very important for evaluating airborne ejections:

- ejection force;
- ejection velocity and acceleration;
- pitch, yaw and roll rates.

Relevant data could be collected by accelerometers, gyroscopes and/or photographic records.

Figure 79: Pit drop testing example.

In is shown a screenshot of a classical tool (TracEye SW) for trajectory reconstruction and pit drop analysis, based on the analysis of high speed

camera data and an example of the outcome of the aforementioned analysis. The activity was performed at the RSV facility in Pratica di Mare by the Aero-mechanic Branch of the Technical Division, integrating a multi-weapons system on a 3rd generation fighter type A/C.

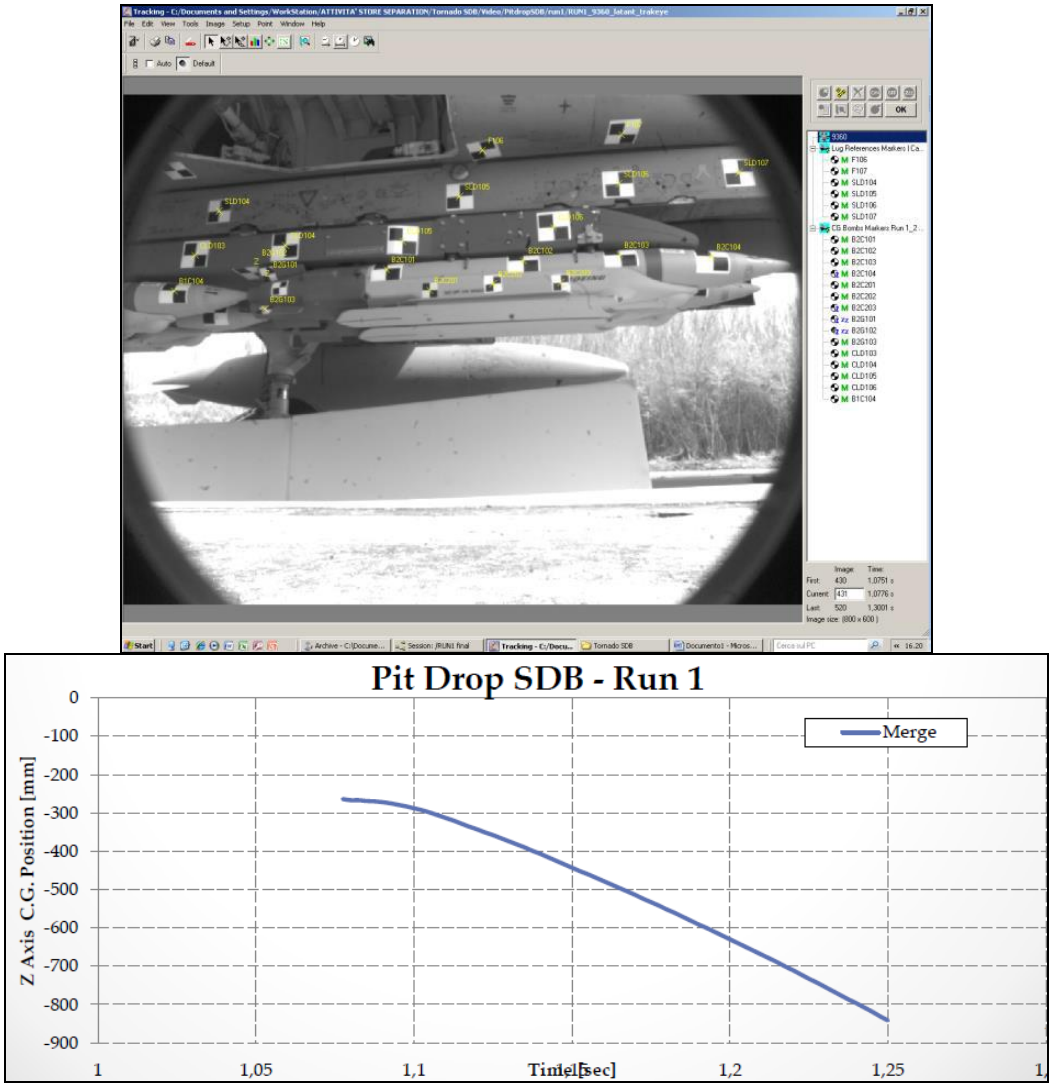

Figure 80: Pit drop post-flight analysis example.

Pit drops are very beneficial, however, flight test, where safe separation is evaluated, is the most critical and relevant step for a new external store certification. Understanding of how a store reacts when released from a flying platform provides engineers, the ability to identify the safety issues

which may cause risks for the aircraft and the pilot. Moreover, understanding how a released store reacts also provides the knowledge required to develop accurate and safer systems. As already stated, a series of experimental data collection have been performed for model validation purposes during the integration of new stores on a 3rd generation jet activity.

6.3 Store separation testing

One of the methods to verify the store-vehicle compatibility is recording of separation using on-board high-speed video cameras. It is important to choose proper air-borne high-speed cameras which may overcome high g loads and high vibrations. Generally high-speed cameras have random memories, and permanent memories. Once powered up the camera begin to record images and store them in a circular buffer to internal random memory. To store the recorded images permanently in cameras internal memory or any other storage, high-speed camera needs to be triggered. This mechanism allows the user to store the images recorded a specified time before triggering, to the random memory. The time gap should be designated so that the stored film covers the whole separation process. Connections of the high-speed cameras should be made depending on test requirements. Arranging the proper connections, high-speed cameras can be triggered by jettison or release signals generated by the aircraft/flying platform.

Stamping time data on the recorded images is also important to match the images and other flight test data on a common time base in means of post-flight analyses. IRIG-B may be used as a common time reference, if available. The high-speed camera should synchronize each frame to this reference time.

High-speed camera locations should be chosen where the separation can be observed clearly. To provide the clear line of sight, high-speed cameras can be located in external wing-pods or in any part of the fuselage in direct free air stream. Also the sunlight exposition, therefore the day-time of the air-drop, is a significant parameter to take into account for this kind of safe separation testing in order to gather usable video/data.

To carry the high-speed cameras in an external pod, the external pod should be modified, or a new external pod should be produced. In Figure 81 is shown an example of a camera pod used in flight test.

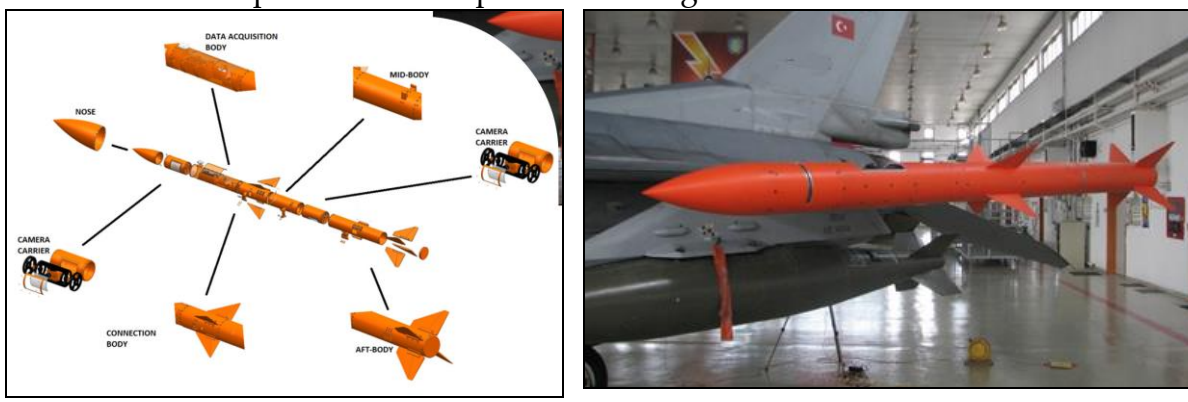

Figure 81: Camera pod example.

Jettisonable store and its background (drop-tanks, wing, fuselage, etc…) need to be marked so that the movement of the marked points on the store can be observed with respect to the background (reference system) by the software that is used for post-process analysis of the recorded images.

Typical targets on the cruise missile and the background are shown in Figure 82.

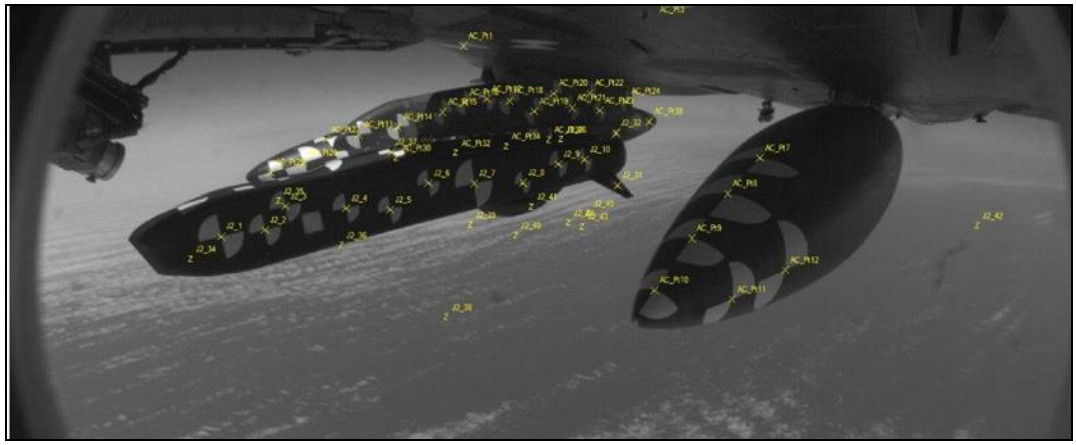

Figure 82: High-Speed Camera Picture

As already noticed, light condition is a big challenge in in-flight high-speed camera recording. Under the wing tip the store may be in shadow and after the release it may be in bright sunlight, after the release there may

also be a variety of backgrounds as white cloud, blue sea, green forest, white snow, etc... The camera system chosen should overcome this lighting and manage the variety of possible conditions.

The safe separation trajectory is identified by post-flight processing of the images recorded by high-speed cameras using photogrammetric methods. After the methodology for photogrammetric safe separation analysis is determined and the analyses are performed, the results are compared to the results of computational fluid dynamic analysis to verify consistency and in case to validate the CFD model.

Photogrammetry is the technique used to extract reliable measurements from video of the test item and the environment. A photogrammetric solution consists of a 6-DOF time history, from which centre of gravity3D position/velocity and Eulerian angles/rates can be computed.

An important parameter that is evaluated based on the 6-DOF analysis is the separation distance between the moving store and the external surface of the test aircraft (fuselage, external loads, etc…).

6.4 Integration of SDB on ItAF Tornado A/C

Verifying the simulated behavior of a store during flight test is a technically complex issue. Specific analysis are performed to quantify a store position and dynamics after its release from an aircraft, using dedicated photogrammetric SW. Information obtained are typically used to validate the accuracy of a prediction model or to determine if the separation characteristics are safe enough to proceed with more severe (less safety margin) release conditions.

A photogrammetric project of a SDB I released from a Tornado aircraft is presented as a case study. The aim of the activity was to provide quantitative data of the separation testing to the store contractor in order to validate the separation aerodynamic model.

The SDB I system is the next generation of low cost precision strike weapons for employment from fighters, bombers, and unmanned combat air vehicles. The SDB I system is comprised of the GBU-39 Precision Guided Munition and the BRU-61 MIL-STD-1760 pneumatic 4-place carriage rack. The SDB I munition leverages a new level of precision guidance and

navigation while delivering a hybrid blast-fragmentation/penetrator warhead that provides the weapon effectiveness of larger weapons. The relatively small size of the SDB I munition allows carriage of 4 PGMs on the BRU-61 thereby enabling larger weapon load-outs on a given number of aircraft pylon stations.

Operational testing of the SDB I system on the USAF's F-15E aircraft, Figure 83, has been completed and USAF declaration of operational capability was issued in October 2006. In addition to its ability to be carried and employed from the F-15E, integration of SDB I has been proved on the F-16, F-22A Raptor and F-35A Lightening II.

Figure 83: SDB I carriage on F-15E.

The SDB I munitions physical properties (size and weight) makes it the ideal weapon for all platforms including unmanned vehicles. Existing weapon systems (including direct attack munitions under development) are deficient in one or more of the following areas: insufficient kills per pass; insufficient weapon load-out capability; no or limited adverse weather capability; insufficient precision munitions capability; insufficient capability against hardened targets; enlarged munitions footprints; insufficient weapons effectiveness against area targets; and higher potential for collateral damage. The SDB I System was designed with urban warfighting capability in mind. The SDB I system enables strike aircraft to increase the number of targets attacked per sortie while inherently limiting collateral damage against unintended targets.

In addition, the SDB I System delivers precise, penetrating weapons, day or night, in adverse weather from stand-off ranges. In the early stages of a

potential conflict, the SDB I System is envisioned to be utilized on surface attack missions against offensive counter air targets. Equally important are Suppression/Destruction of Enemy Air Defenses (SEAD/DEAD) missions where achieving air superiority is the primary objective. Increased load-out (leading to multiple kills per sortie) of SDB I weapons allows a limited number of initial combat forces to achieve operational objectives early in the conflict, paving the way for follow-on forces.

GBU-39/B Munition

The 250 pounds class GBU-39 munition, Figure 84, comes equipped with an Anti-Jam Global Positioning System/Inertial Navigation System (AJGPS/INS) guidance system that provides navigation of the weapon to the target coordinates. Typical target set includes Command Control Communication Intelligence bunkers, air defense assets, airfield targets, infrastructure targets, missiles, artillery. A wing assembly is also attached to the weapon providing additional range. This increased range capability puts more enemy aim-points within the footprint of the releasing aircraft thereby allowing the launch aircraft to prosecute more targets on a single pass. The GBU-39/B payload is a highly effective hybrid warhead affording the warfighter both penetration and blast and fragmentation capabilities. The warhead is coupled with a cockpit selectable electronic fuze. The weapon's
design has been optimized to limit the effects of collateral damage due the combination of its precise accuracy and a smaller 250 pounds class warhead containing thirty-six pounds of energetic explosive fill. In addition, the warhead has been qualified to meet Insensitive Munition requirements. A Height of Burst sensor is incorporated to provide additional flexibility in defeating a variety of threats.

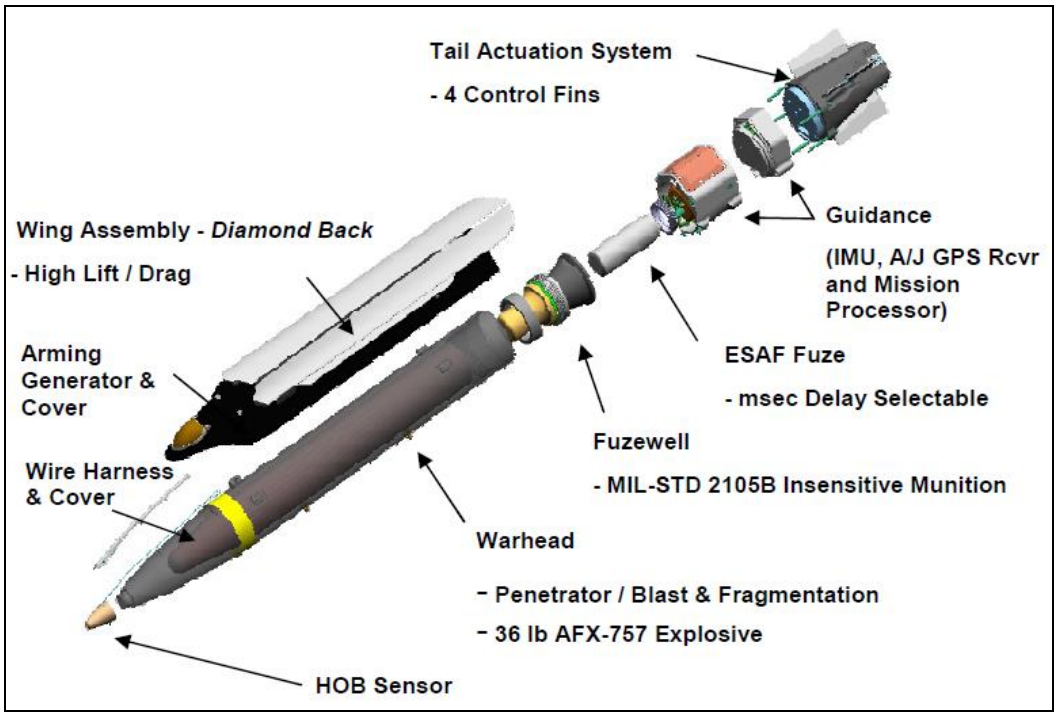

Figure 84: GBU-39/B munition.

BRU-61/A Carriage System

The 4-place pneumatic carriage system has its own avionics and four weapon ejectors units. The carriage system interfaces with the aircraft via a MIL-STD-1760 umbilical cable connected to the aircraft stores pylon, providing both aircraft electrical power and 1553 digital data aircraft stores management interfaces. The carriage system is uploaded and fixed to the aircraft pylon by standard weapon suspension lugs configured to support either standard 30 inch or 14 inch spacing. The carriage avionics provide stores management functions, weapon initialization and control including Launch Acceptability Region generation, weapon health monitoring, and aircrew training functions. The management of these functions by the BRU-61 rack results in a simplified aircraft integration while providing feature to facilitate in-flight planning. The pneumatic ejector units provide a long ejection stroke with lateral constraint and selectable end of stroke velocity/pitch rate. This further simplifies aircraft integration tasks associated with weapons clearance process per individual aircraft type. The

BRU-61, Figure 85,with its rechargeable energy source requires little maintenance resulting in design results in low life cycle costs.

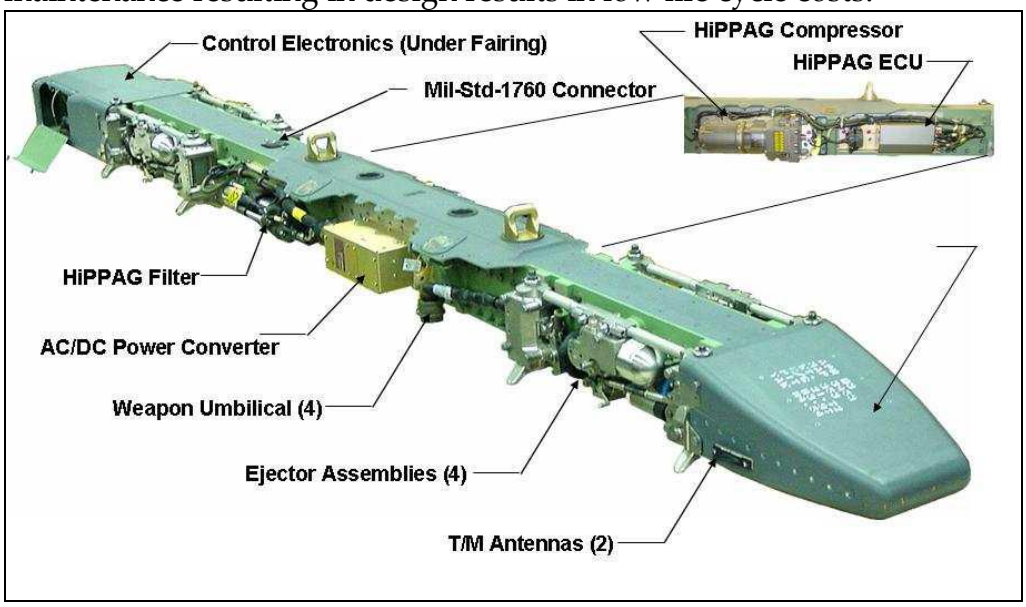

Figure 85: BRU-61 carriage system.

A photogrammetric project of a Small Diameter Bomb released from a Tornado aircraft is presented.

The post-flight analysis activity was performed in order to analyze the store separation videos, gathered during different test flights executed in different A/C load-out configurations (operational representative), and obtain time complete 6DoF data by using Image System TrackEye photogrammetric SW.

In Figure 86 is showed the typical interface of the TrackEye SW to generate the algorithm necessary for the image sequence analysis, in case of a two high speed camera merging (a sort of stereoscopic view analysis). The relevant steps to be performed are the following:

- Image & Camera setting;
- 2D tracking options definition;
- Merging for multiple cameras analysis;
- Cameras calibration & reference points setting;
- Cameras distortion correction;
- 6DOF calculation;
- 2D diagram and data generation.

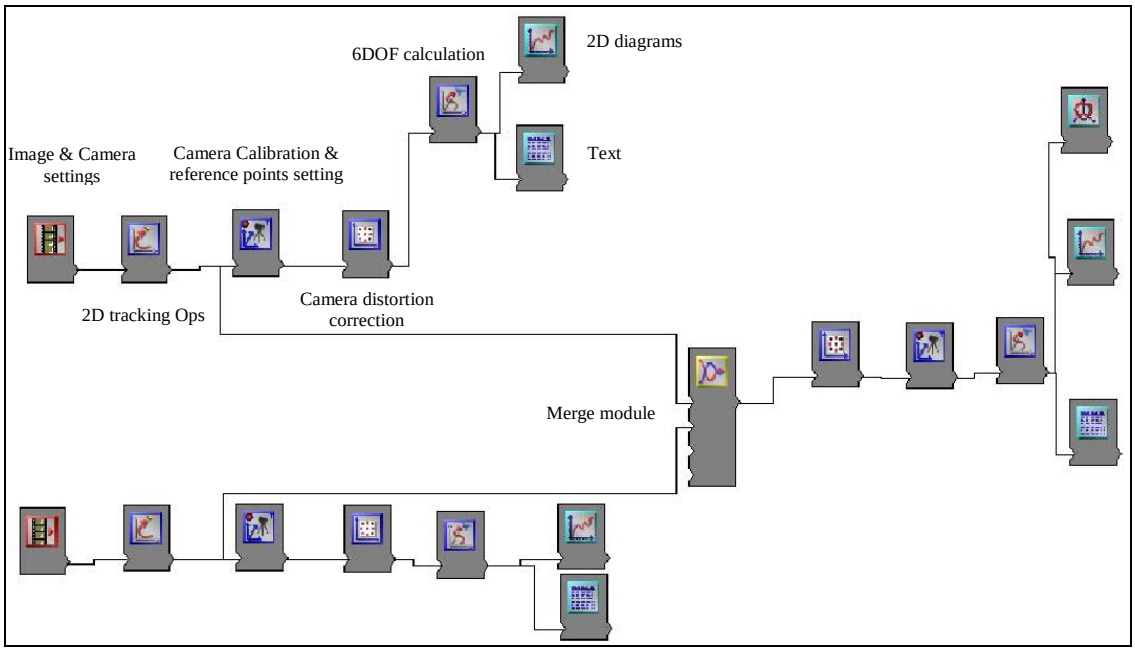

Figure 86: TrackEye analysis sequence.

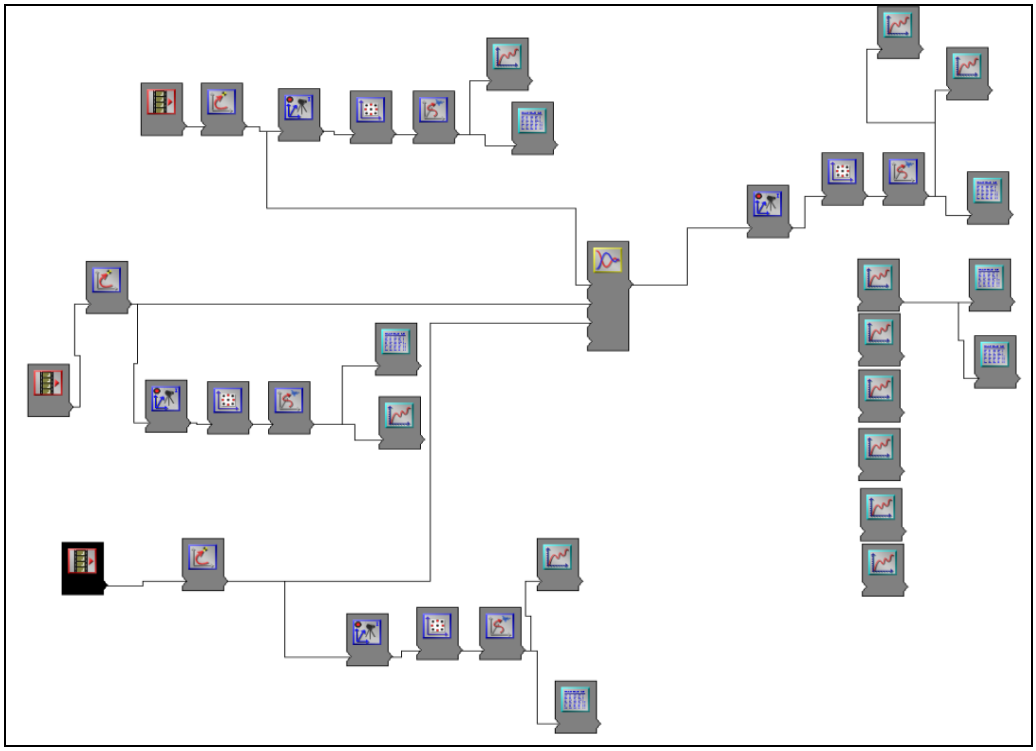

Figure 87: TrackEye algorithm used for post-test analysis.

In

Figure 87 is presented the algorithm used in order to analyze data gathered in a three cameras high speed camera (Phantom MIRO3) configuration: two cameras accommodated in left/right underwing pods and one housed in the forward avionic bay behind the nose landing gear compartment looking backward, Figure 88. The latter algorithm and cameras configuration has been used to gather, reduce and elaborate data for the following presented results.

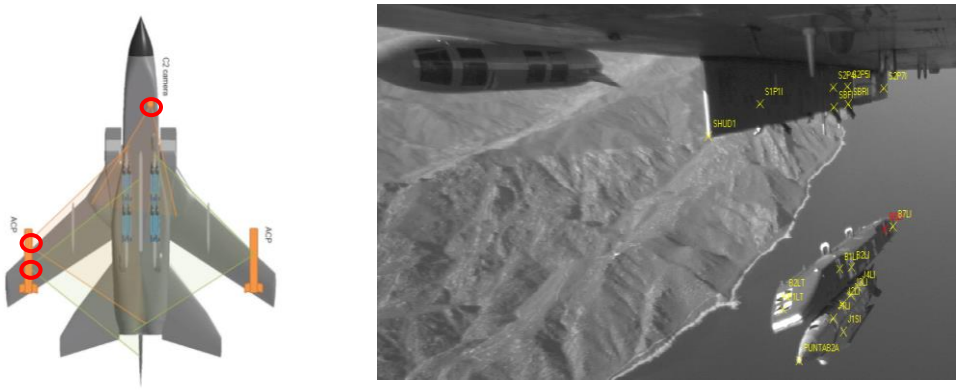

Figure 88: On-board cameras installation.

Several store release conditions were tested during the flight test campaign (12 in total), however, in this thesis, only the results of two configurations, Figure 89, safe separation analysis are presented.

Config. nr	Store to be released	Carrier starting configuration	Mach nr	KCAS	Altitude
J3	C	A+C	0.90	400	--
B2	Carrier + A	A	--	350	5000

Figure 89: Stores release conditions.

The aircraft, carrier and stores were properly targeted. Released test item targets are called *moving targets*, while the ones integral to the aircraft structure or portion of the test item not to be released during the test are called *reference targets*. While only three targets are required for a photogrammetric solution, many targets were affixed to ensure a minimum number of targets was available in each video frame and visible by almost all cameras. Relative position of aircraft and stores targets in the reference A/C coordinate system were obtained by using FaroScene laser scanner already presented in chapter 3.

The recorded videos as well as the geometry model built by using the laser scanner RE technique were loaded in the TrackEye SW. Before proceeding with the tracking procedure, distortion correction and camera calibration were applied at the input videos. The tracking procedure consisted essentially in tracking the center of each moving targets, within the reference targets system, frame by frame for the entire duration of the captured experimental video, each point was manually tagged and verified by the user at each time step in order to improve the accuracy level with respect to the automatic tracking feature, provided by TrackEye SW, but deemed too much error prone for the proposed analysis. The most common issue was the loss of targets due to the sunlight reflection or shadowing that had to be fixed by the user performing a kind of interpolation between relative positions of consecutive frame. Unfortunately there is no rule working all the time, user experience a main factor driver. The tracking process was repeated for videos from all cameras. At the end of the tracking process the three cameras tracking outputs were merged and the 6DOF data were computed providing the store (or carrier + store) spatial position (three coordinates x, y, z in the A/C reference system) and relative velocity as well as the three Eulerian angles (roll, pitch, yaw) and relative rates. The merging technique is based on a weighted average of the data provided by the different cameras according to the estimated accuracy of the same data.

Figure 90 shows the data reconstruction process for one of the tested configuration.

Figure 91 e Figure 92show the results obtained from the post-flight analysis of J3 and B2 configuration release flight, executed on behalf of ItAF RSV for Boeing/AleniaAermacchi model validation purposes.

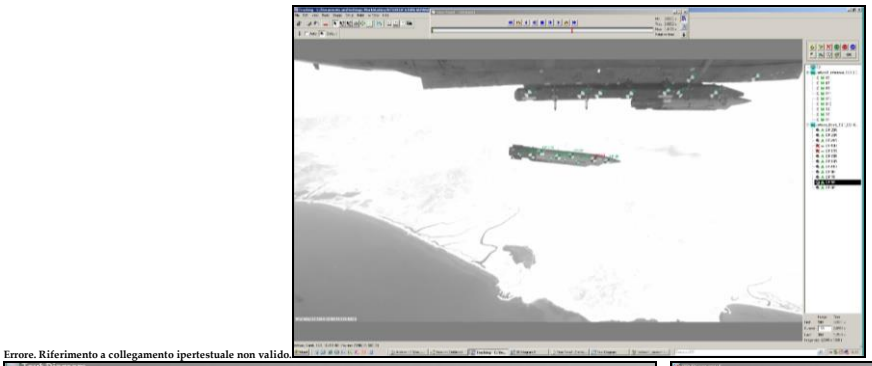

Errore. Riferimento a collegamento ipertestuale non valido.

Test Diagram

File Edit View Setup Window Help

1	CS1:1	CS1:2	CS1:3	CS1:4	CS1:5	CS1:6
Time [s]	Jettison_Bomb_TG... 6D position (m_E2) pos/x [mm]	Jettison_Bomb_TG... 6D position (m_E2) pos/y [mm]	Jettison_Bomb_TG... 6D position (m_E2) pos/z [mm]	Jettison_Bomb_TG... 6D position (m_E2) attitude/roll [degrees]	Jettison_Bomb_TG... 6D position (m_E2) attitude/pitch [degr...	Jettison_Bomb_TG... 6D position (m_E2) attitude/yaw [degre...
0,8166	10872	-399	1359	38,268	-17,999	-36,730
0,8196	10871	-410	1352	38,078	-17,779	-36,802
0,8226	10871	-416	1340	37,962	-17,590	-36,968
0,8256	10872	-422	1329	37,708	-17,386	-37,113
0,8287	10871	-432	1320	37,544	-17,167	-37,232
0,8317	10871	-442	1311	37,286	-16,954	-37,337
0,8347	10871	-450	1301	37,258	-16,747	-37,452
0,8378	10870	-460	1293	37,037	-16,533	-37,532
0,8408	10870	-469	1285	36,721	-16,312	-37,638
0,8438	10871	-474	1273	36,508	-16,126	-37,804
0,8469	10871	-480	1262	36,447	-15,913	-37,969
0,8499	10872	-488	1250	36,445	-15,700	-38,129
0,8529	10871	-502	1242	36,460	-15,438	-38,154
0,8559	10871	-512	1233	36,199	-15,196	-38,269
0,8590	10871	-520	1223	36,069	-14,984	-38,406
0,8620	10872	-526	1211	35,883	-14,769	-38,560
0,8650	10873	-531	1200	35,821	-14,583	-38,731
0,8681	10873	-541	1191	35,717	-14,353	-38,844
0,8711	10873	-552	1181	35,709	-14,117	-38,955
0,8741	10874	-561	1171	35,553	-13,884	-39,091
0,8772	10874	-573	1161	35,525	-13,613	-39,193
0,8802	10876	-579	1147	35,447	-13,390	-39,392
0,8832	10877	-588	1136	35,268	-13,147	-39,538
0,8863	10878	-595	1123	35,268	-12,924	-39,720
0,8893	10878	-609	1113	35,263	-12,639	-39,793
0,8923	10879	-619	1101	35,273	-12,371	-39,930
0,8953	10880	-626	1088	35,212	-12,135	-40,110
0,8984	10882	-632	1075	35,088	-11,905	-40,292
0,9014	10882	-642	1064	34,841	-11,642	-40,420

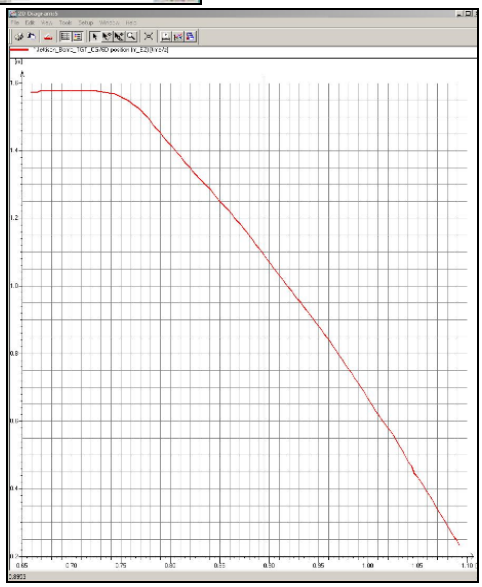

Figure 90: Post-flight trajectory identification.

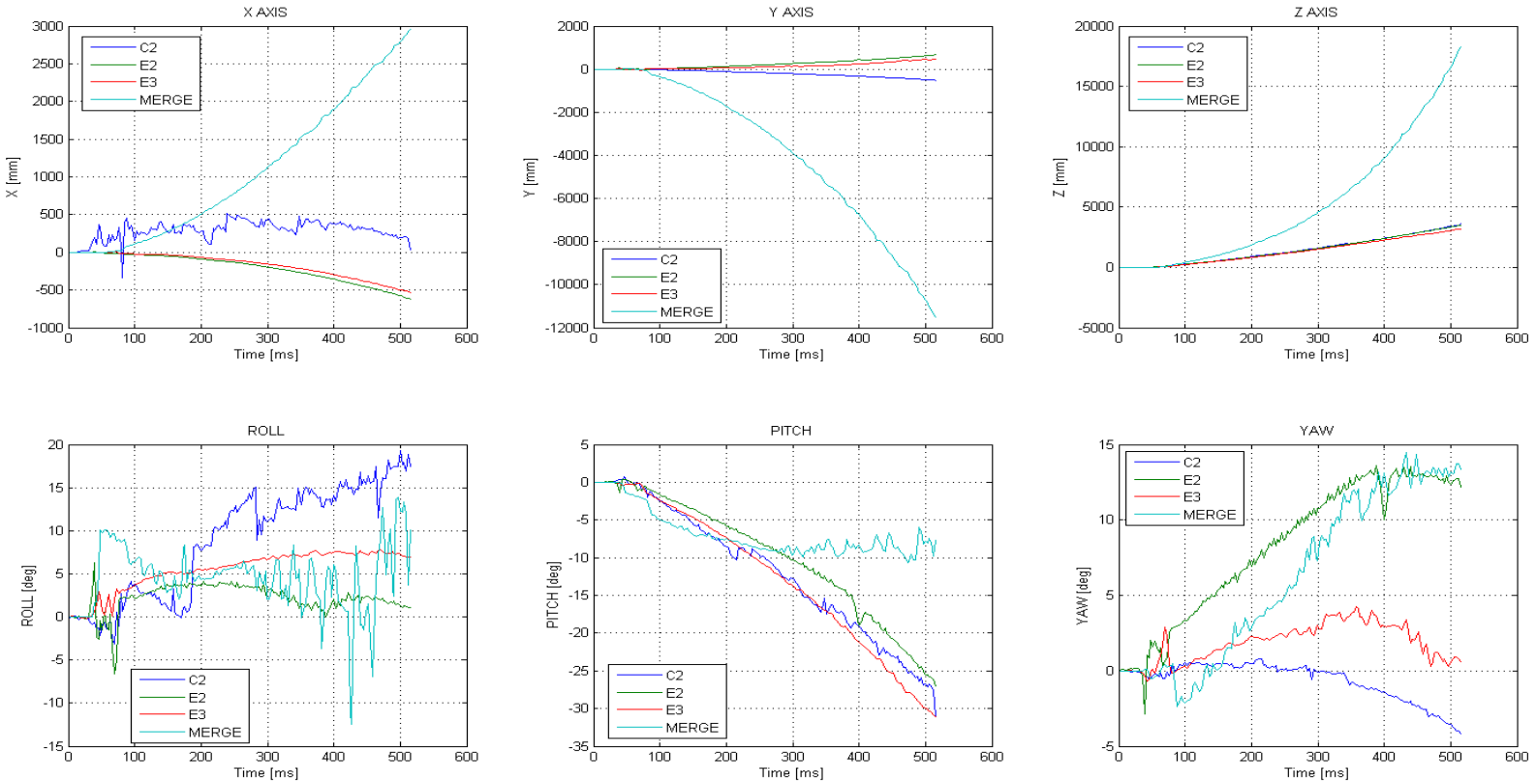

Figure 91: J3 configuration analysis.

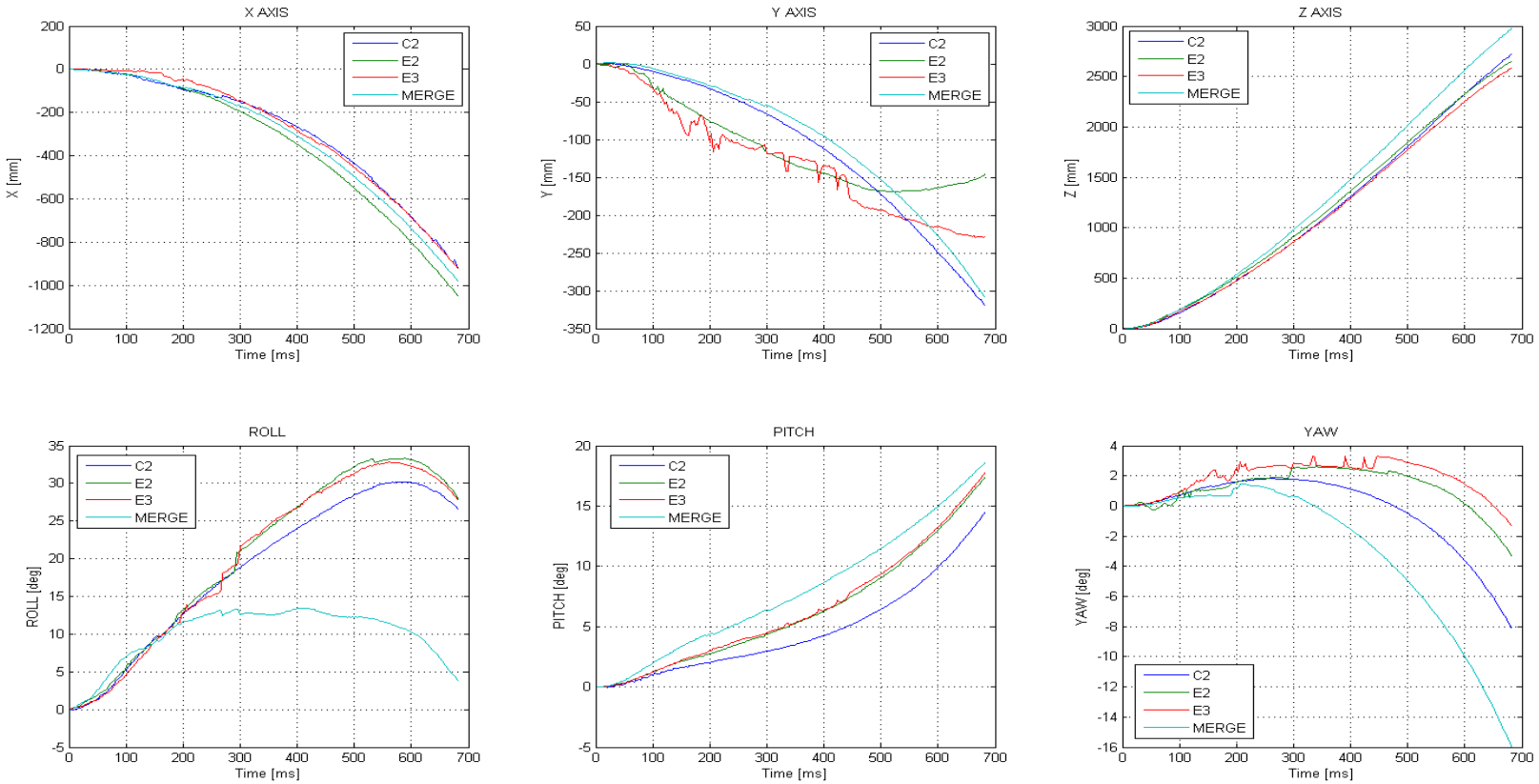

Figure 92: B2 configuration analysis.

CONCLUSIONS

Flight testing has always been a balance between research and risk management; within the risks to be taken into account there are not only technical issues (i.e. in-flight mishap risk mitigation activity) but also programmatic concerns related to time constraints and cost containment.

Safety of flight is paramount in the experimental field where huge amount of money and skilful (almost priceless) crew are necessary to perform the required envelope expansion flights.

Furthermore, the cost of one hour of flight test on a unique prototype jet aircraft could range between of 15-20K€ and 1M€ and in case of failure or mishap, the test program could stop from days to months with increasing costs.

Many test program are driven by urgent operational needs, therefore a timing response to the customer is relevant for the success of the experimental process.

The mind-set change from the fly-fix-fly philosophy to the predict-test-validate paradigm has introduced a different approach into flight test environment, expanding the focus to prediction and model validation phases. Increasing computational capabilities, paired to the development of adequate SW solver, and reliable reverse engineering methodologies have improved the opportunity for a successful fluid dynamic numerical analysis.

Cost reduction, safety risk analysis and time efficiency have been improved by the introduction of these new technology.

However, proliferating the driving factors it is essential to focus the attention on coordination among the single procedural steps of this complex process. Most times the inefficiency resides in interface moments where the gaps of information transfer produce delays and uncertainty. Furthermore, the choice of the right tool per each test/certification step is essential in order to standardize the test approach and therefore the associated analysis and results.

In this study itinerary and in particular in this thesis, an all-encompassing test management method has been analysed and proposed for the testing and certification process of a new store integration on a fighter type aircraft. Of course,

many of the tools identified could be used *sic at simpliciter* to different case studies or testing activities, other would need some adaptations.

Optimization has been achieved developing forward and reverse engineering geometry acquisition technique (identifying associated SW and tools), innovative TPs management and test matrix identification, proposing new CFD model, FTTs and approach analysis and eventually setting a validation process based on trajectory reconstruction technique.

Each step of the test/certification process has been tested against a real activity and a final graduation exercise overarching the majority of the aimed objective has been conducted for a new reconnaissance pod integration on a 5th generation fighter type A/C.

The appointed level of ambition has been met and the way ahead of the research path introduced should be the integration of the current procedure defined for store integration with additional prediction tools based on a structural model of the assembly A/C + store load-out usable for FSI and, therefore, aero-elastic analysis. The declared aim is not to replace flight test, this would be unrealistic and counterproductive, but to improve safety of flight and speed up test campaign conclusion and cost reduction via a comprehensive test management approach based on innovative tools, techniques and ideas.

REFERENCES

[1] Seeking the Proper Balance Between Simulation and Flight Test. AIAA Flight Test Technical Committee, 01 October 1999.

[2] ANSYS webpage: www.ansys.com

[3] Hou G., Wang J., Anita Layton, Numerical Methods for Fluid-Structure Interaction, Commun. Comput. Phys., 12 (2012), pp. 337-377.

[4] Michler, C., Hulshoff, S. J., van Brummelen, E. H. and de Borst, R., A monolithic approachto fluid-structure interaction, Computers & Fluids, Vol. 33, 2004, pp. 839-848.

[5] Basar T. and Olsder G.J. (1999), Dynamic non-cooperative game theory, Reprint of the second (1995) edition. Classics in Applied Mathematics, 23. Society for Industrial and Applied Mathematics (SIAM), Philadelphia, PA.

[6] Drezner, Z. (1995) Facility Location: a Survey of Applications and Methods, Springer Verlag New York.

[7] Fudenberg, D. and Tirole, J. (1993) Game theory. The MIT Press, Cambridge, Massachusetts.

[8] Hansen, P., Peeters, D., Richard, D. and Thisse, J.-F. (1985) The mini-sum and mini-max location problems revisited Operation Research vol. 33, pp. 1251-1265.

[9] Hotelling, H. (1929) Stability in Competition Economic Journal vol. 39, pp. 41-57.

[10] Mallozzi, L. (2007) Non-cooperative facility location games, Operation Research Letters vol. 35, pp. 151-154.

[11] Deb, K. (2001) Multi-Objective Optimization using Evolutionary Algorithms, Wiley.

[12] Mallozzi, L., D'Amato, E., Daniele, E. and Petrone, G. (2011) N leader - M follower coalition games with genetic algorithms and applications. Evolutionary and deterministic methods for design, optimization and control, C. Poloni, D. Quagliarella, J. Periaux, N. Gauger and K. Giannakoglou (Eds.), CIRA, Capua, Italy.

[13] Mallozzi, L., De Paolis, P., Di Francesco, G. and d'Argenio, A. (2013) Computational Results for Flight Test Points Distribution in the Flight Envelope, EUROGEN 2013, Las Palmas de Gran Canaria (Spain), 07th-09th October 2013.

[14] Mallozzi, L. (2013) An application of Optimization Theory to the study of equilibria for games: a survey, Central European Journal of Operations Research vol. 21, Issue 3, pp.523-539.

[15] Monderer, D. and Shapley, L.S. (1996) Potential games, Games and Economic Behavior vol. 14, pp. 124-143.

[16] Periaux, J., Chen, H.Q., Mantel, B., Sefrioui, M. and Sui, H.T. (2001) Combining game theory and genetic algorithms with application to DDM-nozzle optimization problems, Finite Elements in Analysis and Design vol. 37, pp. 417-429.

[17] Anderson, John D. (2007) Fundamentals of Aerodynamics, 4th edition, McGraw-Hill, New York USA. ISBN 978-0-07-295046-5.

[18] Clarich A., Periaux J. and Poloni C. (2003) Combining game strategies and evolutionary algorithms for CAD parametrization and multi-point optimization of complex aeronautic systems, Barcelona, EUROGEN 2003.

[19] Eiselt, H. A., Marianov, V.: Foundations of Location Analysis. International Series in Operations Research & Management Science, Vol 115, Springer (2011).

[20] Hansen, P., Peeters, D., Richard, D., Thisse, J.-F.: The minisum and minimax location problems revisited. Oper. Res. 33, 1251–1265 (1985).

[21] Branzei, R., Mallozzi, L., Tijs, S.H.: Supermodular games and potential games. J. Math. Econ. 39, 39–49 (2003).

[22] d'Argenio: Computational Fluid Dynamics in support to Flight Test Experiments using Optimization Techniques (2015).

[23] Simulation in Support of Flight Testing, RTO-AG-300 Vol.19, September 2000.

[24] Cenko A., Store Separation lessons learned during the last 30 years, 27th International Congress of the Aeronautical Sciences.

[25] Sepe A.M., Integration of a underwing store on a fighter type aircraft: CAD drawing of a rockets launcher for CFD analysis, Aerospace Master Degree, Naples 2013.

[26] Mallozzi L., d'Argenio A., Di Francesco G, De Paolis P., Design of a Flight Test Matrix and Dynamic Relocation of Test Points, EUROGEN 2013, Las Palmas de Gran Canaria (Spain), 07th-09th October 2013.

[27] Mallozzi L., d'Argenio A., Di Francesco G, De Paolis P. (2015), Computational results for flight test points distribution in the flight envelope, Advances in Evolutionary and Deterministic Methods for Design, Optimization and Control in Engineering and Sciences, Edited by: D. Greiner, B. Galván, J. Periaux, N. Gauger,

K. Giannakoglou, G. Winter, Computational Methods in Applied Sciences Series, Springer.

[28] d'Argenio A., de Nicola C, De Paolis P., Di Francesco G., Mallozzi L. (2014), Design of a Flight Test Matrix and Dynamic Relocation of Test Points, Journal of Algorithms and Optimization Vol.2, Issue 3, pp.52-60.

[29] Bock, K.-W., Fuchs, H., Lehra, H., The missile coefficient program AAV, Dornier Report BF 9/87 B, May 1987.

[30] Cebeci T., Shao J.P, Kafyeke F., Laurendau E., Computational Fluid Dynamics for Engineers, Ed. Springer.

[31] Anderson J.D., Computational Fluid Dynamics, Ed. McGraw Hill.

[32] Blazek J., Computational Fluid Dynamics: Principles and Applications, Ed. Elsevier.

[33] Pope S.B., Turbulent flows, Ed. Cambridge University Press.

[34] NASA, Dryden Flight Research Center, Information Summary. Wind-Up Turn, June 2010.

[35] USAF Air University - Test Pilot School Graduate Course, Edwards AFB (CA), 2010.

[36] Aircraft Performance Flight Test Handbook, S. Corda, 25 Jul 2005.

[37] Anderson J. D., Introduction to flight, Ch. 6 Ed.6, 2008.

[38] Losito V., Fondamenti di Aeronautica Generale, Accademia Aeronautica, 1991.

LIST OF FIGURES

LIST OF TABLES

SYMBOLS AND ACRONYMS

α	Angle of attack, degree
2D	Bi-dimensional
3D	Tri-dimensional
6DOF	6 Degrees Of Freedom
A/C	Aircraft
AIAA	American Institute of Aeronautics and Astronautics
a.k.a.	also known as
AoA	Angle of Attack
AoS	Angle of Sideslip
ARL	Aircraft Rocket Launcher
CAD	Computer Aided Design
CAE	Computer Aided Engineering
CAM	Computer Aided Manufacturing
CATIA	Computer Aided Three-dimensional Interactive Application
C_D	Drag coefficient
C_L	Lift coefficient
CMMs	Coordinate Measuring Machines
CTS	Captive Trajectory System
CFD	Computational Fluid Dynamics
DoE	Design of Experiments
DREAM	Dual Rockets Engagement Automatic Mechanism
EAS	Equivalent Air Speed
FCS	Flight Control System
FSI	Fluid Structure Interaction
FT	Flight Test
FTE/P	Flight Test Engineer/Pilot
FTI	Flight Test Instrumentation
FTT	Flight Test Techniques
g	Normal acceleration
GA	Genetic Algorithm

GVT	Ground Vibration Testing
H_C(=H)	Pressure Altitude
HW	Hardware
i.e.	*id est*
ItAF	Italian Air Force
KEAS	Knots Equivalent Air Speed
M	Mach number
M&S	Modeling and Simulation
MIT	Massachusetts Institute of Technology
OFAT	One Factor At Time
OT&E	Operational Test and Evaluation
N-S	Navier-Stokes
NURBS	Non Uniform Rational Basis-Splines
PITL	Pilot-in-the-Loop
RE	Reverse Engineering
RSV	Reparto Sperimentale Volo
SAGE	Semi-Automatic Ground Environment
SDB I	Small Diameter Bomb I
StE	Structure Engineers
SW	Software
SyE	Systems Engineers
TOF	Time Of Flight
TP(s)	Test Point(s)
USAF	United States Air Force
V_E=(V)	Equivalent Airspeed
WRB	Weapon Release Button
WTT	Wind Tunnel Test
WUT	Wind Up Turn

RINGRAZIAMENTI

I miei più sentiti ringraziamenti vanno alle persone che in questo lungo cammino di studio e ricerca mi sono state affettivamente e fattivamente vicine.

A mia moglie Maria Grazia e a mia figlia Ludovica un grazie di cuore per il tempo che mi hanno consentito di dedicare a questa attività avvincente e per il sostegno morale che non mi hanno fatto mai mancare. Non si può fare ricerca e la mente non può produrre se il cuore non è sereno e l'animo non è leggero…loro sono state la mia spinta e la mia forza quotidiana, il carburante necessario per macinare i tanti chilometri richiesti. La loro dolcezza e il loro amore, nonché i ritmi a cui mi hanno abituato, hanno fatto sembrare questo cammino una passeggiata in lieta compagnia. Le parole non potrebbero mai descrivere il senso di gratitudine, appagamento e la meraviglia che provo ogni giorno nel rivedervi accanto a me.

A mia madre Maria Teresa e a mia sorella Alessandra un abbraccio sincero per l'appoggio incondizionato che hanno sempre saputo darmi, specialmente nei momenti difficili, a volte stressanti: un porto sicuro in cui trovar conforto. Grazie sorellina, per me sei sempre stata uno sprone a migliorarmi, un importante confronto.

Inoltre, un grazie di cuore a mio padre, che anche se da molto lontano starà sicuramente sorridendo pieno di soddisfazione; assieme a mia madre è sempre stato per me una guida sicura e forte in una vita non priva di ostacoli. La verità è che il miglior complimento che posso fare ai miei genitori è forse l'emblema della banalità, ma ha un significato profondo che esprime a mio avviso l'essenza del rapporto genitori-figli e ciò che ho nel cuore: "mamma, papà…grazie per essere stati il miglior esempio da seguire che un figlio potesse avere".

Un sentito ringraziamento va sicuramente al carissimo Professor Carlo de Nicola, Maestro di tante cose, fra queste senza dubbio anche l'Aerodinamica con la A maiuscola, "quella che fa volare gli aerei" per dirla con parole mie e non quella che rimane staticamente confinata fra rotori e divergenze su lavagne polverose. Mi ha fatto ragionare su molte cose, spesso, e di questo non posso che essergli grato. Mi ha guidato in questi anni in un percorso di crescita non solo culturale, ma anche professionale e per certi versi umana.

Un ringraziamento particolare alla Professoressa Lina Mallozzi, un vulcano di energia e idee, sempre propositiva…a volte credevo che avesse più motivazione lei di me nell'affrontare le problematiche legate alle mie ricerche. Un esempio di entusiastica dedizione, oltre che docente dall'altissimo profilo accademico dalla quale ho appreso tanto in campi a me prima sconosciuti, quale quello della Teoria dei Giochi, solo per citarne uno.

All'Aeronautica Militare ed al Reparto Sperimentale Volo in particolare ho dedicato e dedico gran parte della mia vita (lavorativa e non) e forse anche parte di quella della mia famiglia…ringraziamento più grande mi riesce difficile pensarlo. È giusto che sia così…non sarei l'uomo, l'ufficiale, l'ingegnere, lo sperimentatore che sono se non grazie all'AM e al RSV…e spero che molto ancora avremo da scambiarci a tante cose da dirci in futuro.

Infine, come non sono nuovo fare nei miei ringraziamenti, ci terrei a ringraziare me stesso per la costanza, la forza d'animo, l'impegno, a volte l'ingegno, ma sicuramente il cuore e la mente che metto nelle cose di tutti i giorni e per quel mio non dare mai per scontato nulla, anche quello che scontato potrebbe sembrare. Un bravo di cuore per il mio vedere sempre nelle difficoltà un'opportunità, nel buio la luce e nella tempesta la serenità. Una pacca sulla spalla simbolica, con un po' di ironia, perché come mi ripeto sempre da anni e come mi piace ripetere sempre a mia moglie, a mia figlia e a quanti mi sono vicini…"un giorno senza un sorriso è un giorno perso" (Charlie Chaplin) e "ridiamo oggi che siamo vivi, che un domani chi lo sa che ci aspetta…*risata di gusto*" (papà - Antonio De Paolis, per tutti noi Tonio).

…alla prossima ☺.